Angle of arrival receiver design for a visible light positioning system

Stefanie Cincotta

Bachelor of Engineering (Hons.)

A thesis submitted for the Degree of Doctor of Philosophy at

Monash University in 2020

Department of Electrical and Computer Systems Engineering

Angle of arrival receiver design for a visible light positioning system

Copyright notices

Stefanie Cincotta

28th February 2020

Abstract

The introduction of light emitting diode (LED) lighting offers a new way of meeting the demand for an accurate, reliable and economical indoor positioning system (IPS); this emerging technology is termed visible light positioning (VLP). In VLP, the LED luminaires, in addition to providing indoor illumination, are used as beacons in an IPS. This is possible because the LEDs can be modulated at high speeds, enabling them to transmit data containing their position. At the VLP receiver, the signals are detected, using either photodiodes (PDs) or cameras. The signals can then be decoded and used in positioning algorithms.

There are several different positioning techniques that can be used in VLP. The focus of this thesis is the angle of arrival (AOA) technique. Firstly, a novel PD-based receiver has been developed and analysed in detail. This receiver, called the quadrant angular diversity aperture (QADA) receiver, consists of a quadrant PD that is located directly below an aperture. Light passes through the aperture to the PD, forming a light spot that is the same size and shape as the aperture. The position of this light spot on the quadrant PD is related to the AOA. Algorithms were developed that use the photocurrents from each quadrant of the PD to calculate the AOA. Experimental and simulation results show that the QADA is able to accurately estimate the AOA under ideal conditions.

In the next contribution, to address the difficulties of using a QADA under non-ideal conditions, the QADA-plus receiver is introduced. This hybrid receiver design combines a QADA with a camera. Accurate AOA calculation is possible from an image captured by a camera, but cameras are not ideal for receiving modulated data. Conversely, the QADA is able to receive the data, but its AOA estimation accuracy is affected by many factors that can be difficult to control, such as luminaire size and shape. In a QADA-plus receiver, the modulated signals are received and decoded by the QADA, which is also used to coarsely estimate the AOA. The decoded data can then be matched to the luminaires that are present in the image using the QADA AOA estimations. Extensive simulation results are presented that show the limitations of the PD-based QADA receiver in the presence of noise and realistic luminaire geometry. When using a QADA-plus, the QADA accuracy only needs to be sufficient to differentiate between luminaires in the image.

Finally, the use of luminaire reference points (LRP) is explored. One challenge in VLP is that, in some indoor scenarios, the field of view (FOV) of the receiver needs to be very large to guarantee enough luminaires are available for triangulation. A LRP is any feature associated with a luminaire that can be identified in an image. Possible LRPs include inconspicuous marks on the frame of the luminaire or a single LED of a different wavelength. The location of each LRP is transmitted by the luminaire, thus the LRPs can be used for triangulation. An important reason for using LRPs is the ability to co-locate multiple LRPs on a single luminaire. If multiple LRPs are located on a single luminaire, then only one luminaire, instead of three, must be in the FOV of the receiver. This is shown by analysing typical indoor environments such as corridors and large rooms where the luminaires are often large and spaced far apart. In these environments, without the use of LRPs, the FOV requirement would be very challenging. The non-ideal beacon geometry imposed by the co-location of LRPs on a single luminaire is analysed using the geometric dilution of precision. It is shown that the positioning error distribution is low and uniform in the majority of locations.

The work presented in this thesis underpins an important new VLP system that is both accurate and robust.

List of Publications

Articles in peer-reviewed journals

1. S. Cincotta, C. He, A. Neild, and J. Armstrong, 'High angular resolution visible light positioning using a quadrant photodiode angular diversity aperture receiver (QADA)', *Opt. Express, OE*, vol. 26, no. 7, pp. 9230–9242, Apr. 2018

2. S. Cincotta, C. He, A. Neild, and J. Armstrong, 'Indoor Visible Light Positioning: Overcoming the Practical Limitations of the Quadrant Angular Diversity Aperture Receiver (QADA) by Using the Two-Stage QADA-Plus Receiver', *Sensors*, vol. 19, no. 4, p. 956, Jan. 2019

3. C. He, S. Cincotta, M. M. A. Mohammed, and J. Armstong, 'Angular Diversity Aperture (ADA) Receivers for Indoor Visible Light Communications (VLC),' *IEEE Access*, vol. 7, pp. 145282–145301, 2019

Peer-reviewed conference papers

1. S. Cincotta, A. Neild, C. He, and J. Armstrong, 'Visible Light Positioning Using an Aperture and a Quadrant Photodiode', in *2017 IEEE Globecom Workshops (GC Wkshps)*, 2017, pp. 1-6

2. S. Cincotta, C. He, A. Neild, and J. Armstrong, 'QADA-PLUS: A Novel Two-Stage Receiver for Visible Light Positioning', in *2018 International Conference on Indoor Positioning and Indoor Navigation (IPIN)*, 2018, pp. 1-8.

3. S. Cincotta, A. Neild, and J. Armstrong, 'Luminaire Reference Points (LRP) in Visible Light Positioning using Hybrid Imaging-Photodiode (HIP) Receivers', in *2019 International Conference on Indoor Positioning and Indoor Navigation (IPIN)*, 2019, pp. 1-8.

PCT Patent

1. S. Cincotta, A. Neild, and J. Armstrong, 'Visible Light Positioning Receiver Arrangement and Two Stage Positioning Method', WO2020000021 (A1).

Declaration of Authorship

I hereby declare that this thesis contains no material which has been accepted for the award of any other degree or diploma at any university or equivalent institution and that, to the best of my knowledge and belief, this thesis contains no material previously published or written by another person, except where due reference is made in the text of the thesis.

This thesis includes five original papers; two have been published in peer-reviewed journals and three have been published in peer-reviewed conferences. The core theme of the thesis is Angle of arrival receiver design for a visible light positioning system. The ideas, development and writing up of all the papers in the thesis were the principal responsibility of myself, the student, working within the Department of Electrical and Computer Systems Engineering (ECSE) under the supervision of Professor Jean Armstrong and Professor Adrian Neild.

The inclusion of co-authors reflects the fact that the work came from active collaboration between researchers and acknowledges input into team-based research.

In the case of Chapters 4 to 8 my contribution to the work involved the following:

Thesis Chapter	**Publication Title**	**Status**	**Nature and % of student contribution**	**Co-author name(s) Nature and % of Co-author's contribution***	**Co-author(s), Monash student Y/N***
4	Visible Light Positioning Using an Aperture and a Quadrant Photodiode	Published	75%. Concept, ideas, simulations, analysis and paper writing	Adrian Neild, input into concept and ideas, review of drafts, overall supervision, 10% Cuiwei He, review of drafts, 5% Jean Armstrong, input into concept and ideas, review of drafts, overall supervision, 10%	No Yes No

5	High angular resolution visible light positioning using a quadrant photodiode angular diversity aperture receiver (QADA)	Published	75%. Concept, ideas, simulations, experiment and paper writing	Cuiwei He, review of drafts 5% Adrian Neild, input into concept and ideas, review of drafts, overall supervision, 10% Jean Armstrong, input into concept and ideas, review of drafts, overall supervision, 10%	Yes No No
6	QADA-PLUS: A Novel Two-Stage Receiver for Visible Light Positioning	Published	75%. Concept, ideas, simulations and paper writing	Cuiwei He, simulation, review of drafts 5% Adrian Neild, input into concept and ideas, review of drafts, overall supervision, 10% Jean Armstrong, input into concept and ideas, review of drafts, overall supervision, 10%	No No No
7	Indoor Visible Light Positioning: Overcoming the Practical Limitations of the Quadrant Angular Diversity Aperture Receiver (QADA) by Using the Two-Stage QADA-Plus Receiver	Published	75%. Concept, ideas, simulations, analysis and paper writing	Cuiwei He, review of drafts 5% Adrian Neild, input into concept and ideas, review of drafts, overall supervision, 10% Jean Armstrong, input into concept and ideas, review of drafts, overall supervision, 10%	No No No
8	Luminaire Reference Points (LRP) in Visible Light Positioning using Hybrid Imaging-Photodiode (HIP) Receivers	Published	80%. Concept, ideas, simulations, and paper writing	Adrian Neild, input into concept and ideas, review of drafts, overall supervision, 10% Jean Armstrong, input into concept and ideas, review of drafts, overall supervision, 10%	No No

I have not renumbered sections of submitted or published papers in order to generate a consistent presentation within the thesis.

Student signature:

Candidate Name: Stefanie Cincotta

Date: 28th February 2020

The undersigned hereby certify that the above declaration correctly reflects the nature and extent of the student's and co-authors' contributions to this work. In instances where I am not the responsible author, I have consulted with the responsible author to agree on the respective contributions of the authors.

Main Supervisor signature:

Main supervisor name: Prof. Jean Armstrong

Date: 28th February 2020

Acknowledgements

I would like to express my sincere gratitude to my supervisors, Professor Jean Armstrong and Professor Adrian Neild, for all their support and guidance during this Ph.D. I have greatly appreciated all the opportunities I have been given to learn and develop my research skills. It has been a genuine privilege to have you both as my supervisors.

I would also like to express my gratitude to my colleagues, Dr Cuiwei He, Dr Mohammed Mohammed, Mr Kelly Kelly and Mr Daniel Morrison. I have appreciated all the times you have offered your feedback and shared your knowledge. Thank you for your friendship and all of the fun times. It has been a pleasure to share the lab with you all.

Finally, none of this would have been possible without the generous financial support of the Australian Government's Research Training Program (RTP) Scholarship and the Australian Research Council's (ARC) Discovery funding scheme (DP 150100003 and DP 180100872).

Contents

List of Figures

List of Abbreviations

AC	Alternating Current
ADA	Angular Diversity Aperture
AOA	Angle of Arrival
BIP	Beacon Information Packet
BLE	Bluetooth Low Energy
CMOS	Complementary Metal-Oxide-Semiconductor
DC	Direct Current
FOV	Field of View
GDOP	Geometric Dilution of Precision
GNSS	Global Navigation Satellite System
GPS	Global Positioning System
HIP	Hybrid Imaging Photodiode
IMR	Imaging Receivier
IMU	Inertial Measurement Unit
IPIN	Indoor Positioning and Indoor Navigation
IPS	Indoor Positioning System
LBS	Location-based Services
LED	Light Emitting Diode
LOS	Line of Sight
LRP	Luminaire Reference Point
MIMO	Multiple Input Multiple Output
NEP	Noise Equivalent Power
NLOS	Non Line of Sight
PD	Photodiode
PDR	Photodiode-based Receiver
QADA	Quadrant Angular Diversity Aperture

RE	Receiving Element
RF	Radio Frequency
rMSE	Root Mean Square Error
RSS	Received Signal Strength
SNR	Signal to Noise Ratio
TDMA	Time Division Multiple Access
TDOA	Time Difference of Arrival
TFT	Thin Film Transistor
TOA	Time of Arrival
US	Ultrasound
UWB	Ultra-wideband
VLC	Visible Light Communication
VLP	Visible Light Positioning

List of Symbols

Chapter 3

h	DC channel gain
m	Lambertian order
A	Area of photodiode
d	Distance between transmitter and receiver
ϕ	Emergence angle
ψ	Incident angle
T	Filter transmission
g	Concentrator gain
ψ_c	Field of View of the receiver
σ^2_{shot}	Shot noise variance
q	Electron charge
R	Photodiode responsivity
p_n	Background spectral irradiance
$\Delta\lambda$	Optical bandwidth
B	Electrical bandwidth

Chapter 4

t	Time
$[x_1(t), y_1(t)]$	Centroid of light spot
$p_x(t)$	Ratio of photocurrents used to find $x_1(t)$
$p_y(t)$	Ratio of photocurrents used to find $y_1(t)$
$i_j(t)$	Photocurrent from j^{th} quadrant
$N_j(t)$	Noise in j^{th} quadrant
$A_j(t)$	Area of overlap in j^{th} quadrant
L	Length of PD quadrant

k	Sample start index
n	Sample index
M	Number of samples
$\hat{x}_1(t)$	Estimate for $x_1(t)$
$\hat{y}_1(t)$	Estimate for $y_1(t)$
$h_c(t)$	DC channel gain
P_R	Received optical power
P_T	Transmitted optical power
H	Distance from transmitter to receiver
h	Distance from aperture to photodiode
N_0	Single sided power density
σ_n^2	Shot noise variance

Chapter 5

L_{PD}	Length of PD quadrant
L_{ap}	Half side length of aperture
k_1	Constant term equal to RP_T/π
$E_n(t)$	Ratio noise term
$\sigma_e^2(t)$	Noise variance of $E_n(T)$

Chapter 6

α	Polar angle
$\sigma_{thermal}^2$	Thermal noise variance
(x, y, z)	Position of the receiver
(x_A, y_A, z_A)	Image coordinates
d_{AB}	Distance between transmitters
$d_{A'B'}$	Distance between transmitters in image
f	Focal length

Chapter 7

$(x_{L,n}, y_{L,n}, z_{L,n})$	Location of n^{th} transmitter
(x_R, y_R, z_R)	Location of receiver
r_n	Distance from n^{th} transmitter to the receiver
h_j	DC channel gain

n	Integer

Chapter 8

H	Geometric design matrix
σ_p	Standard deviation of position error
σ_a	Standard deviation of angle estimation error
(x_i, y_i, z_i)	Location of i^{th} transmitter
r_i	2D Euclidean Distance from transmitter to receiver
R_i	3D Euclidean Distance from transmitter to receiver

Chapter 1

Introduction

Indoor positioning is the ability to locate a person or an object in an indoor environment. This ability brings with it the ability to navigate. Humans have long been driven to find ways to position and navigate the world; from celestial navigation to radio-wave navigation, the innovation and interest in the field of positioning and navigation has been enduring and increasing over a very long period of time [1].

In recent years, with the decreasing cost of global navigation satellite system (GNSS) receivers and the explosion of smart phone usage [2], the ability to accurately and easily navigate the outdoor world has become standard. However, this is still not the case for the indoor world. Despite humans spending most of the time indoors [3], there is currently no indoor positioning system that rivals the utility of GNSS.

In order to localise using GNSS, a receiver must have line-of-sight (LOS) to at least four satellites [4]. This is easily achieved in the majority of outdoor environments, however it is typically

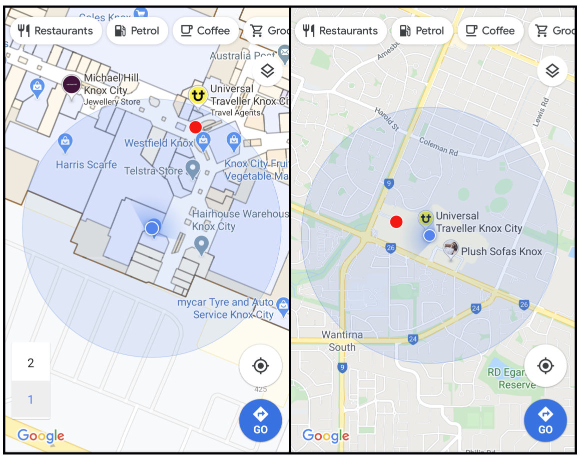

FIGURE 1.1: GNSS position estimates in a shopping centre for two different positions.

not possible indoors. Due to signal attenuation and multipath effects, even where the signals can be received, it is not possible to accurately estimate position. This means that the typical five meter accuracy of GNSS [5] is further degraded and its position estimations are often not useful indoors. This is demonstrated in Fig. 1.1 where the Google maps application is used in a large shopping centre. The blue dot represents the position estimate and the large blue circle represents the uncertainty in the position estimate. The red dot shows the true position.

There are currently over one hundred GNSS satellites orbiting the earth [6]–[9], providing accurate and reliable positioning in almost all outdoor locations. This huge investment in infrastructure, spanning four major systems, makes it clear that the desire for outdoor positioning is extremely high. Originally motivated by military applications, GNSS has become extremely popular since the United States' Global Positioning System (GPS) became fully available for civilian use in 2000. Whilst the primary use of GNSS has been vehicle navigation, it is also used in mapping, surveying, geofencing, search and rescue, social networking, entertainment and more [10]. With so many unforeseen uses, it is reasonable to assume that similar potential exists for indoor localisation.

Despite no widespread indoor positioning system (IPS) currently available, market research has shown that indoor positioning has the potential to be a multi-billion-dollar industry [11]. This is driven, in part, by the desire to provide location-based services (LBS) in retail environments, but also by the integration of smartphones into everyday life and the increasing drive for autonomous supply chains. A reliable, robust and economical IPS is highly desirable and it will have a huge impact on the way the indoor world is utilised and experienced, much like GNSS did for the outdoor world.

1.1 Visible Light Positioning motivation

The demand for indoor positioning has been well established, as demonstrated by a large body of literature, significant interest from industry, several international competitions and an annual international conference [12]–[14]. In recent years, a new technology called visible light positioning (VLP) has demonstrated great potential for indoor positioning. In VLP, light emitting diode (LED) luminaires transmit their positions, in a local or global coordinate system, and the signals are detected and decoded by photodiodes (PDs) or cameras. If a sufficient number of signals are received, the receiver can calculate its position.

There are many different ways to approach VLP, based on various properties of the received signal [15]–[18]. All of these positioning techniques (discussed in Chapter 3) have demonstrated potential, in both simulation and experimental results, to achieve good positioning accuracy. The focus of this thesis is the use of angle of arrival (AOA) techniques. These techniques have many useful properties in VLP [19]. However, to use AOA techniques, a receiver which can detect the AOA is required. These receivers could either be PDs or cameras. There have been many different PD-based AOA receiver designs, which will be discussed in detail in Chapter 3. These designs rely on the PDs facing in different directions, and they can theoretically provide good angular diversity and accurate AOA estimation [20]–[24]. However, the physical structure of the receiver is very important in many applications. An ideal receiver would have a compact and planar form factor so that it can be easily incorporated into a smartphone or used in an unobtrusive stand-alone device.

The research presented in this thesis is focused on AOA techniques for VLP and specifically the design, analysis and verification of a novel angular diversity receiver.

1.2 Thesis outline

In Chapter 2, the topic of indoor positioning is introduced, with a broad overview of the different technologies and positioning techniques that have been reported in the literature. The many and varied applications are discussed and the important metrics for assessing an indoor positioning system are outlined. Visible light positioning is highlighted as a promising technology for indoor positioning as it performs well in many of the metrics described.

In Chapter 3, visible light positioning is explored in more detail. This chapter provides a deeper understanding of this exciting new technology and how it can provide accurate, reliable indoor positioning in a wide variety of applications. The various techniques are discussed with angle of arrival emphasised because of its many advantages. Finally, potential receiver designs are introduced, focusing on the receivers used in AOA techniques.

Chapter 4 introduces a new receiver structure for AOA detection in VLP. The quadrant angular diversity aperture (QADA) receiver combines a quadrant PD and an aperture. One feature of this receiver structure is that it has a compact and planar form. Analytical and simulation results are presented that demonstrate the potential accuracy of this receiver.

In Chapter 5, the QADA receiver is explored further including experimental validation. The results from an experiment on an optical bench are shown to align well with simulation results for the same scenario. Further analysis of the noise variance for a QADA is presented and an adapted algorithm is introduced for the QADA geometry used in the experiment.

In Chapter 6, QADA-plus is introduced. This new receiver structure combines a QADA with a camera to provide more robust and accurate positioning. Reference points are also introduced. These are distinct features that can be identified in an image. The advantages of using reference points for VLP are discussed. Finally, the challenges of using a QADA alone are demonstrated with simulations showing the impact of various parameters on the AOA estimation.

In Chapter 7, further limitations of QADA are explored with a focus on the impact of real luminaire geometry. Luminaires are often modelled as point sources, however this is not true in practice. In this chapter, the impact on AOA and position estimation of various luminaire geometries is shown. Other sources of error for PD receivers are also analysed and the use of the hybrid receiver structure of QADA-plus to overcome these problems is discussed.

In Chapter 8, reference points are analysed further. In particular, the impact on accuracy of using multiple reference points on a single luminaire is analysed. Using the geometric dilution of precision (GDOP), the degradation of accuracy from having non ideal beacon geometry is shown. It is also shown that, despite the loss of accuracy, that co-locating multiple reference points on a single luminaire makes it possible to localise in environments where it would otherwise not be possible. These environments include corridors, which typically have a linear arrangement of widely spaced luminaires, and large rooms that install widely spaced, large luminaires.

Finally, Chapter 9 provides a summary of the contributions and conclusions from the work presented in this thesis and suggests possible avenues for future research.

Chapter 2

Indoor Positioning

2.1 Overview

There has been a large amount of research in recent years that has been dedicated to finding a reliable indoor positioning system suitable for widespread market adoption [13], [25]–[28].

This chapter explores the potential applications for indoor positioning so as to understand why there has been so much interest in this topic. The various metrics used for evaluating an IPS will be discussed to provide a good understanding of the design goals. Finally, to understand the state of the art, a brief outline of the various indoor positioning techniques and technologies that have been used for indoor positioning is presented.

2.2 Applications of Indoor Positioning

In order to understand why there has been so much research into indoor positioning, it is worth considering the potential applications.

The applications for indoor positioning are vast and varied, spanning a range of industries. Due to the large number of applications, it is useful to break them down into categories. Although there are many different ways to categorise the applications, for simplicity, the following sections use three broad categories; those where the user is directly utilising the position information (i.e. first-person navigation or client-based positioning), those where a control unit or other agent is utilising the position information (i.e. tracking or server-based positioning) and location-based broadcasting. In all these applications, various different technologies and techniques have been investigated [28].

2.2.1 Navigation

Arguably the most obvious and easiest to envisage application for indoor positioning is pedestrian navigation. Shopping centres, airports, museums, hospitals, universities; it is not difficult to think of a large number of indoor locations where it is challenging to navigate. This could be due to a variety of reasons such as building size, complex layouts or lack of familiarity with the location. Indoor positioning technology could also be used to guide emergency services [29], [30] or vision impaired people [31]. Navigation applications are not just limited to human use, but also apply to robots, autonomous vehicles and drones. In general, for this category of applications, the user is equipped with a receiver that is able to determine its position, and decisions on how to use the position information are made by the user. User privacy is possible for technologies where all processing can be carried out on the receiving device.

2.2.2 Tracking

Tracking applications are those in which some sort of central server or control unit is tasked with monitoring the location of users or equipment in the indoor environment. In contrast to navigation type applications, the user that is being tracked may not have access to the position information. Examples of tracking type applications include factory automation, customer tracking, workforce tracking, asset tracking, big data analytics and research [32]–[35]. For these applications it is possible to operate in one of two modes. Either the receiver is carried by the tracked user or object, and a communication uplink must be established to send the position information to a central control unit [33], or the user carries a transmitter and the indoor space is equipped with receiving units that send data to the central control unit [36].

2.2.3 Location-based broadcasting

Location-based broadcasting is dominated by LBS such as advertising, marketing and point of interest (POI) information [37], [38]. They also include entertainment applications like augmented reality gaming and social networking. These application types may be integrated with the other categories of applications (navigation and tracking) or they may exist as a simple, stand-alone system.

2.3 Performance metrics

When considering a positioning system, its performance should be assessed based on the requirements of the application. Whilst some applications may require high levels of accuracy, others may be capable of tolerating lower accuracy in order to keep costs down. It is often very difficult to directly compare the positioning systems proposed in the literature due to the variety of experimental scenarios, that are typically highly controlled, and the arbitrary choice of a subset of performance metrics to measure and report. Indoor positioning competitions, such as the one hosted by the annual Indoor Positioning and Indoor Navigation (IPIN) conference [14], allow direct comparison of systems by standardising the scenario, however the only performance metric used to determine the winner is accuracy. Similarly, the Microsoft indoor localisation competition, last held in 2018, focused on accuracy. However, unlike the IPIN competition, teams were allowed to deploy infrastructure if needed, thus providing another point of comparison [12].

The following section outlines some important performance metrics and the potential trade-offs involved when trying to achieve specific design goals.

2.3.1 Accuracy and Precision

Accuracy is probably the most common metric by which a positioning system is judged, however it is not necessarily the most important in all applications. In general, accuracy is considered to be the average Euclidean distance between the estimated position and the true position. This is often reported using the cumulative distribution function or plotted as a function of position. Depending on the application, this may be in two or three dimensions. Precision, however, is related to the variability of the estimate. In general, it is desirable for position estimates to be both accurate and precise.

A common requirement for an IPS is that the position estimate must be sufficiently accurate to differentiate between floors in a building [39]. Whilst this requirement is not particularly onerous, generally only requiring accuracy that is less than approximately three meters, it can be quite challenging for some technologies to achieve reliably [40].

The trade off with accuracy is often update speed [41]. This is a problem as the applications that tend to be most demanding on accuracy, such as autonomous vehicles and robots, may also be the ones that have high requirements for rapid, real-time updates. Most human applications, with the exception of vision impaired navigation, have lower accuracy demands due to the ability to simultaneously utilise the position estimates and visually process the world.

2.3.2 Infrastructure, Scalability and Cost

Economic performance metrics are important for an IPS to achieve commercial success. These metrics relate to the cost of installation, operation and maintenance of the system.

Battery operated beacons can be challenging in both the short and long term [42]. These beacons typically need to be installed densely due to short reception range, thus the flexibility of battery operation is advantageous. However, the amount of time needed for initial installation and configuration can become very lengthy [42]. Long term, maintenance can be difficult as it may be challenging to find a replace malfunctioning units. Whilst a system like this is suitable for some applications, such as proximity advertising, it will suffer from poor scalability and thus is not suitable for more demanding applications.

Another solution that suffers from poor scalability and difficult maintenance is fingerprinting [43]. The initial offline stage of gathering fingerprints is time consuming for large buildings and management of the fingerprint map quickly becomes challenging due to the dynamic nature of indoor environments. Indoor environments experience regular changes, such as furniture or people moving around, that can affect the fingerprints. One proposed solution is crowd-sourcing fingerprints [44], [45]. Privacy concerns aside [37], this solution is reliant on uplink communication and cloud-based processing which will impose other limitations on the system.

Whilst infrastructure-free technologies can be desirable for some systems, dual-use technologies, such as VLP, also have merit. As indoor locations are already illuminated, much of the infrastructure cost in VLP is absorbed in the initial installation or retrofit of the lighting infrastructure. Added to this, the opportunity currently exists to piggyback on the large scale migration to energy efficient lighting.

2.3.3 Energy Consumption

Energy efficiency is important for receivers, as they are generally mobile devices, but it is also important for technologies that require transmitting infrastructure.

Transmitters may be battery operated or mains powered. It is clearly important for battery operated beacons to be energy efficient to minimise battery drain and decrease maintenance costs, as discussed in the previous section. However, transmitters connected to mains power should also aim to be energy efficient. It would be very difficult for an emerging technology to be accepted if it was energy inefficient [46].

For most pedestrian applications it is expected that position information is delivered visually on a display, such as a smartphone screen. Regardless of technology used, the screen-on time will cause a non-negligible battery drain, which is difficult to avoid. However, if the receiver and associated processing is also significantly draining the battery, then people will be less inclined to use the device for navigation. GNSS receivers in vehicles are able to get around this by drawing power from the vehicle, however this is clearly not possible in typical indoor positioning applications.

For stand-alone devices, such as those that are attached to autonomous vehicles, the need for a screen output is no longer present and the possibility of adding additional battery may be possible. Although this means that a greater amount energy is potentially available, efficiency is still important as these applications often impose other demands on the system such as rapid update speed, which is discussed in the next section.

2.3.4 Update frequency and latency

The position update frequency is linked closely with the application requirements and thus the movement speed of the user. However, it is also linked to the achievable accuracy of the system. As an example; the typical indoor walking speed for humans is around 1.3-1.4 m/s [47]. If the accuracy of the IPS is one to two meters, there is little to be gained from rapid position updates. A related, but slightly different metric is latency. In many applications, near real-time updates are desirable. This may mean sacrificing accuracy as algorithms would need to be optimised for speed instead of accuracy [13].

Autonomous vehicles have the potential to move faster than humans, especially in warehouse and factory environments, thus rapid position updates will be desirable for these applications. However, the demand for frequent updates is energy intensive and increases the complexity of the system. Computational speed and efficiency become important and the reliance on any external database will likely slow down update speed due to round trip times. These factors combined make it very difficult for some technologies to be adopted in these applications.

2.3.5 Reliability and Robustness

Reliability and robustness relate to the system's ability to perform well, and without failure, under different conditions, many of which are not ideal. Many indoor spaces are very challenging for IPS, whether due to their sheer size, their ever-changing environment, the presence of interfering signals or even the abundance of reflective surfaces [48], [49]. For some applications, such as emergency services, reliability is vital. However, other applications, such as navigating a shopping centre, may be able to accept an occasional, momentary failure.

2.4 Indoor Positioning Techniques

Indoor positioning can be achieved in a variety of ways using a variety of technologies. In order to better understand the potential technologies, the most common techniques are first introduced.

Received signal strength (RSS) systems measure the intensity of the signal at the receiver and relates it to the transmitted power in order to estimate the distance the signal has travelled. This technique relies on accurate channel models and accurate knowledge of the transmitted power. If enough distances are known trilateration algorithms can then be applied.

Angle of arrival systems, as the name suggests, measure the AOA of the received signals. This technique relies on angular diversity at the transmitter or the receiver. For this technique, triangulation algorithms can be applied assuming a sufficient number of angles were estimated.

Time-based (Time of Arrival (TOA), Time Difference of Arrival (TDOA), etc.) systems rely on very precise measurements of the time in order to estimate how far the signal travelled. As the times that are measured are generally very small, very accurate (and potentially synchronised) clocks are needed. Spherical lateration algorithms are used for TOA and hyperbolic lateration algorithms are used for TDOA [50].

Proximity techniques use the strongest signal to estimate the position with low precision. This technique tends to be useful only in location based broadcasting applications, or potentially where very low accuracy is acceptable.

Fingerprinting techniques require an off-line stage where sensor measurements are gathered for all positions to create a map. Later, during use, the received signals are compared to the map to estimate position.

Dead Reckoning relies on measurements, typically from inertial sensors, which are combined with kinematic equations to estimate position. As each successive estimate is based on the previous estimate, errors will build up and there needs to be a way to recalibrate the receiver periodically.

2.5 Indoor Positioning Technologies

Many different technologies have been explored for indoor positioning, each with their strengths and weaknesses. This section briefly looks at some of the technologies that have been discussed in the literature, with a focus on the current challenges each technology faces.

2.5.1 WiFi

The indoor world has become increasingly blanketed in WiFi. This is particularly true in the last decade as the technology has matured and the demand for connectivity has increased. Due to the high availability of WiFi signals, there has been a lot of research into utilising them for indoor positioning [40], [51]. WiFi transmits radio-frequency (RF) signals in the 2.4 Ghz and 5 Ghz bands [52] and it can be received up to 70 m away [53]. As wireless access points are already present in most indoor locations for communication and smartphones are already equipped with WiFi receivers, there is no need for additional infrastructure. However, it is difficult to directly apply the RSS or AOA techniques due to multipath effects, so most WiFi systems rely on fingerprinting to achieve usable accuracy [51], [54]. As mentioned earlier, fingerprint maps are difficult to maintain as the fingerprints are affected by features in the indoor environment that frequently change such as furniture, people and temporary WiFi hotspots. Added to this, constant WiFi scanning draws considerable battery power and update frequency is limited due to the WiFi scans taking several seconds [53].

2.5.2 Bluetooth

Bluetooth also transmits RF waves in the 2.4 GHz band, however unlike WiFi the range is much shorter, particularly for the Bluetooth low energy protocol (BLE) which has a typical range of 20 m [37]. The accuracy of a BLE IPS is related to the density of beacon installation [53]. This means battery operated beacons are preferable because it is easier to install them densely. Similar to WiFi, fingerprinting is the most common approach to achieve navigation and tracking functionality. However, higher levels of accuracy can be achieved when compared to WiFi.

The Apple iBeacon protocol is an example of a BLE IPS that is already on the market [55]. The beacons periodically broadcast a standardised advertising packet that is received by nearby devices. This is well suited to providing LBS with the use of proximity techniques, but, to be used in any other application, fingerprinting is still required.

2.5.3 Ultra-wideband

In ultra-wideband systems (UWB), RF signals are transmitted that have extremely short pulse width and a low duty cycle. Due to the short pulse length, it is less sensitive to multipath because of the ability to differentiate the reflected signal. This means that, unlike WiFi and BLE, there is no absolute need to rely on fingerprinting techniques and thus several different techniques have been applied successfully with time-based techniques being most common [55]–[59]. High levels of accuracy are possible, however specialised infrastructure needs to be deployed to transmit the signals [60]. As time of flight is the most common technique, there is a requirement that there is a LOS path available. Thus, there could be a substantial amount of infrastructure, depending on the environment layout.

Whilst all smartphones already have WiFi and BLE receivers, it is only recently that a UWB receiver was introduced into the latest Apple iPhone [61]. Although it is too early to say what impact this will have on the popularity of UWB for indoor positioning, it is an interesting advancement for the technology.

2.5.4 Acoustic

Although there have been IPS that use audible sound [62], it is more common to use ultrasound (US) (frequencies greater than 20 kHz) [63], [64]. The most common techniques used are time-based, thus many of the same requirements specified for UWB also apply to US. However, because the speed of sound is much less than the speed of light, less expensive clocks can be used, making it a potentially more economical alternative. Unfortunately, update speed is limited, and difficulties arise when users are moving due to Doppler shift [64].

2.5.5 Magnetic

The magnetic fields that have been used for indoor positioning are split into two categories - passive and active. Passive systems rely on measuring the earth's magnetic field [65], whilst active systems use coils and either direct current (DC) [66] or alternating current (AC) [67] power to induce magnetic fields in the area. In both cases, the most common technique applied is fingerprinting. Systems that rely on creating magnetic fields tend to have the disadvantage of requiring significant amounts of power to achieve usable reception range. The passive systems, on the other hand, require no additional infrastructure, however the accuracy is limited [68].

2.5.6 Inertial

Inertial measurement units (IMU) provide estimations of movement in three dimensions, generally using accelerometers and gyroscopes. Whilst most smartphones are equipped with these sensors, foot mounted IMUs are more commonly used for indoor positioning [69]–[71]. These systems use dead reckoning. As each successive estimate is based on the previous estimate, errors will accumulate and thus there must be a method to combat or periodically correct this. One advantage of this type of system is that it does not require any additional infrastructure, however, good quality receivers are expensive, and the foot-mounted approach may have difficulty finding mainstream acceptance.

2.5.7 Visible Light Positioning

In VLP, LED luminaires transmit signals that are received by light sensors such as photodiodes or cameras. The signals generally contain information about the position of the luminaire, either in a global or local coordinate system. A major advantage of VLP is that luminaires are already present in almost all indoor locations, thus installing a VLP system could be as simple as changing a lightbulb [19]. In VLP it is possible to achieve very accurate positioning using very cheap sensors [18]. As VLP is the main focus of this thesis, an in depth exploration of VLP is presented in Chapter 3.

2.5.8 Fusion and other technologies

Many systems have been described in the literature that combine two or more of the above technologies, usually in an attempt to overcome the deficiencies of using only one technology [72]–[75]. This is common for inertial systems that need some way of overcoming the growing errors [71], [76]–[78].

Other less common techniques that have been reported include infrared [79], [80], radio-frequency ID [81], [82], Zigbee [83] and 5G [84]. With the exception of infrared, the other techniques listed are all based on RF signals and experience many of the challenges listed for other RF technologies.

2.6 Summary

This chapter has examined many of the technologies and challenges for indoor positioning. It is clear that with so many diverse applications, and diverse requirements, that it is difficult to find one single technology that can achieve everything. Whilst there has been a large amount of interest in indoor positioning, in both industry and academia, and a number of products have entered the market [60], [85]–[90], there is still no system that has been able to achieve widespread adoption. When beacon technology was released into the market in 2013 there was much excitement and many large organisations invested heavily in the infrastructure [42], [91], [92]. However, in the ensuing years, despite continual interest in the technology and indoor positioning, beacon systems still experience difficulties with installation, maintenance and usage [93].

The next chapter will go into further detail about one particular technology, VLP. This technology has the unique advantage of performing well in all the metrics mentioned and does not suffer from the major issues that plague RF technologies. Importantly, it is potentially suitable for a wide variety of indoor positioning applications, making it a very attractive technology for research and investment.

Chapter 3

Visible Light Positioning

3.1 Overview

The previous chapter provided an overview of indoor positioning. It highlighted the increasing demand for indoor positioning in a broad range of applications and discussed the important features of an IPS along with the various technologies that have been applied. This chapter will go into further detail on one technology, visible light positioning. A typical VLP scenario is shown in Fig. 3.1. The luminaires transmit information that makes it possible to use them as beacons for positioning and the receiver calculates its position.

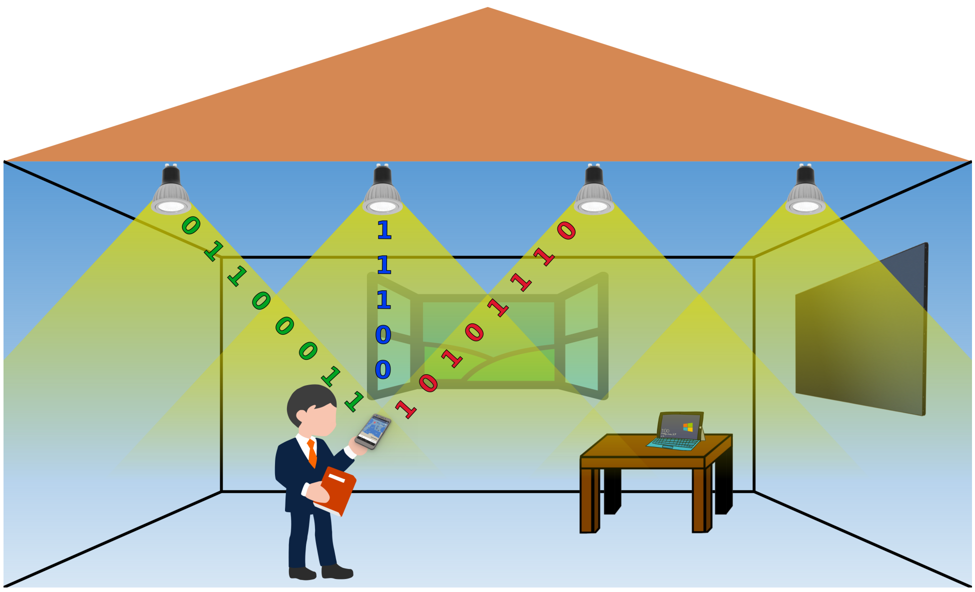

FIGURE 3.1: A typical VLP scenario

To understand why VLP is an interesting technology this chapter begins by discussing the characteristics of a VLP system, particularly when compared with other indoor positioning technologies. This is followed by detailed discussion of the important features and requirements for the transmitters and receivers in VLP, along with the various positioning techniques that have been applied to VLP.

3.2 Characteristics of VLP

VLP offers many advantages over other positioning technologies, particularly when compared to RF technologies [19]. The multipath propagation of radio waves presents a significant challenge for RF technologies like WiFi and BLE. This has mostly forced these technologies to rely on fingerprinting techniques for positioning, the challenges of which were extensively discussed in the previous chapter. Whilst light does reflect off surfaces, it has been shown that the reflected light does not impact VLP greatly [49], [94], [95]. Thus, in VLP, it is possible to use techniques that rely on LOS, making very accurate and precise positioning possible.

A lot of research has been dedicated to quantifying the accuracy of VLP [22], [96]–[106]. Although it is difficult to give an exact figure, it is clear that it is possible to achieve sub decimetre accuracy, or better, depending on the technique that is applied [17], [18], [107]–[110]. This is important because it opens up many more applications than less accurate technologies. Whilst accuracy is not the only metric used to evaluate an IPS, it is particularly important for applications in robotics and autonomous vehicles. These applications are likely to see significant growth in the coming years [48], [111].

Another important feature of VLP is that almost all indoor locations are illuminated, and it is becoming increasingly common for white LEDs to be the lighting of choice. This makes VLP a dual-use technology, where the luminaires simultaneously provide indoor illumination and positioning. This is important because it minimises the need for extensive additional infrastructure. Also, because there is no need to install a large number of RF transmitters, VLP can also be used in areas that are sensitive to RF, such as hospitals or mines [112], [113].

The receivers used in VLP also have useful characteristics. It is possible to create an accurate receiver that is very cheap, low power and compact. This type of receiver structure can easily be integrated into smart phones which is a very important feature for any indoor positioning technology. Also, this compact, low power form factor is ideal as a stand-alone receiver that can be tailored to other applications that do not require a smartphone. VLP is very attractive for a wide range of applications due to the flexibility in implementation [109]. For lower accuracy requirements, simple systems can be deployed relatively cheaply. For more demanding applications, it is possible to customise the infrastructure to achieve the desired characteristics.

3.3 VLP System Overview

A VLP system consists of three major components: the transmitters, the receivers and the channel. This is shown in Fig. 3.2. The transmitters are the LED luminaires that are installed in most indoor locations and the receivers are typically PDs or cameras. The channel is the free space through which the light can take any path from the transmitter to the receiver.

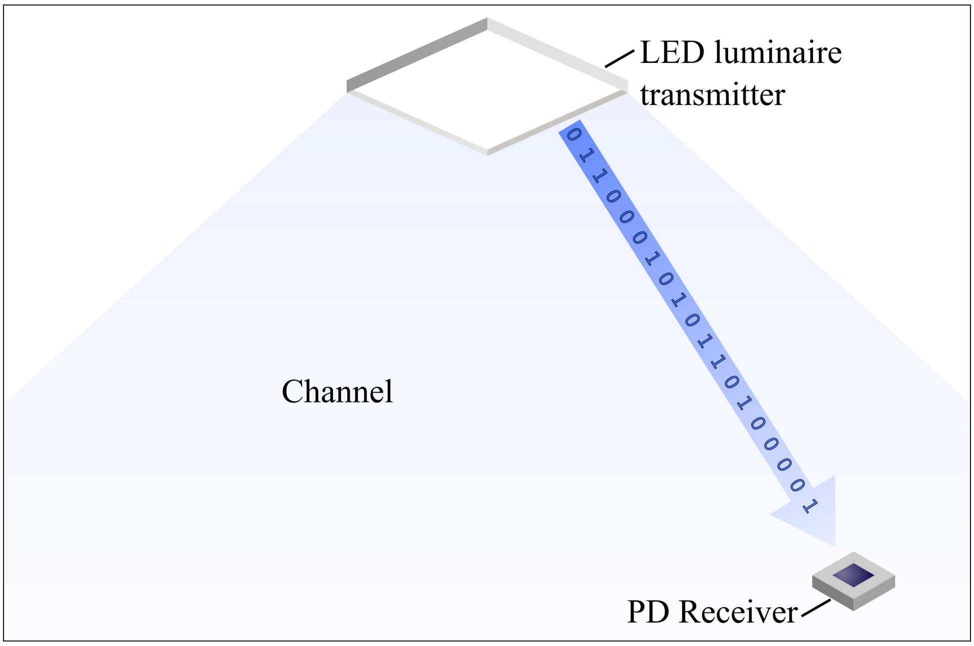

FIGURE 3.2: VLP system showing with a LED luminaire transmitter and a PD receiver

This section provides an understanding of the each of these components.

3.3.1 Transmitter

Whilst attempts have been made to use older lighting technologies, such as compact fluorescent lamps, for VLP [114]–[116], it is the emergence of solid state lighting in the form of LEDs that has driven much of the interest in VLP.

LED lighting has been increasing in popularity since first becoming commercially available 20 years ago [117]. One of the main reasons for the popularity of LEDs is their very high luminous efficacy, meaning they produce a relatively large amount of visible light for the amount of power they use. This makes them very economical to operate and more environmentally friendly than older technologies. Added to this they have longer lifespans and can be manufactured cheaply. Thus, it is unsurprising that they have become the standard choice for indoor illumination in most environments [118], [119].

However, what makes them most interesting for VLP is their ability to be modulated at high speeds [120], meaning they can be used to transmit data. This allows the luminaires to be used as beacons in a positioning system. The transmission of data using LEDs, called visible light communication (VLC), has received a great deal of research interest [121]–[125] since it was first described in the literature almost 20 years ago [126]. In VLC, data is transmitted by varying the intensity of the LED at a rate that is imperceptible to the human eye [127]. Importantly, the rate of intensity variation must be above 3 kHz due to human health concerns, such as epilepsy and migraines [128]. At the receiver, direct detection occurs where a photocurrent is generated in proportion to the received light. Whilst relatively high data rates have been reported with VLC [129], [130], they are not required for VLP as the amount of data that needs to be transmitted is typically small. Although, higher data rates will allow more rapid position updates and be useful for LBS.

In general, the transmitted data contains information that makes it possible to determine the position of the luminaire. The specific details are dependent on the receiver type (discussed in Section 3.3.2), the required accuracy and the system type.

In some systems a database is used and so it is sufficient for each LED to transmit an ID [131]–[133]. The ID is used to look up the position of the luminaire. As it is straightforward to transmit a small ID value, this type of system is useful where data rates are limited, however it does transfer complexity from the transmitter to the receiver. Also, a database lookup will add some additional latency to the system.

In other systems, the luminaires transmit their position, in either a global or local coordinate system. The advantage here is that the system is stand-alone and does not need to access any databases. This is similar to the way GNSS operates. This type of system has the potential to provide rapid, real-time position updates.

Many VLP systems that are reported in the literature do not focus on the communications aspect, however an important key requirement is multiple access [134]. The receiver must be able to receive signals from multiple luminaires as positioning algorithms typically require at least three beacons. The multiple access scheme of choice will depend on the structure of the system. If the luminaires are all connected to the same central control unit, then it is possible to use time division multiple access (TDMA). This is often used in small-scale experimental scenarios as it is simple to implement [135], [136]. However, the synchronisation requirement is a significant additional infrastructure burden in real world scenarios. An alternative is to avoid the need for a control system by using a multiple access technique where luminaires are able to operate asynchronously. This type of system will be cheaper and easier to install. Frequency division multiple access, wavelength division multiple access and orthogonal frequency division multiple access have all been discussed as potential solutions [137]–[141].

3.3.2 Receivers

In VLP, it is possible to use either PDs or cameras as receivers. The chosen receiver type will dictate many of the details of the system.

Photodiodes are the most common receiver used in VLP. PDs convert the incident light into a current using the photoelectric effect. The photocurrent output of the PD is the product of the received optical power and the responsivity. The responsivity is a function of the wavelength of the light and is an intrinsic property of the PD. PDs have a high bandwidth and thus are well suited to receiving modulated data.

Receivers may have one or more PDs, depending on the positioning technique being applied. Larger PDs have the potential to provide more accurate positioning [99] at the cost of reduced electrical bandwidth. However, given the bandwidth requirement for VLP is not large, the greater consideration is the overall size of the receiver. A more compact receiver is desirable for many applications. PDs can be used with or without optical filters and/or concentrators, depending on the requirements of the system [142].

An alternative to using a PD, is to use a digital camera. A camera is effectively a large array of very small light sensors with a focusing lens. Cameras have become very cheap and very common. Most smartphones are equipped with multiple high quality cameras and the quality is improving each year as new models enter the market and manufacturers seek ways to distinguish their devices from the competition [143]. Due to the high pixel density, it is possible to infer a large amount of information from a photograph. However, this comes at the cost of speed. Limitations in the associated circuitry mean that the frame rate of a camera is too slow to receive very high speed signals. Whilst high speed cameras exist [144], they have a relatively low resolution, high power consumption and are very expensive, which makes them less suitable as VLP receivers. So, to receive modulated data for VLP either undersampling is used [145], or more commonly, the rolling shutter mechanism is exploited [131], [146]–[149].

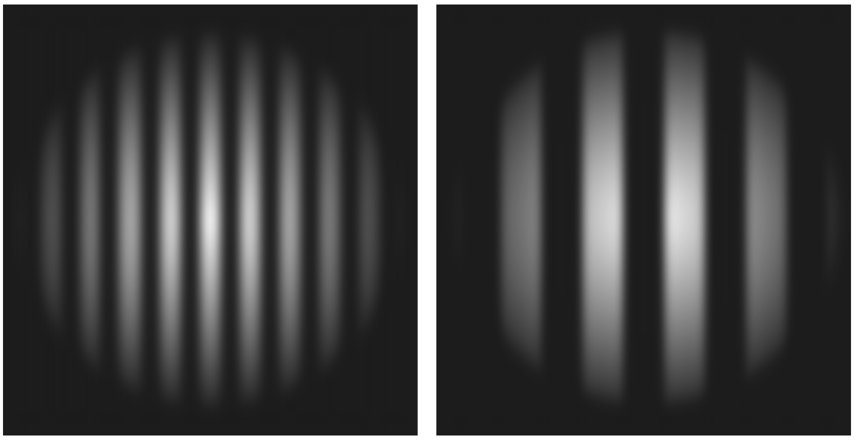

FIGURE 3.3: Examples of the rolling shutter effect for two different frequencies

The rolling shutter is common in most complementary metal-oxide-semiconductor (CMOS) cameras. Rather than capture an entire frame in an instant, each pixel line is read out in succession. For rapidly changing scenes this leads to some interesting artefacts, see Fig. 3.3, and it is these artefacts that are useful in receiving data from the luminaires. In the image, the modulated LED shows a banding pattern that relates to the frequency of the transmitted signal. The actual size of the bands will also be related to the geometry of the scene where higher ceilings will result in narrow bands. This limits the frequencies that can be used and hence the amount of data that can be encoded. Thus, rolling shutter systems tend to transmit an LED-ID and not co-ordinates. This means these systems must rely on a small database to find the corresponding co-ordinates from the LED-ID.

This work introduces a new type of receiver structure - the hybrid receiver. A hybrid receiver combines both PDs and cameras [150], [151], as shown in Fig. 3.4. This receiver structure is appealing because the individual receivers have complementary features, so by combining

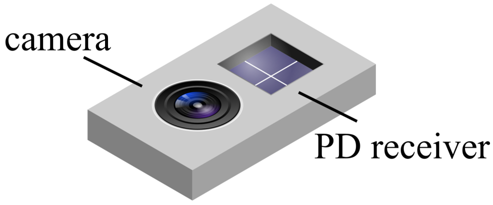

FIGURE 3.4: Hybrid receiver structure with a camera and a QADA

them together it is possible to create a very robust receiver. The PDs are used to receive the modulated data and the camera is used for accurate identification of the luminaires. If the PD receiver is an AOA detector, it is possible to match the decoded position information to the luminaires identified in the image. This receiver structure is discussed in detail in later chapters.

3.3.3 Channel

The light that travels from the transmitter to the receiver can take multiple paths, shown in Fig. 3.5. The LOS path is the direct straight-line path between the transmitter and the receiver, whilst the non line-of-sight (NLOS) path is any other path that involves the light reflecting off one, or more, surfaces. The impact of the reflected, or diffuse, light on the accuracy of the VLP system is generally small [152]. However, it will vary depending on the positioning technique that is used.

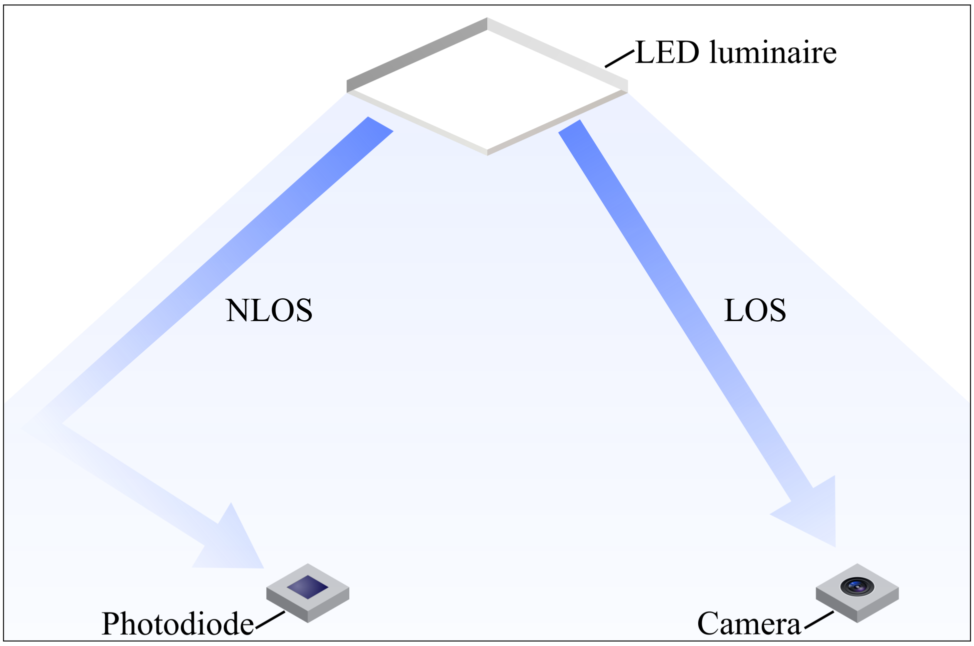

FIGURE 3.5: VLP system showing a LOS link and a NLOS link

For PD receivers, the received optical power at the PD is related to the transmitted power by the DC channel gain, h. In general, the LEDs are assumed to have a Lambertian emission pattern, thus the channel gain is given by [153]:

$$h = \begin{cases} \frac{(m+1)A}{2\pi d^2} \cos^m(\phi) T(\psi) g(\psi) \cos(\psi) & 0 \leq \psi \leq \psi_c \\ 0, & \psi > \psi_c \end{cases}, \tag{3.1}$$

where m is the Lambertian order, A is the area of the PD, d is the distance separating the transmitter and the receiver, $g(\psi)$ is the concentrator gain, $T(\psi)$ is the filter transmission, ϕ is the emission angle, ψ is the incident angle and ψ_c is the field of view (FOV).

The noise in the receiver is the combination of the shot noise, due to background light, and the thermal noise, due to the electronics [153]. Shot noise will typically be the dominant noise in the system. The variance of the shot noise is expressed as the product of the single-sided power density and the electrical bandwidth. Thus, it is expressed as:

$$\sigma_{shot}^2 = 2qRp_n A \Delta\lambda B, \tag{3.2}$$

where q is the charge of an electron, R is the responsivity of the PD, p_n is the background spectral irradiance, $\Delta\lambda$ is the optical bandwidth and B is the electrical bandwidth.

The thermal noise is related to the feedback resistance in the preamplifier. Low resistance values will increase the frequency response, but lead to higher noise levels [154], [155].

3.4 System Design

LED transmitters are commonly modelled as point sources with a Lambertian emission pattern. However, in reality, the luminaires used for indoor illumination have a finite size as they are made up of an array of LEDs. The luminaires also have diffusers that are used to spread the light uniformly. The diffusers used in LED luminaires are generally made from plastic or glass and they are designed to achieve specific illumination goals, such as low glare, high uniformity and specific beam width [156]–[158]. The impact of realistic luminaire geometry on positioing accuracy is discussed in Chapter 7.

As the most commonly used positioning techniques in VLP rely on the LOS path, the location of the luminaires is also important. In general, the luminaire locations are determined by the building standards and requirements. Fortunately, in many indoor locations it is often possible to have LOS to at least one luminaire. Whilst some work has been published on the ideal luminaire layout [159]–[161], it is important to remember that one of the advantages of VLP is the minimal need for additional infrastructure. Hence, it is preferable for a system to be able to work within the existing luminaire layout rather than making major modifications. There is a strong possibility that the geometry of the luminaire layout will not be ideal, and some geometries may be extremely challenging, e.g. corridors. A non-ideal beacon layout will have an impact on the accuracy of the system [162], however a small decrease in accuracy may be preferable to large infrastructure changes.

One limitation on the accuracy of position estimation is the accuracy of luminaire positions. The position of each luminaire is assumed to be known, reliable information that is hard-coded into the system. As VLP has the potential to provide sub decimetre positioning, any small error in this beacon information will propagate through to the position estimates. This has been discussed in several papers and suggestions have been made on how to accurately determine the luminaire positions [131], [163], [164]. It is important to note that this issue is not just limited to VLP, but it is a challenge for almost all positioning technologies that rely on beacons.

3.5 Positioning techniques in VLP

In the previous chapter the various techniques for indoor positioning were introduced. This section provides a more detailed discussion of those positioning techniques, with a focus on how they are applied in VLP.

3.5.1 Received Signal Strength

Received signal strength techniques rely on the attenuation of the light in the channel to estimate the distance the light has travelled and then use trilateration algorithms. To use this technique, accurate knowledge is required of both the channel and the transmitted optical power.

It is difficult to know the transmitted optical power accurately. It can be affected by a variety of factors like LED aging or temperature [165]. Even dust on the luminaire or the receiver will affect the accuracy of the estimates. As the light has travelled several metres to reach the receiver, and the PDs used are typically quite small, the received powers are very small. Thus, the variation caused by the factors above can lead to considerable position estimation errors.

Much research has been published on RSS, some with simulation results showing high accuracy [166]–[169]. There has also been experimental work showing high accuracy is possible, but this tends to be in highly controlled and calibrated environments [170], [171]. One notable example of RSS in a more realistic environment is the Epsilon system [172]. This work describes a VLP IPS that was deployed in an office environment using a single PD receiver. The results showed median accuracy of around 30 cm, which is acceptable for some applications. However, the authors acknowledge that the system requires active participation from the user to avoid shadows, in particular from their own body. This is a common problem for any technique, regardless of LOS requirements. However, it is particularly problematic for techniques that rely on the magnitude of the received signal, as opposed to time-based techniques or AOA which rely on other properties of the signal.

Recently, instead of utilising the RSS directly, there has been a trend towards using a hybrid approach of RSS channel modelling and fingerprinting [173]–[175].

3.5.2 Time of Arrival/Time Difference of Arrival

Time-based techniques include TOA and TDOA. TOA, sometimes called time of flight, involves measuring the time the signal takes to travel from the transmitter to the receiver. This allows the distance the signal has travelled to be calculated. However, the time measurements rely on precise synchronisation of the transmitters and the receivers, which is difficult to achieve. Thus, TDOA is more commonly utilised. This is the well-known technique that is applied in GNSS. In TDOA, only the transmitters need to be synchronised. As the signals are travelling at the speed of light, the time differences that are being measured will be very small. Thus, extremely accurate clocks are needed. In GNSS, expensive atomic clocks are used. Whilst there have been studies published using TOA, TDOA and other related techniques [96], [104], [176]–[179], they are often simulation only and assume extremely accurate clocks and precise synchronisation. Theoretically, this technique offers extremely accurate positioning, with millimetre accuracy reported [178], however it would be prohibitively expensive to equip the luminaire infrastructure with expensive clocks.

3.5.3 Fingerprinting

Fingerprinting was previously introduced in the last chapter in the context of RF systems. In VLP, many of the same principles apply [180]–[182]. An offline phase is required before the system is in use for the collection of fingerprints, which are light intensity values for VLP. Later, when using the system, the received signals are matched to the fingerprint to determine the position. One of the advantages of VLP is the potential for high accuracy. However, to achieve high accuracy using fingerprinting, a high density of fingerprints is needed. This is challenging because it would take a very long time to gather the data, the size of the database could be many gigabytes [174], and it would take a long time to search the database for a match, even with efficient algorithms. Thus, to solve this problem, there has been work published on how to introduce sparseness into the fingerprints [174].

3.5.4 Angle of Arrival

Angle of arrival, as the name suggests, involves estimating the arrival angle of the incoming light. This technique has several advantages over other techniques: it does not rely on knowledge of the transmitted power, there is no need for accurate clocks and no additional offline phase is required. However, the challenge for this technique is that receiver must be able to detect the AOA.

One way to achieve angular diversity is at the transmitter [183], [184], however the more common way is at the receiver by using multiple PDs and arranging them so that the signal received on each PD is different, allowing angular information to be inferred. This means that instead of relying on the magnitude of the received signal, it is the relative magnitudes that are important. Impairments in the channel, such as partial obstructions, will affect AOA less severely than other positioning techniques.

Many different PD arrangements have been described, such as cubes, pyramids and hemispheres [20], [21], [185]–[187]. Some of them have been experimentally verified, showing that high levels of accuracy may be possible. However, the feature they all have in common is that the overall structure of these receivers is usually very bulky. This protrusion is likely to be unacceptable in smartphones or other consumer electronics.

Another way to create diversity is to use apertures. This was first described in [188] with the angular diversity aperture (ADA) receiver. This receiver was designed for VLC [189], [190], but has been shown to also be useful for VLP [191], [192]. It is made up of multiple receiving elements (RE), each consisting of a bare PD and an aperture. By varying the relative location of the PD and the aperture, each RE effectively 'faces' in a different direction. In this thesis, a variation on the ADA receiver that is designed specifically for VLP is introduced. This receiver, called a QADA, consists of a quadrant PD and a single aperture. It is described in detail in the next chapter.

An alternative to using PDs for AOA positioning is to use a camera [41], [131], [146], [193]. Whilst cameras have certain limitations in VLP (described in Section 3.3.2), they can provide very accurate information due to their high pixel density. The most common work-around for the low frame rate is to use the rolling shutter. In [131], the Luxapose system is described. This system used a smartphone to capture images and offloaded processing to a laptop. It was able to experimentally achieve 7 cm accuracy. However, the authors have acknowledged that the system was limited by the distance between the transmitter and receiver due to camera resolution. It was also limited by the need to process the images on a separate device. It is worth noting that this work was published in 2014, and smartphones have seen large increases in both processing power and camera quality since then [194]. Thus, the limitations mentioned by the authors would have less of an impact today.

Instead of using the rolling shutter, one other possibility is to use coloured LEDs. In [195], a smartphone camera is used to capture images of coloured LED arrays. The authors describe a space-colour coding scheme where the LED arrays contain information that can be used to determine the coordinates of several LEDs in the array. These LEDs are then used as reference points for triangulation. Experimental results were presented that showed average positioning errors of 1.24 cm in three-dimensions. The authors state that the number of red, green and blue LEDs in the array should be equal, which will lead to a near white appearance. However, it is unclear if these coloured LED arrays are compatible with indoor illumination colour standards [196]. None the less, this system does demonstrate, once again, the accuracy potential for camera-based VLP systems.

The final receiver type for AOA positioning is the hybrid receiver which combines a camera-based receiver with a PD-based receiver. These receivers have both the accuracy potential of camera-based systems and high bandwidth of the PD. This novel receiver structure is the focus of later chapters in this thesis.

3.6 Summary

This chapter has provided a detailed introduction to VLP. VLP has the potential to provide robust and reliable indoor positioning in a wide variety of applications. The important requirements and features of the system have been discussed, followed by the various positioning techniques that can be used. AOA has been highlighted as a technique that has many useful characteristics.

Chapter 4

Visible Light Positioning using an Aperture and a Quadrant Photodiode

4.1 Overview

The following publication introduces a new type of aperture-based receiver structure designed for AOA VLP. A useful feature of a VLP receiver is a compact form factor so that it can be easily incorporated into devices like smartphones. This can be difficult to achieve when angular diversity is required. Many three-dimensional structures have been proposed and experimentally demonstrated to provide good angular diversity [20]–[23], [41], [136], [185]–[187]. These structures rely on the PDs facing in different directions to achieve angular diversity. However, an alternative way to achieve angular diversity is to use an aperture-based receiver [102], [188]–[190], [192]. An aperture receiver is made up of one or more REs. Each RE consists of a PD located below an aperture which exists on a parallel plane. The angular diversity arises when the horizontal offset between the aperture and the PD is different in each RE. Aperture receivers have the advantage of having a planar structure that can easily be embedded into a smartphone without causing any unacceptable protrusions.

A QADA is a type of aperture receiver that consists of a quadrant PD and a single aperture. It has a very compact structure and exhibits good angular diversity. Quadrant PDs have previously been used in laser light applications such as beam centring and atomic force microscopy. However, it is the addition of the aperture that makes it possible to use the quadrant PD for VLP. The light that arrives at the quadrant PD has passed through the aperture so that it forms a light spot that is of equal size and shape to that of the aperture. The location of the light spot on the PD depends on the location of the original light source relative to the receiver. Thus, by using the ratios of the photocurrent induced in each quadrant, the centroid of this light spot can be calculated. This value can be used in conjunction with the fixed and known height of the aperture to determine both the incident and polar angles.

Two important design parameters for a QADA are the aperture size and the aperture height. The aperture size determines the amount of light that reaches the quadrant PD. However, the size of the aperture cannot exceed the size the quadrant PD because this would result in ambiguity when determining the light spot centroid. Thus, to maximise the SNR, the aperture size is chosen to be the same size as the quadrant PD. The aperture height, which is the vertical distance separating the aperture from the quadrant PD, determines the FOV. A trade off exists between the FOV and the AOA estimation accuracy where a larger FOV will result in a decrease in accuracy.

This paper details the process by which the centroid of the light spot is derived from the quadrant photocurrents and explores the effect on incident angle estimation of varying the design parameters mentioned above. Simulation results are presented that demonstrate the potential accuracy of a QADA receiver under ideal conditions.

4.2 Publication

> S. Cincotta, A. Neild, C. He, and J. Armstrong, “Visible Light Positioning Using an Aperture and a Quadrant Photodiode,” in *2017 IEEE Globecom Workshops (GC Wkshps)*, 2017, pp. 1–6.

The following publication was published in the Proceedings of the 2017 IEEE Globecom Workshop on Optical Wireless Communications. It has been reproduced with the permission of the IEEE.

The references are [19] [197] [131] [172] [107] [198] [104] [199] [182] [102] [200] [23] [21] [188] [190] [201] [202] [203] [204] [205]

Visible Light Positioning using an Aperture and a Quadrant Photodiode

Stefanie Cincotta, Adrian Neild, Cuiwei He and Jean Armstrong
Monash University,
Melbourne, Australia
{Stefanie.Cincotta, Adrian.Neild, Cuiwei.He, Jean.Armstrong}@monash.edu

***Abstract*— This paper describes a new form of angle of arrival (AOA) detector which can be applied in an indoor visible light positioning system using LED luminaires. In this new detector, a quadrant photodiode (PD) is placed below a transparent aperture in an opaque screen. Light passing through the aperture creates an illuminated area on the quadrant PD. This light spot has the same shape and size as the aperture. The position of the light spot on the PD depends on the AOA of the light. It is shown that this position can be determined by measuring the relative optical power of the light reaching each of the four quadrants of the PD. For the case of a square aperture and a square photodetector, a simple algorithm can be used to determine the *x* and *y* coordinates of the center of the light spot on the PD. From this, the AOA can be calculated. Simulations for an indoor visible light positioning system using LED luminaires and realistic parameters show that accurate AOA estimation is possible. If different luminaires transmit different orthogonal signals, digital signal processing can be used to separately estimate the received signal powers from each of the transmitting luminaires. Thus, this new detector has the potential to provide accurate three-dimensional positioning using a single quadrant PD.**

Keywords—Indoor Positioning, Visible Light, VLP, Quadrant photodiode, Aperture, ADA receiver

I. Introduction

Visible light positioning (VLP) and visible light communications (VLC) are emerging as important new technologies that use LED luminaires to transmit signals which can be used for positioning [1] or communications [2]. The VLP systems described to date have used two broad classes of receivers; those using a general purpose camera to detect the light signals and those using separate photodiodes (PDs). While a number of innovative camera based systems have been described [3], [4], their performance is limited by a combination of the limited frame rate of the camera and the requirement for the frequency of signals transmitted by the luminaires to be above the flicker level [5]. PD based systems do not face this limitation.

In a typical VLP system, each LED luminaire transmits a signal which contains information about the position of the luminaire within a room. Based on properties of the received signals, the receiver can determine its relative distance or direction from the luminaire. Many different VLP approaches have been described in the literature, including those based on received signal strength (RSS) [6], time of arrival (TOA) [7], time difference of arrival (TDOA) [8], fingerprinting [9], angle of arrival (AOA) [10] and other techniques [11]. The different approaches have various advantages and disadvantages. RSS systems estimate the distance from the receiver to the transmitter based on the measured RSS and knowledge of the transmitted power and radiation pattern of the transmitter. As such, while conceptually simple, RSS techniques are vulnerable to changes in transmitted power caused by practical aspects such as aging of the LEDs or even an accumulation of dust on the luminaire. TOA and TDOA depend on accurate synchronization and accurate measurement of very small time intervals. Properties that are unlikely to be achieved in consumer products. The use of AOA has many advantages, as the position of the transmitters and hence the AOA of light at a given receiver position does not change over time. However, the major challenge for AOA systems using PDs is to design compact AOA receivers. For VLP to achieve widespread adoption, receivers will have to be incorporated in devices such as smart phones.

A number of papers have described receivers which show that accurate AOA positioning systems can be designed, but most of these have used PDs mounted on three dimensional structures such as pyramids [12] or cubes [13]. However, these are incompatible with incorporation in a smart phone as they have a protruding structure which would be unacceptable to consumers. If they were modified to have a recessed structure, this would limit the overall field of view (FOV). This restricted FOV would mean that for many positions the receiver would not be able to detect signals from enough transmitters to achieve accurate positioning. A solution to this problem is the angular diversity aperture (ADA) receiver [14], [15].

In this paper, we describe a new form of ADA receiver specifically designed for VLP. This receiver needs only a single receiving element due to its novel use of a quadrant PD with an aperture.

Section II provides a detailed system description, initially discussing aperture receivers, followed by quadrant PDs and finally the combination of the two into a novel receiver design. Section III describes the position detection algorithm that is used and Section IV demonstrates the performance of the receiver in the presence of noise. A discussion follows in Section V and finally the conclusion in Section VI.

II. System Description

The new AOA detector combines two key components – an aperture and a quadrant PD. The important aspects of each of these are described in this section. We have previously shown how the combination of an aperture and a PD can be used to create a directional optical receiving element and how multiple apertures and PDs can be used to design a multiple input ADA receiver. Multiple aperture ADA receivers have been shown to be very effective in both VLP applications [10] and in MIMO VLC systems [15]. In this paper, we show how a single aperture positioned above a quadrant PD can be used to create an AOA detector.

A. Aperture receivers

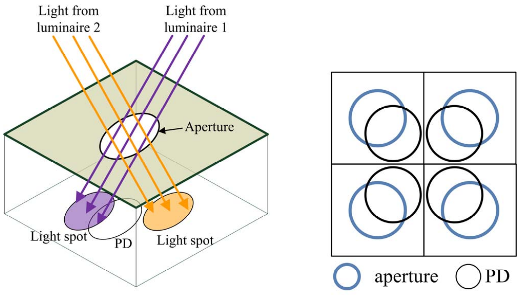

(a) (b)

Fig. 1 Structure of the optical ADA receiver, (a) a single RE, (b), Top view of the ADA receiver with four REs

Fig. 1(a) shows a single receiving element as used in a conventional aperture receiver. Each receiving element consists of a PD and a transparent aperture in an opaque screen. The directionality of a single RE is demonstrated by considering the effect of light emitted from two different luminaires[1]. Consider light from luminaire 1. (For clarity, this is shown as purple on the figure but the color of the light is not significant.). The light creates a spot which partially overlaps with the PD. The current output from the PD is proportional to the area of overlap. Light from the other ('orange') luminaire also creates a spot of light, but as this does not overlap with the PD it is not detected. Thus, the output of the PD depends on the angle of arrival of the light. Fig. 1(b) shows how four of these receiving elements can be combined to create a multiple input receiver. In Fig. 1, round apertures and PDs are depicted, however, different shapes can be used. In this paper, we show that, for AOA estimation, it is advantageous to use a square aperture and square PD.

B. Quadrant photodiodes

Quadrant, or segmented, PDs consist of four active areas separated by a very narrow gap. These detectors are normally used in conjunction with a laser beam. As can be seen from Fig. 2, the PD is aligned so that the laser spot falls on the intersection between the quadrants. By detection of the relative photocurrents produced by each segment, any deflection in the laser beam can be accurately measured.

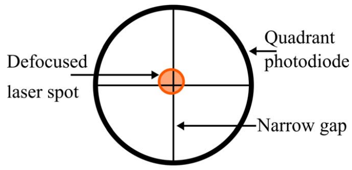

Fig. 2 Quadrant PD with small laser light spot overlapping all quadrants

Such an arrangement is widely used in atomic force microscopy [16]. Another example of widespread usage is in optical trapping [17], [18]. The common features of these systems are the use of the quadrant PD to track the movement of a beam of laser light, the size of the light spot cast is considerably smaller than the outer diameter of the receiver, and the spot shape is usually circular. Additionally, unlike our new detector design, none of these past applications use an aperture.

C. Receiver design

The receiver, shown in Fig. 3, consists of a quadrant PD located on a plane directly below an aperture that has been created in an opaque screen. The aperture plane is separated from the quadrant PD plane by a vertical distance, h. In contrast to an aperture receiver that uses conventional PDs, there is no additional benefit to a lateral offset between the aperture and the quadrant PD. Light, emitted from the LED luminaires, passes through the aperture and casts a light spot on the quadrant PD. Given knowledge of the aperture height, h, and the displacement of the light spot from the center of the quadrant PD, the AOA of the incident light can be determined.

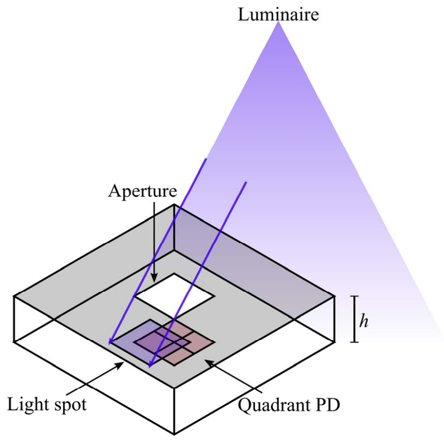

Fig. 3 Aperture receiver using a square quadrant photodiode

[1] The technical term for a light fitting is a 'luminaire'. We use this in preference to the terms 'light' or 'LED' because of the multiple meanings of 'light' and the fact that a single luminaire can be made of one or multiple LEDs

In contrast to typical quadrant PD applications, here, there is a freedom to optimize the light spot shape. The light source, primarily for room lighting, is omnidirectional. In order to cast a light spot on the quadrant photodiode, an aperture is used, the design of which can be chosen to create the desired spot shape and size. In general, for a quadrant PD, the light spot need only be larger than the gap separating the quadrants for position information to be available. However, in this receiver design, it is optimal to match the light spot to the size of the quadrant PD. A smaller aperture reduces signal strength and restricts the FOV because the light spot overlaps all four quadrants of the PD for a smaller range of arrival angles. A larger aperture leads to ambiguous results as multiple arrival angles can yield identical outputs.

In addition, by combining a square shaped aperture with a square quadrant PD, the overlap area in each quadrant changes linearly with the movement of the light spot across the PD [19]. This simplifies the algorithm required to determine incident angle from the measured photocurrents.

III. Position Detection Algorithm

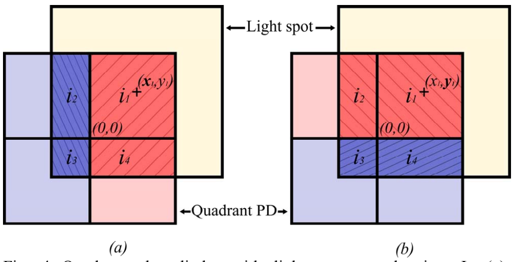

Fig. 4 Quadrant photodiodes with light spots overlapping. In (a), displacement in x is indicated by the ratio of the top and bottom quadrant pairs. In (b), displacement in y indicated by the ratio of the left and right quadrant pairs

In this section, we discuss the algorithm used to detect the position of the light spot center. In general, if the receiver is in motion, the position of the light spot will be time varying. Let $[x_1(t), y_1(t)]$ be the position at time, t. The algorithm is introduced by analyzing $x_1(t)$, and this is later extended to include both $x_1(t)$ and $y_1(t)$. The light spot center can be determined using a ratio between the photocurrents in adjacent pairs of quadrants. The photocurrent generated in each quadrant depends on the received optical power, which in turn, depends on the area of the overlap. In Fig. 4(a), $x_1(t)$ is determined by the ratio, $p_x(t)$, between the currents in the left and right quadrant pairs. This is expressed in (1), where $i_j(t)$ and $N_j(t)$ are the photocurrent and noise at time, t, received by the j^{th} quadrant of the PD, after filtering. Similarly, in Fig. 4(b), $y_1(t)$ is determined by the ratio, $p_y(t)$, between currents in the top and bottom quadrant pairs, as expressed in (2).

$$p_x(t) = \frac{i_1(t)+i_4(t)+N_1(t)+N_4(t)}{i_2(t)+i_3(t)+N_2(t)+N_3(t)} \tag{1}$$

$$p_y(t) = \frac{i_1(t)+i_2(t)+N_1(t)+N_2(t)}{i_3(t)+i_4(t)+N_3(t)+N_4(t)} \tag{2}$$

We first consider the algorithm in the absence of noise. The functions (1) and (2) reduce to a ratio of quadrant area overlaps, shown in (3), and an estimator for $x_1(t)$, or $y_1(t)$, can be derived.

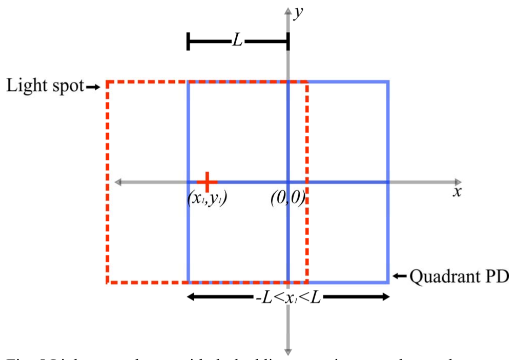

Fig. 5 Light spot, shown with dashed lines, passing over the quadrant

Initially, we will restrict the analysis to the case where the light spot passes horizontally over the quadrant PD from left to right when $y_1(t)=0$, as shown in Fig. 5. The ratio of the overlap areas can be simplified to

$$\begin{aligned} p_x(t) = \frac{A_1(t)+A_4(t)}{A_2(t)+A_3(t)} &= \begin{cases} \dfrac{2L^2+2Lx_1(t)}{2L^2}, & -L < x_1(t) \le 0 \\ \dfrac{2L^2}{2L^2-2Lx_1(t)}, & 0 < x_1(t) < L \end{cases} \\ &= \begin{cases} \dfrac{L+x_1(t)}{L}, & -L < x_1(t) \le 0 \\ \dfrac{L}{L-x_1(t)}, & 0 < x_1(t) < L \end{cases} \end{aligned} \tag{3}$$

where $A_j(t)$ is the overlap area of the j^{th} quadrant, L is the length of a single PD quadrant and $x_1(t)$ is the x co-ordinate of the light spot center. Only values of $x_1(t)$ that result in the light spot overlapping all four quadrants are considered. For a typical case where aperture height is equal to PD length, this leads to a FOV ranging from -45° to 45°. Due to symmetry, this function is unaffected by the value of $y_1(t)$. However, the photocurrents are not independent of $y_1(t)$ as they are proportional to the overlap area. Thus, from (1), it can be seen that the signal to noise ratio (SNR) will be reduced when $y_1(t)$ is not equal to zero.

Rearranging (3) gives

$$x_1(t)=\begin{cases} L\left(p_x(t)-1\right), & -L<x_1(t)\le 0 \\ L-\dfrac{L}{p_x(t)}, & 0<x_1(t)<L \end{cases} \tag{4}$$

In (4) we derive an estimate for $x_1(t)$ from the ratio of received powers. We consider the case where low pass filtering in the electrical domain limits the bandwidth of the received signal to bandwidth B hertz. The filtered signal is then sampled at the Nyquist rate, $2B$. The estimate, at time $t=(k+M)/2B$, is then based on the average of a sequence of M samples as shown in (5). As we will show later, the statistical properties of the estimator depend on the length of this window and on the bandwidths of the optical and electrical filters at the input to the receiver.

$$\hat{x}_1\left[\frac{k+m}{2B}\right]=\begin{cases} \dfrac{1}{M}\displaystyle\sum_{n=k}^{k+M-1} L\left(p_x\left[\frac{n}{2B}\right]-1\right), & -L<x_1\left(\dfrac{k+m}{2B}\right)\le 0 \\ \dfrac{1}{M}\displaystyle\sum_{n=k}^{k+M-1} L-\dfrac{L}{p_x\left[\dfrac{n}{2B}\right]}, & 0<x_1\left(\dfrac{k+m}{2B}\right)<L \end{cases} \tag{5}$$

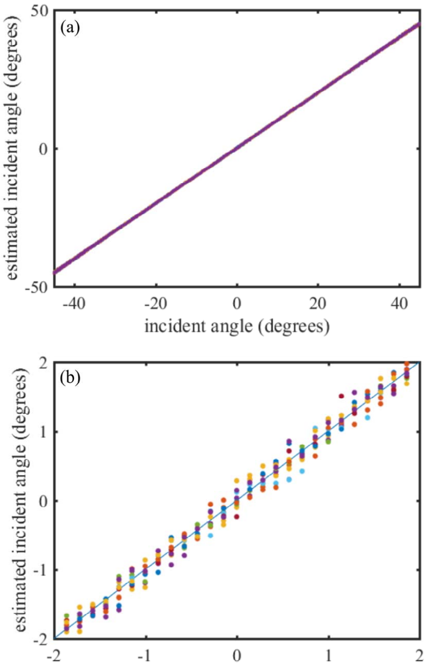

Fig. 6 (a) estimated incident angle from multiple simulations of single Nyquist samples and (b) magnification between -2 and 2 degrees

The symmetry of the receiver means that the same analysis can be applied to generate the function for $p_y(t)$ and, subsequently, $\hat{y}_1(t)$. The estimate for $[x_1(t), y_1(t)]$ can then be used, coupled with knowledge of the aperture height, to determine the incident and polar angles.

Fig. 6(a) shows an example of the estimated angle of arrival versus the actual angle for the parameters discussed in the next section. It shows that even in the presence of high levels of noise the estimated angles are in close agreement with the true incident angle for the entire FOV. Closer inspection, in Fig. 6(b), further highlights the accuracy of the estimated angle. Each spot represents the estimation from a single Nyquist rate sample, thus if multiple samples were captured, there would be an improvement in the performance. The effect of noise is discussed further in the following section.

IV. Analysis and Simulations in the Presence of Noise

In this section, we will consider the effect of noise on the algorithm and present simulation results. The noise and photocurrents are calculated using properties and dimensions of both the transmitting luminaire and quadrant PDs, combined with the position of the receiver.

The photocurrent generated by a PD can be expressed as

$$\begin{aligned} i_i(t) &= RP_R \\ &= RP_T h_c(t) \end{aligned} \tag{6}$$

where R is the responsivity of the PD, P_T and P_R are the powers transmitted and received respectively and $h_c(t)$ is the DC channel gain. For simplicity, we consider the typical VLP case where the incidence and emergence angles are equal and the Lambertian order of the LED is 1. Changes to these values will change the absolute received powers, however will not change the ratio. The DC channel gain is then given by

$$h_c(t)=\frac{A_i(t)}{\pi d^2}\cos^2\left(\psi(t)\right) \tag{7}$$

The distance from the LED transmitter to the receiver is $d=(H+h)/\cos(\psi(t))$, $\psi(t)=\arctan\left(\sqrt{x_1(t)^2+y_1(t)^2}/h\right)$ is the incident angle, h is the vertical height from the PD to the aperture and H is the vertical height from the receiver to the transmitter.

We consider only the dominant noise source, which is the shot noise induced by background illumination. This is modelled as white Gaussian noise with single sided power density given by

$$N_0 = 2qRp_n A\Delta\lambda \tag{8}$$

where q is the charge of an electron, R is the responsivity of the PD, p_n is the spectral irradiance, A is the area of one PD quadrant, $\Delta\lambda$ is the bandwidth of the optical filter. The variance is then given by

$$\sigma_n^2 = N_0 B \tag{9}$$

where B is the bandwidth of the electrical filter. Unlike the received optical power signal, the noise is added in the electrical domain and is thus bipolar. This variance will be an over estimate as the receiver is directional and the opaque screen will block some of the ambient light. Simulation parameters can be seen in Table 1.

TABLE 1 SIMULATION PARAMETERS

Parameter	Value
Power transmitted (P_T)	3 W
Responsivity (R)	0.65 A/W
Optical filter bandwidth $(\Delta\lambda)$	300 nm
Electrical filter bandwidth (B)	1 MHz
Spectral irradiance (p_n)	6.2 x 10^{-6} W/(nm.cm^2)

In the presence of noise, the function previously described in (3) now becomes

$$p_x(t) = \begin{cases} \dfrac{2k_1\cos^4(\psi(t))L^2 + 2k_1\cos^4(\psi(t))Lx_1(t) + N_1(t) + N_4(t)}{2k_1\cos^4(\psi(t))L^2 + N_2(t) + N_3(t)} \\ \quad = \dfrac{L + x_1(t) + E_1(t)}{L + E_2(t)}, \quad -L < x_1(t) \le 0 \\ \dfrac{2k_1\cos^4(\psi(t))L^2 + N_1(t) + N_4(t)}{2k_1\cos^4(\psi(t))L^2 - 2k_1\cos^4(\psi(t))Lx_1(t) + N_2(t) + N_3(t)} \\ \quad = \dfrac{L + E_1(t)}{L - x_1(t) + E_2(t)}, \quad 0 < x_1(t) < L \end{cases} \tag{10}$$

$E_1(t)$ and $E_2(t)$ have a normal distribution with zero mean and variance $\sigma_e(t)^2$ given by

$$\begin{aligned}\sigma_e(t)^2 &= \left(\frac{1}{2k_1\cos^4(\psi(t))L}\right)^2 \times 2\sigma_n^2 \\ &= \frac{\pi^2 (H+h)^4 q p_n \Delta\lambda B}{R P_T^2 \cos^8\left(\arctan\left(\sqrt{x_1(t)^2 + y_1(t)^2} \big/ h\right)\right)}\end{aligned} \tag{11}$$

The magnitude of the variance is dependent on multiple variables. It is directly proportional to the optical and electrical bandwidths and inversely proportional the square of the transmitted power. The $\cos^8(\psi(t))$ term is related to the geometry of the receiver and, depending on the ratio of the PD length to the aperture height, has substantial effects on the root mean square error curve. Fig. 7 shows the root mean square error of the estimate for the case where only a single sample is used, i.e. $M = 1$. For the worst case, where $h = 0.5L$, the root mean square error in the angle is less than 1 degree and much smaller for the majority of the incident angles. As the aperture height increases, the root mean square error decreases dramatically, however the receiver FOV also decreases and the receiver becomes more bulky. In photography, a similar phenomenon called natural vignetting is seen where the illumination is dependent of the fourth power of the cosine of the incident angle and the geometry of the system. [20].

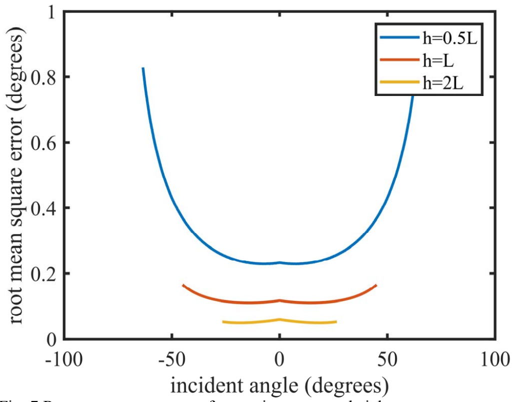

Fig. 7 Root mean square error for varying aperture height

In Fig. 8, we keep the PD length equal to the aperture height, $h = L$, so that we can see the effect of increasing the PD area. Although the variance in (11) is not directly dependent on the area of the PD, as the PD becomes larger, the error in the detection of the light spot center, $[x_1(t), y_1(t)]$, will remain constant and thus an increased PD size will result in increased accuracy. This can be seen in Fig. 8 where the root mean square error in arrival angle detection is shown for increasing PD length, and thus area. Significant improvements can be gained by increasing the PD area, however it will also increase the overall size of the receiver. Typical off the shelf quadrant PDs can have an area of up to 100mm^2, thus it is practical to choose a quadrant PD around this size.

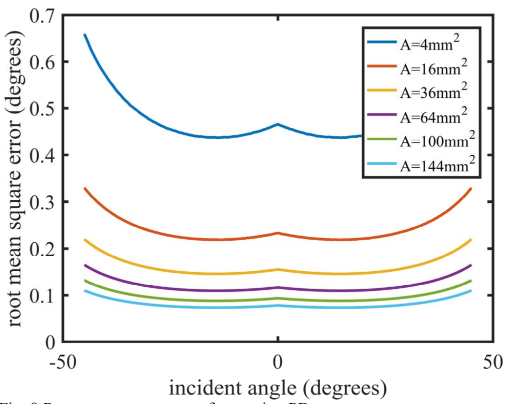

Fig. 8 Root mean square error for varying PD area

V. DISCUSSION

The results show that the new AOA detector can provide accurate angle of arrival estimation. The simulation results which have been presented are for the case of one transmitter, and to simplify the description of the new technique are based on the dc component of the optical power received from that transmitter. In practice it would be better to use a modulated signal as this would allow any dc component due to background light to be eliminated. In the case of a modulated signal the estimate should be based on the output of a matched filter, which is matched to the known transmitted signal. In this case the accuracy of the estimate depends on the SNR at the output of the matched filter. The technique can readily be extended to calculating the AOA for signals from multiple transmitters. To do this the transmitters should transmit orthogonal signals. As long as orthogonal signals are used, single quadrature detector can be used to simultaneously estimate multiple AOAs, by using multiple matched filters each matched to one of the orthogonal signals,

The simulations show that very accurate estimates can be made based on a single sample. However if necessary the robustness in the presence of noise can be improved by using an average of the samples rather than a single sample for the estimate. As the position of the receiver in a typical indoor application will not change rapidly, estimates can be based on multiple samples taken over a relatively long time (e.g. ms).

In practice the accuracy of position estimation may be limited by other factors, such as the size and shape of luminaires, slight imbalances in the properties of the four quadrants of the PD, and if the aperture or PD is not perfectly square or it the aperture and PD are not perfectly aligned. These effects will be the subject of future research.

VI. Conclusion

This paper has presented a novel detector for visible light positioning. The new receiver combines an aperture with a quadrant PD. It is shown that the position of the spot of light on the quadrant PD caused by light passing through the aperture gives information about the position of the receiver relative to the transmitter. A new angle of arrival estimation algorithm is presented which uses the relative received power in each quadrant to estimate the direction of the received light. Analytical and simulation results are presented which show that for a square aperture and a square photodiode the x and y coordinates of the receiver can be separately estimated. The properties of the new estimator in the presence of noise are analyzed. It is shown that the variance of the estimates is smallest when the transmitting luminaire is directly above the receiver and increases as the offset between transmitter and receiver increases. This is because of the reduced received optical power as the angle of incidence of light on the quadrant photodiode increases. It is shown that the variance of the estimator depends on the bandwidths of the optical and electrical filters at the receiver front end, and on the time integration window used. Long integration time windows are possible in typical VLP positioning applications as receivers are typically stationary or moving very slowly. The new receiver can be used to simultaneously detect position relative to a number of transmitters as long as the transmitters transmit known orthogonal signals. No extra apertures or photodetectors are required. In this case the position of the receiver can be calculated using triangulation or trilateration.

Acknowledgment

This work was supported by the Australian Research Council's (ARC) Discovery funding scheme (DP150100003)

References

[1] J. Armstrong, Y. A. Sekercioglu, and A. Neild, 'Visible light positioning: a roadmap for international standardization', *IEEE Commun. Mag.*, vol. 51, no. 12, pp. 68–73, Dec. 2013.

[2] T. Komine and M. Nakagawa, 'Fundamental analysis for visible-light communication system using LED lights', *IEEE Trans. Consum. Electron.*, vol. 50, no. 1, pp. 100–107, Feb. 2004.

[3] Y.-S. Kuo, P. Pannuto, K.-J. Hsiao, and P. Dutta, 'Luxapose: indoor positioning with mobile phones and visible light', in *Proc. of the Annual International Conference on Mobile Computing and Networking,* Maui, United States, 2014, pp. 447–458.

[4] L. Li, P. Hu, C. Peng, G. Shen, and F. Zhao, 'Epsilon: A Visible Light Based Positioning System', in *Proceedings of the 11th USENIX Symposium on Networked Systems Design and Implementation*, Berkeley, Calif, 2014, pp. 331–343.

[5] T.-H. Do and M. Yoo, 'An in-Depth Survey of Visible Light Communication Based Positioning Systems', *Sensors*, vol. 16, no. 5, May 2016.

[6] W. Gu, W. Zhang, M. Kavehrad, and L. Feng, 'Three-dimensional light positioning algorithm with filtering techniques for indoor environments', *Opt. Eng.*, vol. 53, no. 10, pp. 107107–107107, 2014.

[7] T. Q. Wang, Y. A. Sekercioglu, A. Neild, and J. Armstrong, 'Position Accuracy of Time-of-Arrival Based Ranging Using Visible Light With Application in Indoor Localization Systems', *J. Light. Technol.*, vol. 31, no. 20, pp. 3302–3308, Oct. 2013.

[8] K. Panta and J. Armstrong, 'Indoor localisation using white LEDs', *Electron. Lett.*, vol. 48, no. 4, pp. 228–230, Feb. 2012.

[9] A. M. Vegni and M. Biagi, 'An indoor localization algorithm in a small-cell LED-based lighting system', in *2012 International Conf. on Indoor Positioning and Indoor Navigation (IPIN)*, 2012, pp. 1–7.

[10] H. Steendam, T. Q. Wang, and J. Armstrong, 'Theoretical Lower Bound for Indoor Visible Light Positioning Using Received Signal Strength Measurements and an Aperture-Based Receiver', *J. Light. Technol.*, vol. PP, no. 99, pp. 1–1, 2016.

[11] G. del Campo-Jimenez, J. M. Perandones, and F. J. Lopez-Hernandez, 'A VLC-based beacon location system for mobile applications', in *2013 International Conference on Localization and GNSS (ICL-GNSS)*, 2013, pp. 1–4.

[12] S. H. Yang, H. S. Kim, Y. H. Son, and S. K. Han, 'Three-Dimensional Visible Light Indoor Localization Using AOA and RSS With Multiple Optical Receivers', *J. Light. Technol.*, vol. 32, no. 14, pp. 2480–2485, Jul. 2014.

[13] L. Wei, H. Zhang, B. Yu, J. Song, and Y. Guan, 'Cubic-Receiver-Based Indoor Optical Wireless Location System', *IEEE Photonics J.*, vol. 8, no. 1, pp. 1–7, Feb. 2016.

[14] T. Q. Wang, C. He, and J. Armstrong, 'Angular diversity for indoor MIMO optical wireless communications', in *2015 IEEE Int. Conf. on Communications (ICC)*, 2015, pp. 5066–5071.

[15] T. Q. Wang, C. He, and J. Armstrong, 'Performance Analysis of Aperture-Based Receivers for MIMO IM/DD Visible Light Communications', *J. Light. Technol.*, vol. PP, no. 99, pp. 1–1, 2016.

[16] S. Alexander et al., 'An atomic-resolution atomic-force microscope implemented using an optical lever', *J. Appl. Phys.*, vol. 65, no. 1, pp. 164–167, Jan. 1989.

[17] S. Keen, J. Leach, G. Gibson, and M. J. Padgett, 'Comparison of a high-speed camera and a quadrant detector for measuring displacements in optical tweezers', *J. Opt. Pure Appl. Opt.*, vol. 9, no. 8, p. S264, 2007.

[18] S. Lakämper, A. Lamprecht, I. A. T. Schaap, and J. Dual, 'Direct 2D measurement of time-averaged forces and pressure amplitudes in acoustophoretic devices using optical trapping', *Lab. Chip*, vol. 15, no. 1, pp. 290–300, Dec. 2014.

[19] 'Quadrant and Bi-Cell Silicon Photodiode Amplifier Module'. OSI Optoelectronics.

[20] Ray, Sidney F., *Applied Photographic Optics,* 2nd edition. Oxford: Focal Press, 1994

Chapter 5

High angular resolution visible light positioning using a quadrant photodiode angular diversity aperture receiver (QADA)

5.1 Overview

In the previous chapter, the QADA receiver was introduced. It was shown, using simulation, that QADA has the potential to provide high quality incident angle estimation, thus making it well suited for VLP. The results also demonstrated the trade-offs when designing the receiver, highlighting the effect of the aperture height and the quadrant PD size. In the discussion, some of the factors that could affect the accuracy of the QADA were raised. To explore these factors further, it is useful to verify the receiver performance experimentally.

In the following work, the QADA receiver is analysed with both simulation and experimental verification. The experiment was performed on an optical bench with a single white LED transmitter and a prototype QADA receiver. Due to resource constraints, the QADA receiver was constructed from a 10 mm diameter circular quadrant PD that was located behind a 4 mm square aperture created in opaque adhesive vinyl. The aperture was held in place using a custom 3D printed mount. Due to use of the circular quadrant PD, the algorithms described in this work were adapted from the previously described algorithms. The experiment focused on incident angle detection only, thus only two axes of movement were used.

As the transmitter was only a single LED, rather than a luminaire containing a large array of LEDs, the transmitted power was relatively low. Thus, the results are presented for separation distances ranging from 100 mm to 300 mm. These results showed a close correlation between experimental data and simulated data with all absolute errors less than 0.5°and root mean square error (rMSE) less than 0.11°.

5.2 Publication

> S. Cincotta, C. He, A. Neild, and J. Armstrong, "High angular resolution visible light positioning using a quadrant photodiode angular diversity aperture receiver (QADA)," *Opt. Express*, OE, vol. 26, no. 7, pp. 9230–9242, Apr. 2018.

The following publication was published in the Optical Society of America's (OSA) Journal Optics Express. It has been reproduced with the permission of the OSA.

The references are [19] [206] [140] [17] [142] [102] [207] [104] [176] [182] [23] [208] [21] [131] [209] [210] [190] [211] [101] [212] [213] [192] [214] [215] [153] [216] [20]

Research Article Vol. 26, No. 7 | 2 Apr 2018 | OPTICS EXPRESS 9230
Optics EXPRESS

High angular resolution visible light positioning using a quadrant photodiode angular diversity aperture receiver (QADA)

STEFANIE CINCOTTA,[1,*] CUIWEI HE,[1] ADRIAN NEILD,[2] AND JEAN ARMSTRONG[1]

[1]*Department of Electrical and Computer Systems Engineering, Monash University, Clayton, Australia*
[2]*Department of Mechanical and Aerospace Engineering, Monash University, Clayton, Australia*
[*]*Stefanie.Cincotta@monash.edu*

Abstract: The increasing use of white LEDs for indoor illumination provides a significant opportunity for Visible Light Positioning (VLP). The challenge is to design a small, unobtrusive sensor that can be incorporated into mobile devices to provide accurate measurements for triangulation. We present experimental results for a novel angle of arrival (AOA) detector that has been designed for use in a VLP system. The detector is composed of a transparent aperture in an opaque screen that is located above a quadrant photodiode (PD), separated by a known vertical distance. Light passing through the aperture from an LED casts a light spot onto the quadrant PD. The position of this spot, coupled with knowledge of the height of the aperture above the quadrant PD, provides sufficient information to determine both the incident and polar angles of the light. Experiments, using a prototype detector, show that detector is capable of accurate estimation of AOA. The root mean square errors (rMSE) were less than 0.11° for all the measured positions on the test bed, with 90% of positions having an rMSE of less than 0.07°.

OCIS codes: (060.4510) Optical communications; (230.5160) Photodetectors; (050.1220) Apertures.

References and links

1. J. Armstrong, Y. A. Sekercioglu, and A. Neild, "Visible light positioning: a roadmap for international standardization," IEEE Commun. Mag. **51**(12), 68–73 (2013).
2. S.-Y. Jung, D.-H. Kwon, S.-H. Yang, and S.-K. Han, "Inter-cell interference mitigation in multi-cellular visible light communications," Opt. Express **24**(8), 8512–8526 (2016).
3. Y. Xu, Z. Wang, P. Liu, J. Chen, S. Han, C. Yu, and J. Yu, "Accuracy analysis and improvement of visible light positioning based on VLC system using orthogonal frequency division multiple access," Opt. Express **25**(26), 32618–32630 (2017).
4. J. Luo, L. Fan, and H. Li, "Indoor positioning systems based on visible light communication: state of the art," IEEE Comm. Surv. and Tutor. **19**(4), 2871–2893 (2017).
5. N. Wu, L. Feng, and A. Yang, "Localization accuracy improvement of a visible light positioning system based on the linear illumination of LED sources," IEEE Photonics J. **9**(5), 7905611 (2017).
6. H. Steendam, T. Q. Wang, and J. Armstrong, "Theoretical lower bound for indoor visible light positioning using received signal strength measurements and an aperture-based receiver," J. Lightwave Technol. **35**(2), 309–319 (2017).
7. H. Zheng, Z. Xu, C. Yu, and M. Gurusamy, "A 3-D high accuracy positioning system based on visible light communication with novel positioning algorithm," Opt. Commun. **396**, 160–168 (2017).
8. T. Q. Wang, Y. A. Sekercioglu, A. Neild, and J. Armstrong, "Position accuracy of time-of-arrival based ranging using visible light with application in indoor localization systems," J. Lightwave Technol. **31**(20), 3302–3308 (2013).
9. T.-H. Do, J. Hwang, and M. Yoo, "TDoA-based indoor positioning using visible light," Photonic Netw. Commun. **27**(2), 80–88 (2014).
10. A. M. Vegni and M. Biagi, "An indoor localization algorithm in a small-cell LED-based lighting system," in *2012 International Conference on Indoor Positioning and Indoor Navigation (IPIN)* (2012) pp. 1–7.
11. S. H. Yang, H. S. Kim, Y. H. Son, and S. K. Han, "Three-dimensional visible light indoor localization using AOA and RSS with multiple optical receivers," J. Lightwave Technol. **32**(14), 2480–2485 (2014).
12. A. Arafa, S. Dalmiya, R. Klukas, and J. F. Holzman, "Angle-of-arrival reception for optical wireless location technology," Opt. Express **23**(6), 7755–7766 (2015).

#320666 https://doi.org/10.1364/OE.26.009230
Journal © 2018 Received 25 Jan 2018; revised 8 Mar 2018; accepted 8 Mar 2018; published 29 Mar 2018

Research Article Vol. 26, No. 7 | 2 Apr 2018 | OPTICS EXPRESS 9231
Optics EXPRESS

13. L. Wei, H. Zhang, B. Yu, J. Song, and Y. Guan, "Cubic-receiver-based indoor optical wireless location system," IEEE Photonics J. **8**(1), 7390202 (2016).
14. Y.-S. Kuo, P. Pannuto, K.-J. Hsiao, and P. Dutta, "Luxapose: indoor positioning with mobile phones and visible light," in *Proceedings of the Annual International Conference on Mobile Computing and Networking (MOBICOM)*, (2014), pp. 447–458.
15. M. H. Bergen, X. Jin, D. Guerrero, H. A. L. F. Chaves, N. V. Fredeen, and J. F. Holzman, "Design and implementation of an optical receiver for angle-of-arrival-based positioning," J. Lightwave Technol. **35**(18), 3877–3885 (2017).
16. P. Huynh and M. Yoo, "VLC-based positioning system for an indoor environment using an image sensor and an accelerometer sensor," Sensors (Basel) **16**(6), 783 (2016).
17. T. Q. Wang, C. He, and J. Armstrong, "Performance analysis of aperture-based receivers for MIMO IM/DD visible light communications," J. Lightwave Technol. **35**(9), 1513–1523 (2017).
18. H. Steendam, T. Q. Wang, and J. Armstrong, "Cramer-Rao bound for indoor visible light positioning using an aperture-based angular-diversity receiver," in *2016 IEEE International Conference on Communications (ICC)*, (2016), pp. 1–6.
19. H. Steendam, T. Q. Wang, and J. Armstrong, "Cramer-Rao bound for AOA-based VLP with an aperture-based receiver," in *2017 IEEE International Conference on Communications (ICC)*, (2017), pp. 1–6.
20. I. Gőzse, "Optical indoor positioning system based on TFT technology," Sensors (Basel) **16**(1), 19 (2015).
21. S. Cincotta, A. Neild, C. He, and J. Armstrong, "Visible light positioning using an aperture and a quadrant photodiode," in *2017 IEEE Globecom Workshops* (2017), pp. 1–6.
22. H. Steendam, "A 3D positioning algorithm for AOA-based VLP with an aperture-based receiver," IEEE J. Sel. Areas Comm. **36**(1), 23–33 (2017).
23. J. Huisstede, K. van der Werf, M. Bennink, and V. Subramaniam, "Force detection in optical tweezers using backscattered light," Opt. Express **13**(4), 1113–1123 (2005).
24. A. M. Nugrowati, W. G. Stam, and J. P. Woerdman, "Position measurement of non-integer OAM beams with structurally invariant propagation," Opt. Express **20**(25), 27429–27441 (2012).
25. J. M. Kahn and J. R. Barry, "Wireless infrared communications," Proc. IEEE **85**(2), 265–298 (1997).
26. A. Haapalinna, P. Kärhä, and E. Ikonen, "Spectral reflectance of silicon photodiodes," Appl. Opt. **37**(4), 729–732 (1998).
27. A. Arafa, X. Jin, and R. Klukas, "Wireless indoor optical positioning with a differential photosensor," IEEE Photonics Technol. Lett. **24**(12), 1027–1029 (2012).

1. Introduction

Demand is increasing for a reliable and economical indoor positioning system [1]. Visible light positioning (VLP), using the new receiver we describe in this paper, has the potential to meet this demand. Recent research has shown that VLP using lighting LEDs can provide extremely accurate indoor positioning information and the increasing uptake of energy efficient LED lighting means that VLP has the potential to become a ubiquitous technology [2,3]. VLP is based on visible light communication (VLC). In VLC, the light transmitted by the LEDs in luminaires is modulated and used to transmit data. In the case of visible light positioning (VLP), the luminaires transmit information about their position and so act as beacons in a positioning system. Receivers, using photodiodes (PDs) or image sensors, can detect these signals and use them to determine the position of the receiver.

Many different approaches to VLP have been described in the literature [4]. These include techniques based on received signal strength, time of arrival, time difference of arrival, fingerprinting, and angle of arrival (AOA). A number of theoretical and experimental papers have shown that in particular circumstances each of these methods can provide accurate positioning, but each has significant disadvantages.

Received signal strength [5–7] is a popular and relatively straightforward method in which the power of the received signal is used to estimate the distance between the transmitter and the receiver. The main limitation of received signal strength is that it relies on accurate knowledge of the radiation pattern of the transmitter, the channel, and the transmitted power. In practice these may be difficult to ascertain and may change over time. Time of arrival [8] and time difference of arrival [9], depend on measuring the times of arrival of signals from different transmitters. Time difference of arrival is very successfully employed in GPS, but an accurate atomic clock is required in each GPS transmitter and all the clocks must be precisely synchronized in order to measure the time differences. This is unsuitable for VLP due to the additional expensive infrastructure and the difficulty in

Research Article Vol. 26, No. 7 | 2 Apr 2018 | OPTICS EXPRESS 9232
Optics EXPRESS

measuring extremely small time differences. The disadvantage of fingerprinting methods is that, before any positioning can take place, measurements must be made and stored for known positions throughout the scenario [10].

AOA systems depend on measuring the angle of arrival of signals from a number of different transmitters and using this information for triangulation-based positioning. Appealingly, the transmitters need not be synchronized or of known power. The challenge for AOA systems is the design of suitable angular diversity receivers. A number of different receivers have achieved this, either using PDs [11–13] or cameras [14–16]. Many of those using PDs have three dimensional structures with the PDs facing in different directions. In [11], tilted PDs in a pyramidal type structure are used, while in [12] a cubic receiver is described. The practical disadvantage of these structures is that they cannot be easily incorporated into smart devices such as modern mobile phones. If VLP is to be extensively used, receivers must be developed that are both compact and planar. The angular diversity aperture (ADA) receiver [17], whilst designed for VLC, does meet these requirements and theoretical and simulation results have shown that accurate positioning is possible [6, 18, 19]. The original ADA receiver used multiple receiving elements each consisting of an aperture and a photodiode. Most work so far on their use in VLP is theoretical and assumes that the size and position of each receiving element is accurately known and that the photodiodes have precisely matched characteristics. A completely different approach that uses an aperture is described in [20] where a thin film transistor (TFT) unit was used to create an aperture that can be used for tracking a light beacon.

In this paper we analyze and present the first experimental validation of a new type of ADA receiver that uses a quadrant PD and a single aperture. This new design removes the requirements for accurate matching between different photodiodes and accurate positioning of multiple apertures and photodiodes. In addition, this new receiver can accurately detect AOA over a wide FOV whilst maintaining a compact structure [21]. Experimental results demonstrate very high accuracy from this detector, making it ideal for use in future VLP systems.

2. System description

The ADA receiver, using multiple apertures and discrete PDs, was initially developed for VLC multiple-input multiple-output (MIMO) systems [17], but was later shown, theoretically, to be effective for VLP [6, 22]. In this paper, we describe the new quadrant photodiode ADA (QADA) receiver which has been designed specifically for VLP. To enable practical operation, it uses a single aperture and a quadrant PD to create an AOA detector.

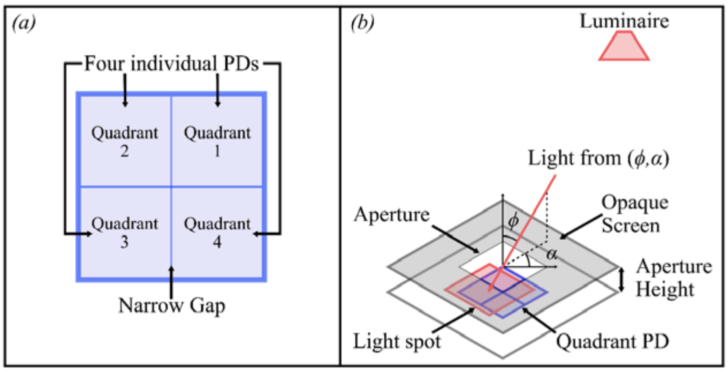

Fig. 1. (a) Quadrant PD showing individual quadrants and narrow gap, and (b) Receiver structure with received light spot overlapping the quadrant PD

Research Article Vol. 26, No. 7 | 2 Apr 2018 | OPTICS EXPRESS 9233

Optics EXPRESS

Quadrant PDs are made up of four individual PDs, separated by a narrow gap, shown in Fig. 1(a). They offer position detection in two dimensions. Previously, they have been used for beam centering and other well-known laser light applications [23, 24]. The key features of our new design are that we use an aperture and that the aperture is located at a known height above the quadrant PD. The aperture is required because the light source in our new application is diffuse. The aperture is used to form a well-defined beam of light that falls on the quadrant PD. The aperture is located at a known height above the quadrant PD as this provides the additional information necessary to calculate the AOA.

We have designed an algorithm that estimates the position of the center of the light spot overlapping the quadrant PD. This information, combined with the height of the aperture, gives both the incident and polar angles of the received light. These angles can then be used with a triangulation algorithm to determine the location of the receiver.

2.1 Concept behind the QADA receiver

The new detector, shown in Fig. 1(b), consists of a quadrant PD located directly below a transparent aperture in an opaque screen. Light passing through the aperture casts a light spot onto the quadrant PD. The position of the light spot is unique for a given AOA, thus, accurately estimating the position of the light spot gives information that is then used to calculate the AOA of the light from the luminaire.

For maximum positioning information, the light spot must overlap all four quadrants of the PD. The vertical distance between the aperture plane and the photodiode plane, termed the aperture height, determines the field of view (FOV) of the detector. As the height becomes larger, the FOV becomes smaller. Because the aperture height is fixed for a given design, it can be combined with the detected displacement of the light spot from the center of the quadrant PD to determine the incident and polar angles.

The aperture and quadrant PD can be any shape desired. However, an important advantage of using a square aperture is that it results in a proportional linear change in the overlap areas of the quadrants as the light spot moves across the detector; this substantially simplifies the algorithm needed to detect position. The size of the light spot is determined by the aperture size. Ideally, the aperture size and shape matches that of the PD as this maximizes the area of the light spot and consequently the strength of the detected signals. However, so long as the light spot is not larger than the quadrant PD, overlaps all four photodiode elements and is not smaller than the gap between quadrants, there will be no ambiguity in position detection.

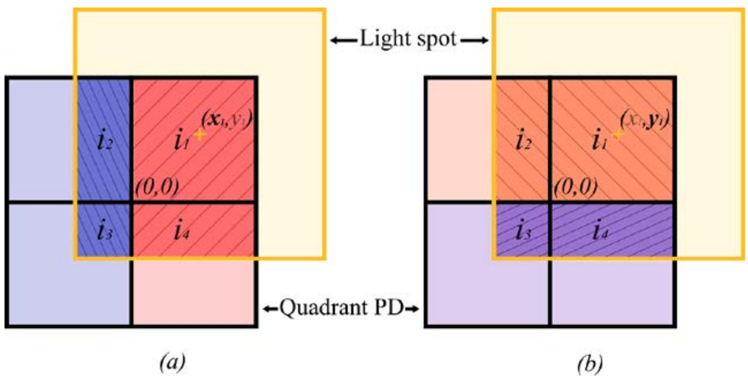

Fig. 2. Light spot, shown in yellow, overlapping a quadrant PD. In (a) we show how the displacement in x is determined using the photocurrents from the left and right quadrant pairs. In (b), we show how the displacement in y is determined using the photocurrents from the top and bottom quadrant pairs.

Research Article Vol. 26, No. 7 | 2 Apr 2018 | OPTICS EXPRESS 9234
Optics EXPRESS

2.2 Algorithm

We initially analyze the ideal case of a square quadrant PD and a square aperture of the same size. To determine position of the receiver, we need to know the displacement of the light spot center from the center of the quadrant PD. In the general case, the receiver is moving and the light spot will vary with time. Thus, we must determine $\left[x_1(t), y_1(t)\right]$, the position of the light spot center at time, t.

The algorithm we have developed to detect the position of the light spot center uses the ratio of the photocurrents generated by adjacent pairs of quadrants. The ratio between the received photocurrents from the left and right quadrant pairs can be used to find displacement in the x direction, shown in Fig. 2(a). Similarly, the ratio between the received photocurrents from the top and bottom quadrant pairs can be used to find displacement in the y direction, shown in Fig. 2(b). These ratios can be expressed as

$$p_x(t) = \frac{i_1(t) + i_4(t) + N_1(t) + N_4(t)}{i_2(t) + i_3(t) + N_2(t) + N_3(t)} \tag{1}$$

$$p_y(t) = \frac{i_1(t) + i_2(t) + N_1(t) + N_2(t)}{i_3(t) + i_4(t) + N_3(t) + N_4(t)} \tag{2}$$

where $i_j(t)$ and $N_j(t)$ are the photocurrent and noise from the j^{th} quadrant, after filtering, at time, t.

The photocurrent generated in each quadrant is proportional to the received optical power, which is dependent on the light spot overlap area. In the absence of noise, the ratios, $p_x(t)$ and $p_y(t)$, can be reduced to ratios of overlap areas, where the areas are a function of the length of the PD quadrant, L_{PD}, and the position of the light spot. Thus, (1) can be expressed as

$$p_x(t) = \frac{A_1(t) + A_4(t)}{A_2(t) + A_3(t)} == \begin{cases} \dfrac{L_{PD} + x_1(t)}{L_{PD}}, & -L_{PD} < x_1(t) \le 0 \\ \dfrac{L_{PD}}{L_{PD} - x_1(t)}, & 0 < x_1(t) < L_{PD} \end{cases} \tag{3}$$

where $A_j(t)$ is the area the light spot overlaps with the j^{th} quadrant of the PD, at time t. And, using symmetry, a similar expression for Eq. (2) can be derived. We can now rearrange Eq. (3) to give

$$x_1(t) = \begin{cases} L_{PD}\left(p_x(t) - 1\right), & -L_{PD} < x_1(t) \le 0 \\ L_{PD} - \dfrac{L_{PD}}{p_x(t)}, & 0 < x_1(t) < L_{PD} \end{cases} \tag{4}$$

which we use to derive an estimate for $x_1(t)$.

From Eq. (3), it can be seen that the ratio, $p_x(t)$, is independent of the value of $y_1(t)$. However, the individual photocurrents, $i_j(t)$, are not. Consequently, when $y_1(t) \neq 0$ the signal to noise ratio (SNR) will be reduced.

We consider the case where the estimate is calculated in the digital domain and the received signal is low-pass filtered in the electrical domain to limit the bandwidth to B

Research Article Vol. 26, No. 7 | 2 Apr 2018 | OPTICS EXPRESS 9235
Optics EXPRESS

hertz. It is then sampled at the Nyquist rate, $2B$, and averaged over M samples so that the estimate at time $t = (k+M)/2B$ is given by

$$\hat{x}_1\left[\frac{k+M}{2B}\right] = \begin{cases} \frac{1}{M}\sum_{n=k}^{k+M-1} L_{PD}\left(p_x\left[\frac{n}{2B}\right]-1\right), & -L_{PD} < x_1\left[\frac{k+M}{2B}\right] \le 0 \\ \frac{1}{M}\sum_{n=k}^{k+M-1} L_{PD} - \frac{L_{PD}}{p_x\left[\frac{n}{2B}\right]}, & 0 < x_1\left[\frac{k+M}{2B}\right] < L_{PD} \end{cases} \quad (5)$$

2.3 Noise analysis

We now consider the impact of noise on the system. We develop an expression for the algorithm in the presence of noise and demonstrate how the resultant noise terms in the ratio function, $p_x(t)$, vary with both the AOA of the light and the vertical distance between the transmitter and receiver.

If we assume the LED is emitting a Lambertian radiation pattern, the general expression for the DC channel gain at time, t, for the j^{th} quadrant of the PD is given by [25]

$$h_c(t) = \frac{(m+1)A_j(t)}{2\pi d^2(t)}\cos^m(\phi(t))T_s(\psi(t))\,g(\psi(t))\cos(\psi(t)) \quad (6)$$

where m is the Lambertian order of the LED, $T_s(\psi)$ is the transmission of the filter, $g(\psi)$ is the concentrator gain, ϕ and ψ are the emergence and incidence angles respectively and d is the distance between the transmitter and receiver. If we restrict our analysis to the case where there is no concentrator or filter, the Lambertian order of the LED is one, and the receiver is pointing straight up at the transmitter so that the incidence and emergence angles are equal, we can then define the photocurrent at time, t, for the j^{th} quadrant as

$$i_j(t) = \frac{RP_T A_j(t)\cos^2(\psi(t))}{\pi d^2(t)} \quad (7)$$

The dominant noise source in an optical wireless system is the shot noise induced by the background illumination [25]. This light is isotropic, however because we use an aperture, the background light reaching the quadrant PD is reduced. Thus, the following analysis will lead to an overestimation of the noise.

We model the shot noise as a white Gaussian process with single-sided noise power density given by

$$N_0 = 2qRp_n A\Delta\lambda \quad (8)$$

where q is the charge of an electron, R is the responsivity of the PD, p_n is the spectral irradiance, A is the area of a single quadrant of the PD and $\Delta\lambda$ is the bandwidth of the optical filter. Thus, the variance of the noise will be the product of the single sided noise power density and the electrical bandwidth, B.

$$\sigma_n^{\,2} = N_0 B \quad (9)$$

For the case where $y_1(t) = 0$, substituting Eqs. (7) and (9) into Eq. (1), gives:

Research Article Vol. 26, No. 7 | 2 Apr 2018 | OPTICS EXPRESS 9236
Optics EXPRESS

$$p_x(t)=\begin{cases}\dfrac{2k_1\cos^4(\psi(t))L_{PD}{}^2+2k_1\cos^4(\psi(t))L_{PD}x_1(t)+N_1(t)+N_4(t)}{2k_1\cos^4(\psi(t))L_{PD}{}^2+N_2(t)+N_3(t)} \\ \quad =\dfrac{L_{PD}+x_1(t)+E_1(t)}{L_{PD}+E_2(t)}, \quad -L_{PD}<x_1(t)\le 0 \\ \dfrac{2k_1\cos^4(\psi(t))L_{PD}{}^2+N_1(t)+N_4(t)}{2k_1\cos^4(\psi(t))L_{PD}{}^2-2k_1\cos^4(\psi(t))L_{PD}x_1(t)+N_2(t)+N_3(t)} \\ \quad =\dfrac{L_{PD}+E_1(t)}{L_{PD}-x_1(t)+E_2(t)}, \quad 0<x_1(t)<L_{PD}\end{cases} \tag{10}$$

where $k_1=(RP_t/\pi)$ is a constant value. The noise terms, $E_1(t)$ and $E_2(t)$, have zero mean and a variance of:

$$\begin{aligned}\sigma_e(t)^2&=\left(\frac{1}{2k_1\cos^4\left(\arctan\left(\sqrt{x_1(t)^2+y_1(t)^2}/h\right)\right)L_{PD}}\right)^2\times 2\sigma_n{}^2 \\ &=\frac{\pi^2(H+h)^4 qp_n A\Delta\lambda B}{RP_T{}^2L_{PD}{}^2\cos^8(\psi(t))}\end{aligned} \tag{11}$$

H is the vertical distance between the transmitter and receiver and h is the vertical distance separating the aperture and the quadrant PD. From Eq. (11), it can be seen that an increase in the electrical filter bandwidth, B, will result in decreased performance as the variance of the noise term is directly proportional to this value.

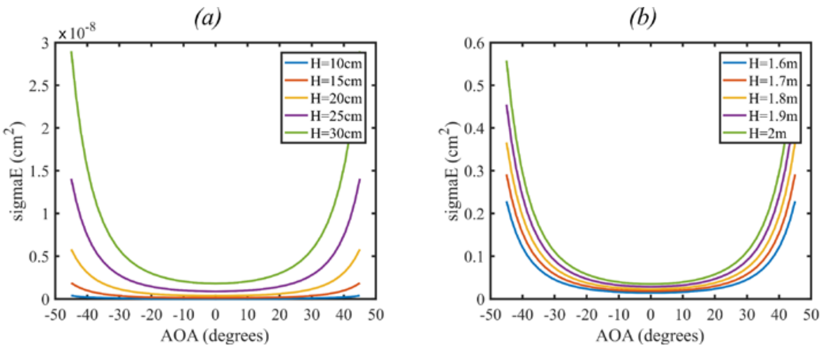

Fig. 3. $\sigma_e{}^2$ for varying AOA and varying vertical distance, *H*, between the transmitter and the receiver, (a) shows the values of *H* used in the experiment and (b) shows more typical values of *H* that are encountered in positioning applications. The variance is larger for large arrival angles and large values of *H* due to the reduced received optical power.

In Fig. 3, $\sigma_e{}^2$ is plotted for varying AOA and vertical distance. In both plots, it can be seen that the magnitude of $\sigma_e{}^2$ is worse for large arrival angles and for large values of H. This is due to the reduced optical power received when the distance separating the transmitter and receiver is increased. The parameters used for this simulation are shown in Table 1.

Research Article
Vol. 26, No. 7 | 2 Apr 2018 | OPTICS EXPRESS 9237
Optics EXPRESS

Table 1. Simulation parameters

Parameter	Value
Power transmitted *(P_t)*	3 W
Responsivity *(R)* (@ 440 nm)	0.15 A/W
Optical filter bandwidth *($\Delta\lambda$)*	300 nm
Electrical filter bandwidth *(B)*	1 MHz
Spectral irradiance *(p_n)*	6.2 x 10^6 W/(nm·cm^2)
Length of PD *(L_{PD})*	2 mm
Aperture height *(h)*	2 mm

3. Experiment

The block diagram of the experiment is shown in Fig. 4. The transmitter, shown in the red box, was a white LED (Luxeon LXML-PWC2) emitting a 200 kHz sine wave. The signal, provided by an arbitrary waveform generator (AWG, Tektronix 3022B), was amplified by a power amplifier (Mini-circuits ZHL-32A-S) before adding a DC bias using a bias-T (Mini-circuits ZFBT-4R2GW).

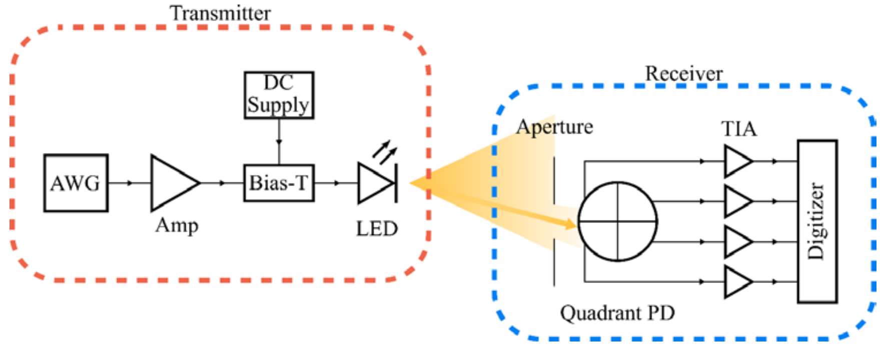

Fig. 4. Block diagram of the experimental set-up. The transmitter circuit, shown on the left, drives a white LED that outputs a 200 kHz sine wave. The light from the LED passes through the aperture and is received by the quadrant PD, shown on the right. It is then amplified and captured by a digitizer.

The receiver, shown in the blue box, consisted of the quadrant PD and an aperture. To optimize the performance, the quadrant PD was operated in photovoltaic mode with no bias. The output of each quadrant of the PD was connected to a transimpedance amplifier (Femto DHPCA-100) before the signals were captured by a digitizer (GaGe CSE8389). The data was analyzed in MATLAB to determine the receiver position.

The experiment was performed on an optical table, shown in Fig. 5, with two perpendicular optical rails, each with a linear stage. The receiver, in the blue box, was mounted on one of the linear stages and the transmitter, in the red box, was mounted on the other. This set-up allowed for the capture of data in varying positions in two dimensions.

The quadrant PD was attached to a breakout board and held in place using a custom 3D printed bracket. In front of the quadrant PD an XY translation mount was used to hold another custom 3D printed bracket that contained the aperture.

Research Article Vol. 26, No. 7 | 2 Apr 2018 | OPTICS EXPRESS 9238
Optics EXPRESS

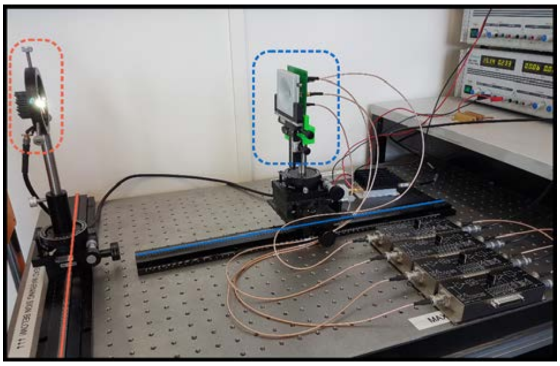

Fig. 5. Photograph of the experiment. The transmitter, in the red box, moves along the optical rail that is highlighted in red. The receiver, in the blue box, moves along the optical rail that is highlighted in blue.

3.1 Experimental algorithm

For this experiment, we selected a readily available circular quadrant PD (OSI SPOT-9DMI) with a diameter of 10 mm. Located directly in front of the quadrant PD was a 4mm square aperture. The distance separating the aperture and the quadrant PD was 2.25 mm. In order to maintain the linear relationship between the movement of the light spot and the change in overlap areas, it was optimal to use a square aperture with a side length that was smaller than the diameter of the quadrant PD.

We replace the general algorithm in Eq. (3) with one that has been designed for this geometry of PD and aperture:

$$p_x(t) = \frac{L_{ap} + x_1(t)}{L_{ap} - x_1(t)}, \quad -L_{ap} \le x_1(t) \le L_{ap} \tag{12}$$

where L_{ap} is half the side length of the aperture. From Eq. (12), we get

$$x_1(t) = \frac{L_{ap}(p_x - 1)}{(1 + p_x)}, \quad -L_{ap} \le x_1(t) \le L_{ap} \tag{13}$$

which can be used to derive an estimate for $x_1(t)$.

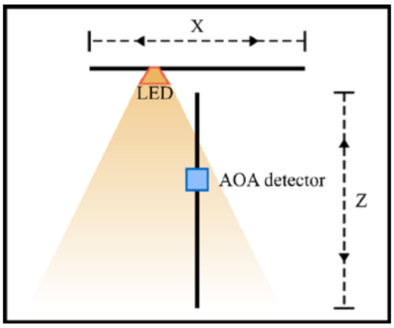

Fig. 1. Schematic showing possible movement of transmitter and receiver

Research Article Vol. 26, No. 7 | 2 Apr 2018 | OPTICS EXPRESS 9239
Optics EXPRESS

3.2 Calibration

Due to the accuracy of the receiver, the experimental set up needed to be carefully aligned. To this end, the calibration of the receiver was performed in several steps. The first step aligned the receiver with the transmitter to find the zero position on the *x*-axis. This was performed without an aperture. The LED transmitter was moved along the *x*-axis, shown in Fig. 6, until the sums of the photocurrents from the left and right quadrants were equal. The height of the transmitter was then adjusted until the sums of the photocurrents from the top and bottom quadrants were equal. Next, the aperture was aligned with the quadrant PD using the XY translation mount and the rotation screw in the 3D printed bracket. Similar to the previous step, adjustments were made until all photocurrents were equal. Finally, the transmitter was moved 5 cm to the left and 5 cm to the right with measurements taken at both positions. These values were used to determine if there was any rotation about the *y*-axis. The receiver was then rotated until these results were symmetric. Note that this calibration is to ensure accuracy in our measurement system, so that we know what the exact angle is and compare that to what is measured, it would not be required in a real system.

3.3 Results

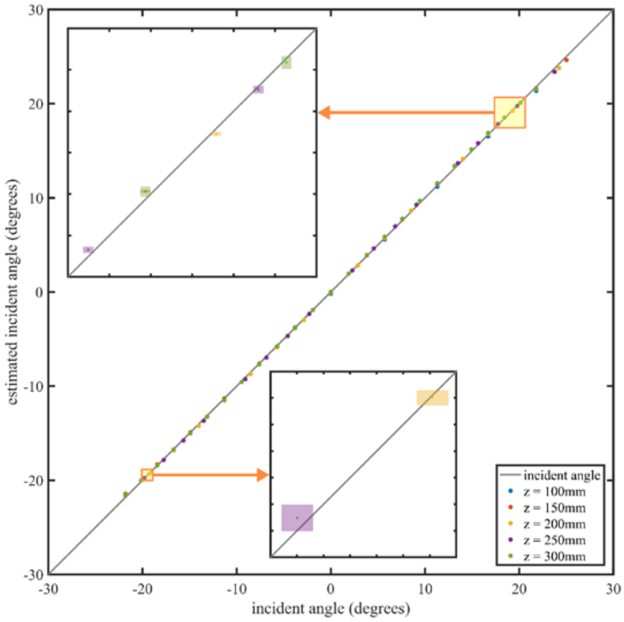

Fig. 7. Estimated incident angle vs true incident angle for all measured positions, demonstrating the accuracy of the QADA. The color patches represent error bars of one standard deviation. Insets at different magnifications for clarity.

Measurements were taken in one centimeter increments along the *x*-axis and five centimeter increments along the *z*-axis. Figure 7 shows the close correlation between the experimental estimated incident angle and the true incident angle. The largest error in estimation of the incident angle was 0.46° and this occurred when the magnitude of the incident angle was highest. Over 90% of the errors in incident angle estimation were below 0.25°.

Figure 8 shows the root mean square error (rMSE) in detection of the incident angle for varying distances. The maximum rMSE was 0.1077° and the minimum was 0.0054°. Over 90% of rMSE were less than 0.07°. As expected, the rMSE are worst when the distance along

Research Article Vol. 26, No. 7 | 2 Apr 2018 | OPTICS EXPRESS 9240
Optics EXPRESS

the z-axis is largest. This is as expected as, from (11), we can see that the variance on the measurement of the position of the light spot is directly proportional to the fourth power of H, the distance between transmitter and receiver. In this experiment the distance along the z-axis is analogous to the height. The rMSE also increases as the magnitude of the incident angle increases. This is due to the reduction in received optical power for increasing incident angle.

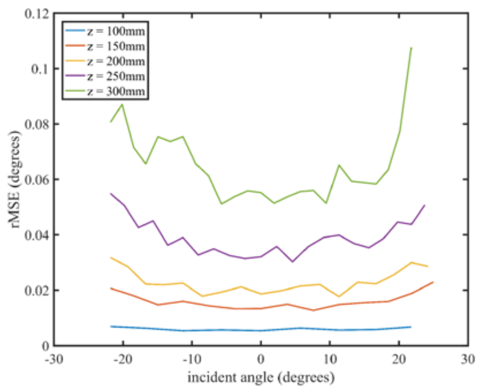

Fig. 8. Experimental results showing root mean square error for varying AOA

4. Discussion

The experimental results we have presented in this paper, using off-the-shelf components and a manual calibration method, demonstrate the accuracy of the detector. Figure 9 shows the experimental results for rMSE plotted on the same graph as the simulation results. The simulation used realistic parameters that were similar to those used in the experiment. It can be seen that there is a very close correlation between simulation and experimental results with the experimental results being slightly worse, as expected. This is probably due to calibration difficulties, combined with the simplified assumptions that are modelled in the simulation. For example, it is unlikely that the LED was a truly perfect Lambertian transmitter. The reduction in FOV for the experimental results is due to the reflectivity of the silicon [26] and the impact of Snell's law, which degrade the results for large incident angles. As both the thickness and refractive index of the glass in the quadrant PD packaging were unknown, it was not possible to correct for the refractive errors.

Due to the precision required to make accurate measurements that were suitable for meaningful comparison with simulation, calibration posed a significant difficulty for this experiment. Most of these calibration difficulties will not be present in a commercial implementation. It is likely that mass fabrication of such a detector will only require a factory calibration step to determine any alignment issues between the quadrant PD and the aperture. Any imperfections found will be corrected for in software. Additionally, the detector should be protected from the atmosphere with a transparent layer built into the structure. Any refractive index introduced by this layer will also need factory calibration and to be accounted for in software.

Research Article Vol. 26, No. 7 | 2 Apr 2018 | OPTICS EXPRESS 9241

Optics EXPRESS

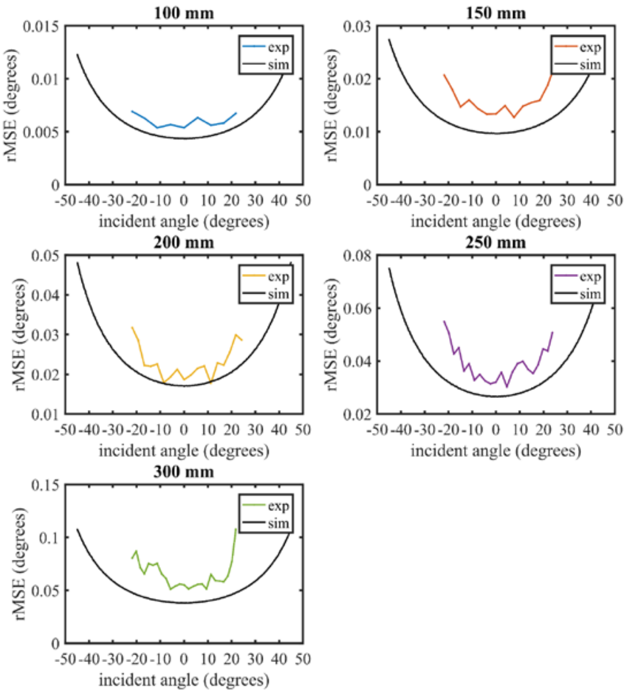

Fig. 9. Simulation and experimental results for root mean square error in incident angle detection. The experimental results, shown in colour, are closely matched to the simulation results, shown in black.

Compared to other AOA detectors that have experimental results published, the QADA receiver has superior performance. In [27], a cubic receiver was able to achieve errors, for the detection of incident angle, in the range of 0.7° – 6.8° and in [13] a different cubic receiver reported errors between 1° and 1.4° in detection of incident angle. Not only are the results for the QADA receiver better (all errors in incident angle detection are less than 0.5°), the QADA receiver has the important advantage of having a thin planar structure which is easier to incorporate into current consumer electronics. Other AOA systems that use cameras are able to achieve high levels of accuracy [15]. However, they have the disadvantages of either needing high frame rates, which add significant expense, or complex algorithms. They also consume a lot of power. By comparison, the QADA receiver is a simple and low power device that can be constructed using relatively cheap components, and clearly meets the requirements for widespread integration.

5. Conclusion

We present analytical and experimental results for our proposed QADA receiver. The results demonstrate that the QADA can support very accurate indoor positioning with centimetre accuracy in typical rooms. A key feature of the QADA is its compact planar structure. Our experiments used an off-the-shelf quadrant PD in a QADA receiver with dimensions compatible with incorporation in a compact portable device like a smart phone. Our experimental results very closely matched our theoretical predictions. These results show that, with rMSE errors less than 0.11°, in addition to being more compact than some of the

Research Article Vol. 26, No. 7 | 2 Apr 2018 | OPTICS EXPRESS 9242
Optics EXPRESS

three dimensional receivers that have previously been described, the QADA is also more accurate. We have demonstrated that the new QADA receiver has the potential to form a key component of future indoor positioning systems.

Funding

Australian Research Council (ARC) Discovery funding scheme (DP130101265, DP150100003); Australian Government Research Training Program (RTP) Scholarship.

Chapter 6

QADA-plus: a novel two-stage receiver for visible light positioning

6.1 Overview

In the previous chapter the AOA estimation capabilities of the QADA receiver were verified with experimental work on an optical bench. Whilst the experiment showed that there was potential to achieve high angular resolution, the challenge in constructing such a device is high. Additionally, the demands for such a high precision detector could make it expensive to manufacture and calibrate. One possible solution is to lower the requirement for high accuracy angle estimation by combining a QADA with an imaging sensor to create a two stage hybrid receiver. The major advantage of this type of receiver structure is that it benefits from the advantages of the individual receivers without adding significant additional complexity.

The following work introduces the new hybrid receiver structure that is called QADA-plus. In this receiver a QADA is used to demodulate the data transmitted by the luminaires and to approximately estimate the AOA. At the same time the imaging sensor captures an image. The AOA estimation from the QADA is used to match the demodulated data to the luminaires that are visible in the image. Then, using the high resolution image and the algorithm described in the paper, accurate position estimates are possible. A further enhancement that is possible when using this type of receiver is to use reference points. A reference point is a feature with a defined location that can be identified using image processing and thus used to improve the positioning accuracy. Whilst this idea is introduced in this paper, it will be discussed in more detail in later chapters.

This chapter presents simulation results that highlight some of the deficiencies in using a QADA, demonstrating why it is useful to use a hybrid receiver. In particular, the sensitivity of the QADA to low received power. Low received power can occur in indoor scenarios with high ceilings or low illumination requirements. In some applications, it would be possible to use the QADA alone, especially if the demands for accuracy are low. However, for more demanding applications a more robust receiver is highly advantageous.

6.2 Publication

> S. Cincotta, C. He, A. Neild, and J. Armstrong, "QADA-PLUS: A Novel Two-Stage Receiver for Visible Light Positioning," in *2018 International Conference on Indoor Positioning and Indoor Navigation (IPIN)*, 2018, pp. 1–8.

The following publication was published in the Proceedings of the 2018 IEEE International Conference on Indoor Positioning and Indoor Navigation (IPIN). It has been reproduced with the permission of the IEEE.

The references are [19] [17] [217] [207] [152] [102] [104] [176] [218] [209] [131] [23] [21] [192] [208] [128] [219] [220] [213] [215] [214] [153] [221] [210] [105] [222] [223] [224]

2018 International Conference on Indoor Positioning and Indoor Navigation (IPIN), 24-27 September 2018, Nantes, France

QADA-PLUS: a novel two-stage receiver for visible light positioning

Stefanie Cincotta, Cuiwei He, Adrian Neild and Jean Armstrong
Monash University
Melbourne, Australia
{Stefanie.Cincotta, Cuiwei.He, Adrian.Neild, Jean.Armstrong}@monash.edu

***Abstract*— In this paper, we introduce a new two-stage receiver structure for visible light positioning (VLP) and a particular implementation of the new structure called the QADA-PLUS receiver. By using two sensors, one a photodiode (PD) based sensor and the other an image-based sensor, the new structure exploits the strengths of both technologies while avoiding their weaknesses. The QADA-PLUS uses a quadrant angular diversity aperture receiver (QADA) for the PD-based stage. The QADA has a very compact, planar structure suitable for incorporation in a smartphone or other small device and has been shown to provide good angular diversity in a proof-of-concept laboratory experiment. The QADA is also, unlike typical image sensors, able to reliably demodulate high frequency visible light signals. In this paper extensive simulation results for a range of typical indoor scenarios and realistic parameters show that the QADA has the potential to accurately estimate the polar and incident angle of light transmitted by LED luminaires. The average absolute error in estimation of incident angle was 0.0006° and for polar angle estimation was 0.005°. A limitation of these simulations is that it is assumed that the luminaires can be modelled as point sources and that the dimensions of the QADA are very precisely known. Incorporation of the QADA in the new two-stage QADA-PLUS receiver removes these limitations in two ways – the image-based receiver provides very accurate angle-of-arrival estimates and the use of visible reference points means that the QADA-PLUS is compatible with luminaires of any shape.**

Keywords—visible light positioning, quadrant photodiode, aperture, QADA, QADA-PLUS

I. INTRODUCTION

Recently, because of the widespread introduction of LED based indoor lighting, there has been significant and increasing interest in the use of visible light communications (VLC) for indoor positioning [1], [2]. Unlike conventional lighting, LEDs can be modulated at high rates. Receivers, using photodiodes (PDs) or imaging sensors, detect the signals and determine the receiver position. A major advantage of visible light positioning (VLP) is that it takes advantage of existing lighting infrastructure and so reduces the cost of installation dramatically [1]. Additionally, unlike radio frequency (RF) based methods, it is not subject to significant multipath propagation issues [3].

This work was supported by the Australian Research Council's (ARC) Discovery funding schemes (DP150100003 and DP180100872) and an Australian Government Research Training Program (RTP) Scholarship.

978-1-5090-1629-7/18/$31.00 ©2016 Crown

There are many different approaches to VLP each with their own strengths and weaknesses. One of the most intuitive approaches is to use the received signal strength (RSS) to determine the distance from the transmitter to the receiver [4]–[6]. However, without very accurate knowledge of the transmitted power and the optical channel, it is difficult to accurately estimate this distance. Alternative well-known methods use time-of-arrival (TOA) or time-difference-of-arrival (TDOA) [7], [8]. Whilst the latter works well for GPS, it is not practical for VLP due to the expensive synchronized clocks that are required and the very small time differences that would need to be accurately measured.

Another alternative is to estimate the angle-of-arrival (AOA) of the received light. This is possible because there is typically a line-of-sight (LOS) path available from the LED beacons to the receiver. AOA estimation requires an angular diversity optical receiver. This can be implemented using either imaging sensors [9]–[11] or PDs [12]–[15]. Imaging sensors generally have high resolutions making them well suited to accurate AOA estimation, but because of frame rate limitations, they are not able to demodulate high-frequency signals. This is a major limitation because to avoid adverse biological effects [16], modulation of LEDs at low frequencies must be avoided. A number of innovative workarounds have been proposed which depend on the rolling shutter mechanism of typical low cost digital cameras [17] but these systems can only provide rough positioning and can demodulate only relatively low data rate signals.

In the past, a number of PD-based receivers have achieved angular diversity by having PDs facing in different directions [13], [15]. These three-dimensional PD structures have been shown to provide good angular diversity, however, they are not well suited to integration into modern consumer electronics due to the awkward protrusion they create. The quadrant PD angular diversity aperture (QADA) receiver solves this problem by combining an aperture with a quadrant PD [18], [19]. We have previously demonstrated that this achieves good angular diversity within a compact and planar structure.

In this paper, we present a completely new approach and describe an all-new hybrid two-stage receiver, called QADA-PLUS. The new receiver has two distinct sensors: one a PD-based sensor and the other an imaging sensor. In this way, we build on the strengths and avoid the weaknesses of each type of sensor. In the system described in this paper, the first stage uses the QADA receiver to demodulate the signals and identify the LED beacons. The second stage captures a still image and

2018 International Conference on Indoor Positioning and Indoor Navigation (IPIN), 24-27 September 2018, Nantes, France

combines this with the information from the first stage to achieve accurate positioning. We also describe how, by associating precise visible reference points with each luminaire, the performance can be further improved.

The significant contributions of this paper include

1. The first publication of the all new two-stage positioning receiver that provides high accuracy.
2. The use of reference point or points to identify precise position(s) associated with each luminaire[1].
3. A detailed analysis of QADA in two dimensions, including angular diversity analysis

Section II provides a detailed description of each of the two stages of the system and the use of reference points. In Section III the results of simulations are presented that demonstrate the suitability of the QADA receiver for stage one. Section IV is a discussion on realistic implementations and Section VI contains the conclusions.

II. System Description

Fig. 1 shows the overall structure of a positioning system using the new QADA-PLUS two-stage receiver. Each LED beacon transmits an optical signal which contains information about its position. In this paper, we call the position information message transmitted by the n^{th} LED beacon the Beacon Information packet (BIP_n). The BIP message contains information about the positions of the reference point, or points, on the luminaire. Reference points are specific points on the luminaire that can be identified by an image sensor. We discuss the use of reference points in detail in a later section.

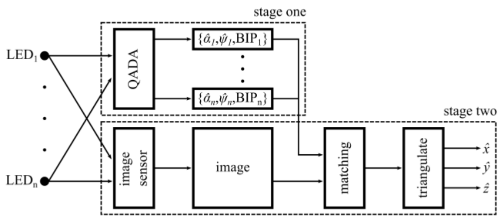

Fig. 1. Block diagram showing the overall structure of the receiver and the flow of information between stage one and stage two.

Light from each transmitter is received by both the PD-based sensor and the image sensor. The PD-based sensor, which in this paper is a QADA, demodulates the signals transmitted by each LED beacon and decodes the BIP messages for all of the transmitters within range. We assume that the LED beacons transmit orthogonal signals so that the signals from each can be readily separated at the receiver. For example, time-division-multiplexed or frequency-division-multiplexed signals could be used. The PD-based sensor simultaneously provides approximate estimates of the incident angle, ψ, and the polar angle, α, of all LED beacons in the field-of-view (FOV). At the same time, the image-based sensor takes a high-resolution image that includes the luminaires. The outputs of the two sensors are then used in the matching stage. The approximate incident angle and polar angle of the LED beacon from the first stage allows each luminaire to be unambiguously identified in the image. This, in combination with the position information contained in the BIP message, allows the precise positions of the reference points in the image plane to be very accurately determined. By using the AOA information from three or more reference points, well-known triangulation algorithms can be used to calculate the x, y, and z coordinates of the receiver. This method is more accurate than using a single-stage QADA receiver.

A. *Stage one – QADA*

The QADA receiver, in Fig. 2, consists of a quadrant PD, shown in blue, positioned directly below a transparent aperture. A quadrant PD is a type of segmented PD that consists of four discrete PDs arranged in a 2 x 2 array. The PDs are separated by a very narrow gap. Segmented PDs are available in varying shapes, sizes and number of segments and are typically used in laser light applications such as beam centering [20], [21] where they are capable of providing position information in two dimensions. In these applications, an aperture is not required. The combination of an aperture with a quadrant PD in the form of the QADA and its potential in indoor positioning applications has only been very recently described [18].

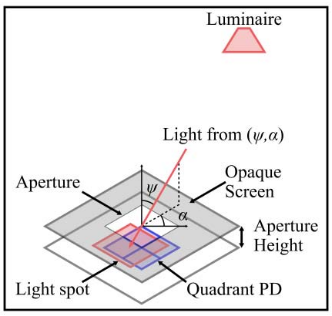

Fig. 2. QADA receiver structure.

The aperture plane is separated from the quadrant PD plane by a known vertical distance, h. We call this distance the aperture height. In Fig. 2, the light from an LED luminaire passes through the aperture and forms a light spot, shown in red, on the quadrant PD. The light spot shape and size match that of the aperture. The position of this light spot is unique for a given AOA provided that the aperture is no larger than the quadrant PD and the dimensions of the light beacon are much smaller than the distance from the beacon to the receiver.

We use a square aperture and quadrant PD so that the position of the light spot maintains a linear relationship as it passes over the quadrant PD [18]. We choose an aperture size that matches the quadrant PD size as we have previously shown that this maximizes the signal-to-noise ratio (SNR) [18].

[1] We use the term ‘luminaire’ as it is the technical term for the light fitting. Luminaires can be made up of one, or multiple, LEDs, of which some, or all, will be transmitting signals. We refer to the LEDs that are transmitting signals as the LED beacons.

2018 International Conference on Indoor Positioning and Indoor Navigation (IPIN), 24-27 September 2018, Nantes, France

First, we analyze how the position information for one beacon is determined, and then we will show how the use of orthogonal signals allows simultaneous calculation of the positions of multiple beacons.

The ratio of photocurrents in adjacent quadrant pairs is used to determine the position of the light spot centroid. In Fig. 3, the light spot, shown in yellow, overlaps the quadrant PD. The colors in the overlap areas represent the quadrant pairs used in the ratio function. In Fig. 3 (a), we determine the x coordinate of the centroid of the spot by using the ratios between the left and right quadrant pairs and in Fig. 3 (b), we determine the y coordinate of the centroid by using the ratios between the top and bottom quadrant pairs. The x and y coordinates of the centroid are estimated independently and then used, in combination with the known aperture height, to estimate the incident and polar angles of the incoming light.

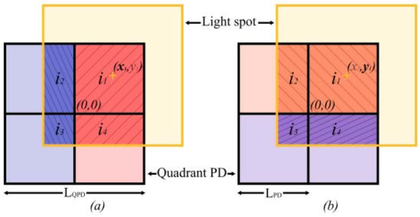

Fig. 3. Light spot overlapping the quadrant PD

These ratios are expressed as

$$p_x(t)=\frac{i_1(t)+i_4(t)+N_1(t)+N_4(t)}{i_2(t)+i_3(t)+N_2(t)+N_3(t)} \tag{1}$$

$$p_y(t)=\frac{i_1(t)+i_2(t)+N_1(t)+N_2(t)}{i_3(t)+i_4(t)+N_3(t)+N_4(t)} \tag{2}$$

where $i_j(t)$ and $N_j(t)$ are the photocurrent and noise generated by the j^{th} quadrant of the PD.

The LEDs are assumed to have a radiation pattern that is Lambertian with an order of $m=1$. We can express the channel gain for the j^{th} quadrant at time, t, as [22]

$$h_c(t)=\frac{(m+1)A_j(t)}{2\pi d^2(t)}\cos^m\left(\phi(t)\right)T_s\left(\psi(t)\right)g\left(\psi(t)\right)\cos\left(\psi(t)\right) \tag{3}$$

where d is the distance between the transmitter and the receiver, ϕ is the emergence angle, ψ is the incidence angle, $T_s\left(\psi(t)\right)$ is the filter transmission and $g\left(\psi(t)\right)$ is the concentrator gain. The QADA does not use any optical filters[2], lenses, or concentrators, thus the photocurrent for the j^{th} quadrant at time, t, is given by

$$i_j(t)=\frac{RP_TA_j(t)\cos^2\left(\psi(t)\right)}{\pi d^2(t)} \tag{4}$$

where R is the responsivity of the PD, P_T is the transmitted optical power and $A_j(t)$ is the area of quadrant j which the light spot overlaps.

From (4), it is clear that the photocurrent is directly proportional to the area of overlap. If we exclude the noise terms from the above functions, we can simplify them to a function of the overlap area. We define L_{PD} as the length of a single quadrant, shown in Fig. 3 (b), and $[x_1(t),y_1(t)]$ as the centroid of the light spot at time, t.Thus, in the absence of noise, the ratios in (1) and (2), can be expressed as:

$$p_x(t)=\frac{A_1(t)+A_4(t)}{A_2(t)+A_3(t)}=\begin{cases}\dfrac{L_{PD}+x_1(t)}{L_{PD}}, & -L_{PD}<x_1(t)\leq 0\\[2ex] \dfrac{L_{PD}}{L_{PD}-x_1(t)}, & 0<x_1(t)<L_{PD}\end{cases} \tag{5}$$

$$p_y(t)=\frac{A_1(t)+A_2(t)}{A_3(t)+A_4(t)}=\begin{cases}\dfrac{L_{PD}+y_1(t)}{L_{PD}}, & -L_{PD}<y_1(t)\leq 0\\[2ex] \dfrac{L_{PD}}{L_{PD}-y_1(t)}, & 0<y_1(t)<L_{PD}\end{cases} \tag{6}$$

We can now rearrange (5) and use the result to derive an estimate for $x_1(t)$. The received signal undergoes low pass filtering to limit the bandwidth to B hertz, before sampling at the Nyquist rate, $2B$, and matched filtering to select the desired signal and reject any orthogonal signals received from other beacons [23]. We then average over M values to find the estimate at time $t=(k+M)/2B$, which can be expressed as

$$\hat{x}_1\left[\frac{k+M}{2B}\right]=\begin{cases}\dfrac{1}{M}\displaystyle\sum_{n=k}^{k+M-1}L_{PD}\left(p_x\left[\frac{n}{2B}\right]-1\right), & -L_{PD}<x_1\left[\dfrac{k+M}{2B}\right]\leq 0\\[3ex] \dfrac{1}{M}\displaystyle\sum_{n=k}^{k+M-1}L_{PD}-\frac{L_{PD}}{p_x\left[\frac{n}{2B}\right]}, & 0<x_1\left[\dfrac{k+M}{2B}\right]<L_{PD}\end{cases} \tag{7}$$

The block diagram showing this process is shown in Fig. 4

We can derive a similar estimate for $y_1(t)$. As can be seen in (7), the estimate for $x_1(t)$ depends only on the value of L_{PD} and p_x. It does not depend on the value of $y_1(t)$. However, the photocurrent, $i_j(t)$, depends on the values of $x_1(t)$ and $y_1(t)$. Thus, the SNR is reduced because of the reduced area of overlap.

2 Optical filters operate in the optical domain before the PD and are used to selectively transmit different wavelengths of light, whilst electrical filters operate in the electrical domain after the PD and remove unwanted electrical frequencies.

2018 International Conference on Indoor Positioning and Indoor Navigation (IPIN), 24-27 September 2018, Nantes, France

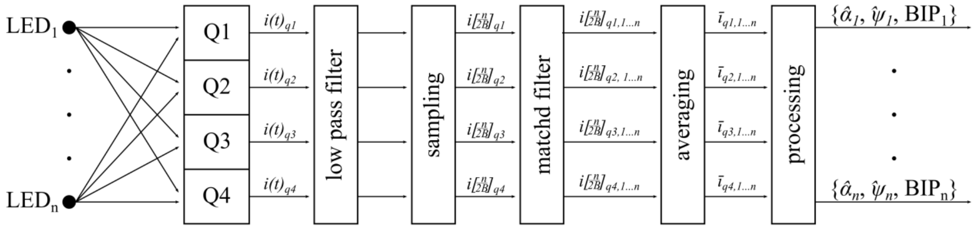

Fig. 4 Digital signal processing path for QADA

The noise in optical receivers is typically a combination of both the shot noise and the thermal noise [22]. The shot noise due to background illumination is the dominant noise source. It is modeled as a white Gaussian process. The variance of the shot noise for an isotropic receiver, expressed in (8), is the product of the single-sided noise power density and the electrical bandwidth, B .

$$\sigma^2_{shot} = 2qRp_n A\Delta\lambda B \tag{8}$$

where q is the charge of an electron, p_n is the spectral irradiance, A is the area of the PD quadrant and $\Delta\lambda$ is the optical bandwidth.

The thermal noise is calculated using the noise equivalent power (NEP). Like the shot noise, it is the product of the spectral density and the electrical bandwidth.

$$\sigma^2_{thermal} = \left(NEP \times R\right)^2 B \tag{9}$$

QADA is a well suited AOA detector for stage one. Using a small 5 mm square quadrant PD, its compact planar structure means that it can be easily incorporated into a smartphone and it provides sufficiently accurate AOA data for input to stage two.

B. Stage two – Image sensor

An image sensors, such as cameras typically found in a smartphone, can provide very high angular resolution as they typically have a large number of pixels. Position accuracy in the sub-decimeter range has been shown to be possible using high megapixel cameras [11], [24], [25]. However, demodulation of transmitted data is difficult without high frame rates or complex algorithms [26]–[28]. In QADA-PLUS, this is avoided by using a PD-based AOA detector to demodulate the signals and identify the LED beacons. This information from stage one, consisting of an AOA estimate and BIP message, is combined with the information gathered in stage two to estimate the position with very high accuracy. As the location of the luminaires is approximately known, the computational complexity of the image processing is significantly reduced.

We use photogrammetry to determine the position of the receiver. After the LED beacons have been identified and the BIP messages, stating the position of the reference points within a local (or global) coordinate system, has been decoded in stage one, the reference points are located in the image plane and, finally, a triangulation algorithm is used.

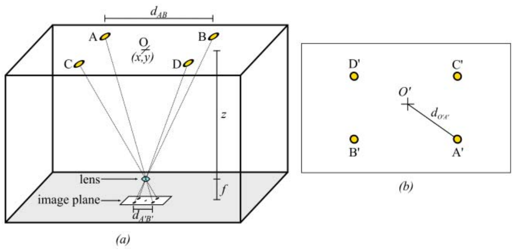

Fig. 5. (a) Room with image of ceiling captured and (b) image plane

In Fig. 5, the camera has captured an image of the ceiling showing four LED beacons. In Fig. 5 (a), the focal length of the camera, f , is a known value. The distance between the LEDs, A and B, can be easily determined in both the image and room coordinates. To determine the position in the room, first we must determine the height, z , using the ratio of the distance between two beacons: $z : f = d_{AB} : d_{A'B'}$. From this relationship, we obtain

$$\hat{z} = f\,\frac{\sqrt{\left(x_A - x_B\right)^2 + \left(y_A - y_B\right)^2}}{\sqrt{\left(x_{A'} - x_{B'}\right)^2 + \left(y_{A'} - y_{B'}\right)^2}} \tag{10}$$

We then repeat the calculation in (10) for all possible combinations of LED beacons and use the mean of these values to estimate the height. Once the height is known, we calculate an estimate for $\hat{x}$ and $\hat{y}$, using

$$\frac{z}{f} = \frac{d_{OA}}{d_{O'A'}} = \frac{d_{OB}}{d_{O'B'}} = \frac{d_{OC}}{d_{O'C'}} = \frac{d_{OD}}{d_{O'D'}} \tag{11}$$

The distance from the origin in the image plane, O' , to each beacon, shown in Fig. 5 (b), can be determined using image processing, whilst the corresponding origin in room coordinates, O , is the (x, y) location of the receiver. From (11), we get

$$\begin{aligned}
\left(d^2_{OA} - d^2_{OB} - x^2_A + x^2_B - y^2_A + y^2_B\right)/2 &= x(x_B - x_A) + y(y_B - y_A) \\
\left(d^2_{OB} - d^2_{OC} - x^2_B + x^2_C - y^2_B + y^2_C\right)/2 &= x(x_C - x_B) + y(y_C - y_B) \\
\left(d^2_{OC} - d^2_{OD} - x^2_C + x^2_D - y^2_C + y^2_D\right)/2 &= x(x_D - x_C) + y(y_D - y_C)
\end{aligned} \tag{12}$$

2018 International Conference on Indoor Positioning and Indoor Navigation (IPIN), 24-27 September 2018, Nantes, France

This overdetermined set of equations can easily be solved using linear least squares regression. In reality, the receiver may be tilted at arbitrary angles and thus additional algorithms are needed to compensate for these rotations.

C. Reference Points

In this section, we describe the use of visible reference points. The use of these in conjunction with the new two-stage receiver has two major advantages – it makes the new receiver more accurate and it makes it compatible with any shape of luminaire. In this paper we use the term ‘reference points’, these play a similar role to anchor nodes or landmarks in other positioning systems.

In principle, reference points can be any specific position within the luminaire as long as they can be unambiguously identified from the image taken in the second stage. For example, a reference point could be a given corner of the luminaire or a single colored LED. The form of the reference point can either be defined for the entire system or, can be transmitted as part of the BIP message. For example, a system could be built where every positioning luminaire has one red LED which is the reference point for that luminaire, or a more versatile system could be built where the BIP messages convey both the type and position of the reference point in each luminaire.

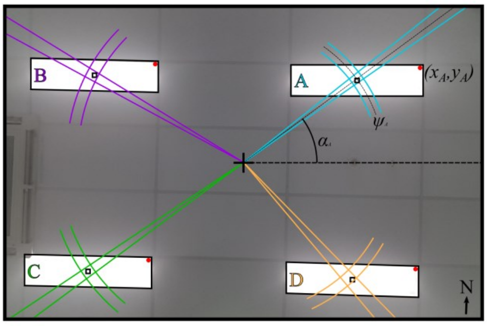

Fig. 6. Example image captured by smartphone camera with overlay showing the information provided by stage one.

Fig. 6 shows a practical example of the use of reference points. It shows an image of a ceiling on which there are four separate batten luminaires. It was captured using a front-facing smartphone camera. Batten luminaires are often used in commercial and industrial settings and consist of many LEDs in a linear array. In our new system some, or all, of the LEDs can be used to transmit positioning information. In this example, we assume a LED in the center of each luminaire is used as the beacon LED. The overlay demonstrates how the incident and polar angle estimates, from stage one, are used to locate the LED beacons and, by extension, the luminaires, in the image plane. For example, the LED beacon in luminaire A is estimated to have an incident angle of ψ_1 and a polar angle of α_1. The colored lines represent the uncertainty in the estimation and thus the intersection of the blue lines should contain the LED beacon. This information is then matched with the BIP message that was decoded by the QADA. So now the second stage knows from the BIP the precise position of the reference point in each luminaire and its position on the image, shown as a red dot. These values are then used in (11) to calculate the receiver position.

Although we do not analyze it in detail in this paper, the concept of reference points can be extended to the use of multiple reference points within one luminaire. This would be particularly useful for large area luminaires such as the batten luminaire as fewer LED beacons are required to support triangulation.

III. Simulation Results

In this section, we investigate the performance of the QADA as the position of the receiver and the height of the ceiling is varied. We start with a room with dimensions $3\,\text{m} \times 3\,\text{m} \times 2.4\,\text{m}$ and a single LED installed in the center of the ceiling, shown in Fig. 7.

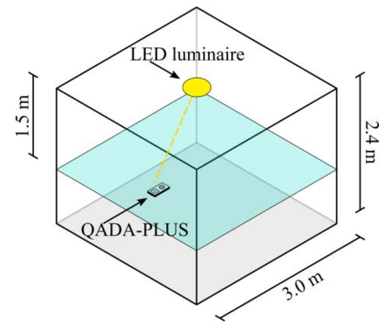

Fig. 7. Schematic of the room with dimensions 3 m x 3 m x 2.4 m that is used in the initial simulation. A single LED is located at the center of the ceiling.

We first assume that the receiver is located at a vertical distance of 1.5 m from the ceiling and that the optical power of the LED beacon is 3 W. For simplicity, we model the LED beacon as a point source. The transmitted signal is sampled at the Nyquist rate and the samples are averaged over 0.01 seconds. This allows for rapid position updates. The rest of the simulation parameters can be found in Table 1.

Table 1. Simulation parameters

Parameter	**Value**
Quadrant PD size	5 mm × 5 mm
Aperture height	2.5 mm
Responsivity	0.25 A/W
Electrical bandwidth	1 MHz
Optical bandwidth	300 nm
Noise Equivalent Power	1.9×10^{-14} W/$\sqrt{\text{Hz}}$
Spectral irradiance	6.2×10^{-6} W/(nm.cm^2)

A. Angular Diversity of QADA

First, we analyze the angular diversity of the QADA receiver. In Fig. 8, the channel gains of the QADA receiver are

2018 International Conference on Indoor Positioning and Indoor Navigation (IPIN), 24-27 September 2018, Nantes, France

presented for all possible receiver positions using the indoor scenario described in Fig. 7. Each subplot in Fig. 8 shows the channel gains between the LED beacon and a single quadrant as a function of the QADA receiver's position. We can see that, when the QADA receiver is located in the center of the room, the channel gains of the four quadrants are relatively large, but have very similar values. However, when the QADA receiver is located close to the corner of the room, the similarity between these four channel gains is significantly reduced. An important feature is that the relationship between these four channel gains is different at every point so the gains, and consequently the photocurrents, uniquely determine the position.

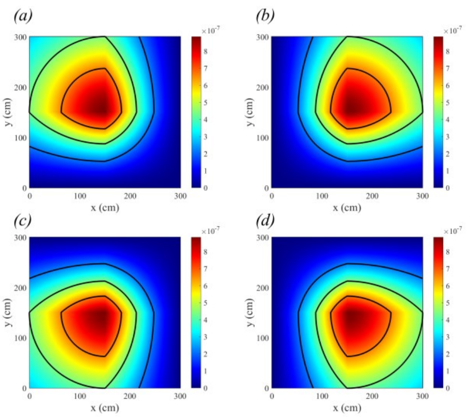

Fig. 8. Channel gain plot for all positions in the room. Each plot represents the channel gain for a single quadrant of the PD.

B. AOA estimation

We now investigate how the accuracy of AOA estimation varies as a function of receiver position. Fig. 9 shows the rMSE and the absolute error in AOA estimation. In Fig. 9 (a) it can be seen that the absolute errors in the estimation of the incident angle are very small for all positions; the largest absolute error in incident angle estimation is only 8.2×10^{-4} degrees. In the corners, where the incident angles are largest, the performance is worst. This is due to the low signal power resulting from lower area of overlap of the light spot and the dependence on d^{-2} and $\cos(\psi)^2$, as expressed in (4). In Fig. 9 (b), it can be seen that the absolute errors in polar angle estimation are also very small for the majority of positions, with most errors below 1×10^{-3} degrees. This is similar in magnitude to the errors in Fig. 9 (a). The largest absolute error in estimation for the polar angle is 0.0117 degrees which is directly below the luminaire. This is because small errors in the estimation of $x_1(t)$ and $y_1(t)$ in these positions can result in large errors in the polar angle estimation.

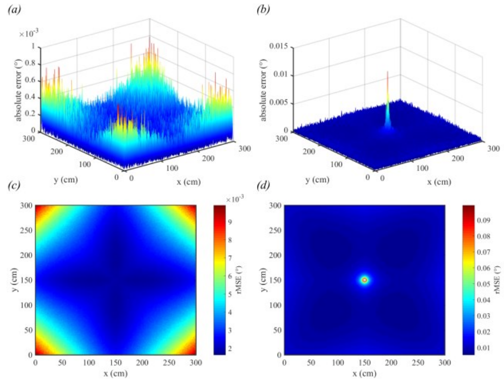

Fig. 9. Absolute error in (a) incident angle and (b) polar angle estimation. rMSE for (c) incident angle and (d) polar angle. For all plots, the receiver is 150 cm below the ceiling and the transmitted power is 3 W.

In Fig. 9 (c) and (d) we look at the root mean square error (rMSE) for incident and polar angle estimation. In general, the rMSE are very small for all positions, but in both plots, we can see that the error is greater at the extremities, as expected. Also, for the polar angle, the central values are also high as we saw in Fig. 9 (b). For clarity, the center values in Fig. 9 (d) have been truncated and thus, the true maximum value was 0.2892°. This is still a very small value. Additionally, the rMSE for the polar angle is smallest when closest to $45°\pm90n°$, where n is any integer. We can extrapolate this data to any LED in any position in the room as it encompasses the entire FOV of the QADA.

To investigate how sensitive the performance of the QADA is to variation in the parameters, we now change the vertical height to 3 m and the transmitted optical power to 1 W. This causes a significant reduction in received optical power. The results are shown in Fig. 10. The overall trends are very similar, however, the magnitude of the absolute error and rMSE are greater. In Fig. 10 (a) we can see that the absolute error for incident angle in the center is worse and in Fig. 10 (b) that a larger portion of the center has a relatively large error than in Fig. 9 (b).

In Fig. 10 (c) and (d) we again look at the rMSE for incident and polar angle estimation. It is important to note that because the height of the room has been increased, the range of incident angles represented is smaller. The rMSE for incident angle are again very small, whilst the rMSE for polar angles have increased but are still small. Again, we have cropped the central values for clarity. It can be seen that the circle of cropped values in the center is larger than Fig. 9 (d). The QADA has difficulty estimating angles when it is directly below the luminaire and these difficulties become more evident as the SNR decreases. The similarities in channel gain for all four quadrants, and hence the lack of angular diversity, at these positions, is a reason for this limitation.

2018 International Conference on Indoor Positioning and Indoor Navigation (IPIN), 24-27 September 2018, Nantes, France

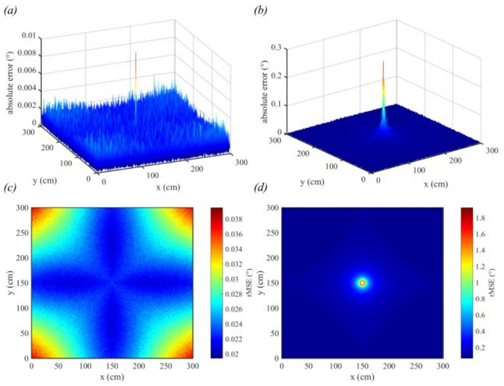

Fig. 10. Absolute error in (a) incident angle and (b) polar angle estimation. rMSE for (c) incident angle and (d) polar angle. For all plots, the receiver is 300 cm below the ceiling and the transmitted power is 1 W

C. Impact of varying height

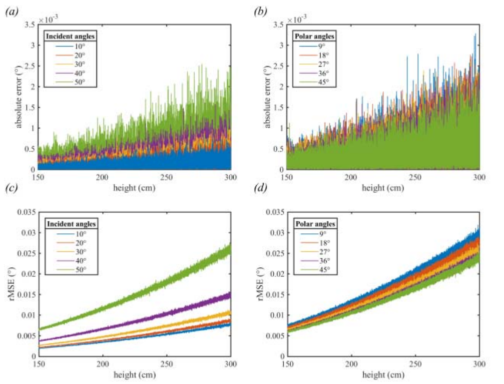

Fig. 11. Absolute error in (a) incident angle and (b) polar angle estimation and rMSE for (c) incident angle and (d) polar angle. Height is varying from 150 cm to 300 cm

We further analyze the impact of increasing the vertical distance, h, between the transmitter and receiver. In Fig. 11, for all angles and heights, the absolute errors and rMSE are small. In Fig. 11 (a) and (c) we keep the polar angle fixed at 45° and vary the incident angle between 10° and 50°. In general, the performance degrades as the height increases for all incident angles due to the reduced optical power received. Larger incident angles are impacted more than smaller incident angles due to the lower SNR.

The rMSE and error in polar angle estimation are shown in Fig. 11 (b) and (d). The incident angle is fixed at 25° and we show polar angles in the first 45° only. These can be extrapolated to other polar angles because of the repeating pattern visible in Fig. 9 (d). The estimation of polar angle is impacted in a similar way to the estimation of incident angle with the worst performance occurring at the largest distance between transmitter and receiver. Also, consistent with Fig. 9, the polar angle 45°performs best.

D. Impact of varying power

We now vary the transmitted power and fix the height at 1.5 m. The power received by QADA is directly proportional to the power transmitted by the LED beacon. The results are shown in Fig. 12. As transmitted power increases, the performance improves, as we expect. The general trends are very similar to the previous example with the varying vertical height, albeit inverted. Interestingly, there is a rapid improvement in performance between 0.5 W and 1 W, with diminishing returns thereafter.

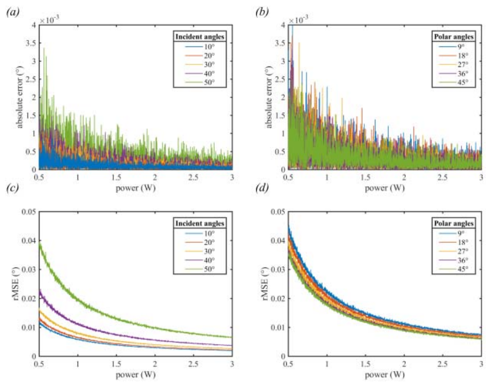

Fig. 12. Absolute error in (a) incident angle and (b) polar angle estimation and rMSE for (c) incident angle and (d) polar angle. Power is varying from 0.5 W to 1 W.

IV. Discussion

The important advantage of this new two-stage hybrid system is that it exploits the strengths of each individual method. In the previous section, it was shown that in ideal circumstances the QADA alone gives excellent estimates of angle of arrival, however, in practice, many factors may degrade the performance, including dust on the aperture, very high ceilings, dimmed luminaires or manufacturing imperfections. By moving to a two-stage system, we relax the requirements for accuracy in the QADA and create a system that is likely to be very robust in most or all realistic applications. The use of visible reference points enables the new two-stage receiver to be used for any shape of luminaire.

The performance of the second, image-based, stage depends very much on the specifications of the camera. As an example, we consider the front-facing camera of a current flagship smartphone. Current flagship smartphones have front cameras with resolution in the range of 7-8 MP, a maximum frame rate of 30 fps, and a wide FOV. Although the back cameras traditionally have higher resolution, it is likely that it will be the front camera that has the luminaires within its FOV, as the user will typically be looking at the screen. If we assume a maximum indoor movement speed of 10 km/hr, which equates to 2.78 m/s, and also assume that images are captured every 0.033 seconds (30 fps), then the position will have only changed by a maximum of 9 cm between estimates. In most indoor applications the receiver position will change much more slowly or even be stationary for long periods of time. So, the accuracy and speed of the new system is likely to be more than adequate for the majority of future applications.

This completely new receiver design opens up many important areas for future study. Questions to be answered include: How can image processing algorithms be optimized for use in the QADA-PLUS receiver, and what accuracy can they achieve? How does the accuracy depend on the position of the LED beacon within the luminaire? What is the optimum type and position of visible reference point? And can multiple reference points within one luminaire improve performance?

V. Conclusion

In this paper, we have introduced a new two-stage receiver structure for visible light positioning. The new structure uses two sensors, one of which is a PD-based sensor and the other is an image-based sensor. We describe how this combination exploits both the ability of PDs to receive and demodulate high frequency signals and the ability of image-based sensors to provide very accurate positioning information. The paper also introduces the use of visible reference points in VLP. These are highly localized features which can be readily identified within an image. Potential reference points are a single colored LED within the luminaire, or a specific corner of the luminaire. The use of precise reference points allows very accurate positioning even when the LED beacons are distributed rather than point sources. Extensive simulation results are presented for the case where the PD-based sensor is a QADA. We have shown that, for a range of practical scenarios, the QADA has excellent angular diversity and can provide very accurate AOA estimation. For the case of a high ceiling and low transmitted power, the majority of errors in estimation of incident and polar angle were below 0.003° and 0.02°, respectively. The QADA sensor has the very important practical advantage over other angular diversity receivers that it has compact planar structure. This advantage is shared by the QADA-PLUS which is the new two-stage structure where a QADA is used in the first stage.

References

[1] J. Armstrong, Y. A. Sekercioglu, and A. Neild, "Visible light positioning: a roadmap for international standardization," *IEEE Commun. Mag.*, vol. 51, no. 12, pp. 68–73, Dec. 2013.

[2] J. Luo, L. Fan, and H. Li, "Indoor Positioning Systems Based on Visible Light Communication: State of the Art," *IEEE Commun. Surv. Tutor.*, vol. 19, no. 4, pp. 2871–2893, Fourthquarter 2017.

[3] H. Liu, H. Darabi, P. Banerjee, and J. Liu, "Survey of Wireless Indoor Positioning Techniques and Systems," *IEEE Trans. Syst. Man Cybern. Part C Appl. Rev.*, vol. 37, no. 6, pp. 1067–1080, Nov. 2007.

[4] H. Zheng, Z. Xu, C. Yu, and M. Gurusamy, "A 3-D high accuracy positioning system based on visible light communication with novel positioning algorithm," *Opt. Commun.*, vol. 396, no. Supplement C, pp. 160–168, Aug. 2017.

[5] W. Gu, M. Aminikashani, P. Deng, and M. Kavehrad, "Impact of Multipath Reflections on the Performance of Indoor Visible Light Positioning Systems," *J. Light. Technol.*, vol. 34, no. 10, pp. 2578–2587, May 2016.

[6] H. Steendam, T. Q. Wang, and J. Armstrong, "Theoretical Lower Bound for Indoor Visible Light Positioning Using Received Signal Strength Measurements and an Aperture-Based Receiver," *J. Light. Technol.*, vol. PP, no. 99, pp. 1–1, 2016.

[7] T. Q. Wang, Y. A. Sekercioglu, A. Neild, and J. Armstrong, "Position Accuracy of Time-of-Arrival Based Ranging Using Visible Light With Application in Indoor Localization Systems," *J. Light. Technol.*, vol. 31, no. 20, pp. 3302–3308, Oct. 2013.

[8] T.-H. Do and M. Yoo, "TDOA-based indoor positioning using visible light," *Photonic Netw. Commun.*, vol. 27, no. 2, pp. 80–88, Apr. 2014.

[9] J. Y. Kim, S. H. Yang, Y. H. Son, and S. K. Han, "High-resolution indoor positioning using light emitting diode visible light and camera image sensor," *IET Optoelectron.*, vol. 10, no. 5, pp. 184–192, 2016.

[10] M. H. Bergen, X. Jin, D. Guerrero, H. A. L. F. Chaves, N. V. Fredeen, and J. F. Holzman, "Design and Implementation of an Optical Receiver for Angle-of-Arrival-Based Positioning," *J. Light. Technol.*, vol. 35, no. 18, pp. 3877–3885, Sep. 2017.

[11] Y.-S. Kuo, P. Pannuto, K.-J. Hsiao, and P. Dutta, "Luxapose: indoor positioning with mobile phones and visible light," in *Proceedings of the Annual International Conference on Mobile Computing and Networking, MOBICOM*, Maui; United States, 2014, pp. 447–458.

[12] S. H. Yang, H. S. Kim, Y. H. Son, and S. K. Han, "Three-Dimensional Visible Light Indoor Localization Using AOA and RSS With Multiple Optical Receivers," *J. Light. Technol.*, vol. 32, no. 14, pp. 2480–2485, Jul. 2014.

[13] L. Wei, H. Zhang, B. Yu, J. Song, and Y. Guan, "Cubic-Receiver-Based Indoor Optical Wireless Location System," *IEEE Photonics J.*, vol. 8, no. 1, pp. 1–7, Feb. 2016.

[14] H. Steendam, "A 3D Positioning Algorithm for AOA-Based VLP with an Aperture-Based Receiver," *IEEE J. Sel. Areas Commun.*, vol. 36, no. 1, pp. 23–33, Jan. 2018.

[15] A. Arafa, S. Dalmiya, R. Klukas, and J. F. Holzman, "Angle-of-arrival reception for optical wireless location technology," *Opt. Express*, vol. 23, no. 6, pp. 7755–7766, Mar. 2015.

[16] "IEEE Recommended Practices for Modulating Current in High-Brightness LEDs for Mitigating Health Risks to Viewers," *IEEE Std 1789-2015*, pp. 1–80, Jun. 2015.

[17] R. Zhang, W. D. Zhong, Q. Kemao, and S. Zhang, "A Single LED Positioning System Based on Circle Projection," *IEEE Photonics J.*, vol. 9, no. 4, pp. 1–9, Aug. 2017.

[18] S. Cincotta, C. He, A. Neild, and J. Armstrong, "High angular resolution visible light positioning using a quadrant photodiode angular diversity aperture receiver (QADA)," *Opt. Express*, vol. 26, no. 7, pp. 9230–9242, Apr. 2018.

[19] S. Cincotta, A. Neild, C. He, and J. Armstrong, "Visible Light Positioning Using an Aperture and a Quadrant Photodiode," in *2017 IEEE Globecom Workshops (GC Wkshps)*, 2017, pp. 1–6.

[20] A. M. Nugrowati, W. G. Stam, and J. P. Woerdman, "Position measurement of non-integer OAM beams with structurally invariant propagation," *Opt. Express*, vol. 20, no. 25, pp. 27429–27441, Dec. 2012.

[21] J. H. G. Huisstede, K. O. van der Werf, M. L. Bennink, and V. Subramaniam, "Force detection in optical tweezers using backscattered light," *Opt. Express*, vol. 13, no. 4, pp. 1113–1123, Feb. 2005.

[22] J. M. Kahn and J. R. Barry, "Wireless infrared communications," *Proc. IEEE*, vol. 85, no. 2, pp. 265–298, Feb. 1997.

[23] J. Proakis, M. Salehi, and G. Bauch, *Contemporary Communication Systems using MATLAB*, 3rd edition. Stamford, USA: Cengage Learning, 2013.

[24] P. Huynh and M. Yoo, "VLC-Based Positioning System for an Indoor Environment Using an Image Sensor and an Accelerometer Sensor," *Sensors*, vol. 16, no. 6, p. 783, May 2016.

[25] R. Zhang, W. D. Zhong, K. Qian, and D. Wu, "Image Sensor Based Visible Light Positioning System With Improved Positioning Algorithm," *IEEE Access*, vol. 5, pp. 6087–6094, 2017.

[26] M. H. Bergen *et al.*, "Design and optimization of indoor optical wireless positioning systems," in *Photonic Instrumentation Engineering III*, 2016, vol. 9754, p. 97540A.

[27] C. Danakis, M. Afgani, G. Povey, I. Underwood, and H. Haas, "Using a CMOS camera sensor for visible light communication," in *2012 IEEE Globecom Workshops*, 2012, pp. 1244–1248.

[28] Y. Nakazawa, H. Makino, K. Nishimori, D. Wakatsuki, and H. Komagata, "Indoor positioning using a high-speed, fish-eye lens-equipped camera in Visible Light Communication," in *International Conference on Indoor Positioning and Indoor Navigation*, 2013, pp. 1–8.

Chapter 7

Indoor Visible Light Positioning: Overcoming the Practical Limitations of the Quadrant Angular Diversity Aperture Receiver (QADA) by Using the Two-Stage QADA-Plus Receiver

7.1 Overview

QADA-plus, introduced in the previous chapter, is a robust receiver structure that overcomes the limitations, in realistic scenarios, of using either a QADA or an imaging sensor alone. The following work provides an in depth investigation into some of the features of realistic scenarios that will influence the accuracy of using a QADA receiver. This includes both the AOA estimation accuracy and the positioning accuracy. Whilst there are many potential sources of error in any positioning system, this work predominantly focused on the impact of luminaire size and shape.

The realistic modelling of luminaires is often overlooked in the literature, with the common assumption that all luminaires are point sources. The shape and size of the luminaire will have a non-negligible impact on AOA estimation with any PD-based AOA sensor, not just a QADA. The simulation results presented here show the accuracy degradation due to luminaire geometry for a QADA receiver, both in the presence and absence of noise. Asymmetric luminaire shapes, such as the common rectangular batten lighting, were shown to perform worse than square and circular luminaires.

Another important consideration with any PD-based receiver is the number of signal samples used to calculate the estimates. In power limited receivers, or when update frequency requirements are high, the number of samples will need to be lower. Large numbers of samples are used to reduce the impact of noise. Thus, reducing the number of samples will lead to an increase in positioning error.

Finally, an extensive discussion emphasises that the presented results examine a limited subset of the potential sources of error and thus should be seen as near to a best-case scenario. Importantly, many of these issues only affect PD-based receivers, such as QADA. In QADA-plus, the AOA estimates from QADA only need to be accurate enough to spatially separate and identify the luminaires in the image. The accuracy of the hybrid receiver is then dependant on the quality of the camera, the image processing, the beacon arrangement and the positioning algorithm.

7.2 Publication

> S. Cincotta, C. He, A. Neild, and J. Armstrong, "Indoor Visible Light Positioning: Overcoming the Practical Limitations of the Quadrant Angular Diversity Aperture Receiver (QADA) by Using the Two-Stage QADA-Plus Receiver," *Sensors*, vol. 19, no. 4, p. 956, Jan. 2019.

The following publication was published in the MDPI journal Sensors. It has been reproduced with the permission of MDPI.

The references are [217] [225] [25] [17] [107] [226] [227] [228] [160] [41] [131] [49] [229] [174] [21] [136] [23] [190] [102] [220] [104] [210] [230] [231] [213] [151] [201] [232] [19] [159] [153] [233] [234] [235] [165] [236]

sensors

MDPI

Article

Indoor Visible Light Positioning: Overcoming the Practical Limitations of the Quadrant Angular Diversity Aperture Receiver (QADA) by Using the Two-Stage QADA-Plus Receiver †

Stefanie Cincotta [1,*], Cuiwei He [1], Adrian Neild [2] and Jean Armstrong [1]

1 Department of Electrical and Computer Systems Engineering, Faculty of Engineering, Monash University, Wellington Rd, Clayton 3800, Victoria, Australia; cuiwei.he@monash.edu (C.H.); jean.armstrong@monash.edu (J.A.)
2 Department of Mechanical and Aerospace Engineering, Faculty of Engineering, Monash University, Wellington Rd, Clayton 3800, Victoria, Australia; adrian.neild@monash.edu
* Correspondence: stefanie.cincotta@monash.edu

† This article is an extended version of our paper published in Cincotta, S.; He, C.; Neild, A.; Armstrong, J. QADA-PLUS: A Novel Two-Stage Receiver for Visible Light Positioning. In Proceedings of the 2018 International Conference on Indoor Positioning and Indoor Navigation (IPIN), Nantes, France, 24–27 September 2018, doi: 10.1109/IPIN.2018.8533733.

Received: 20 December 2018; Accepted: 20 February 2019; Published: 24 February 2019

check for updates

Abstract: Visible light positioning (VLP), using LED luminaires as beacons, is a promising solution to the growing demand for accurate indoor positioning. In this paper, we introduce a two-stage receiver that has been specifically designed for VLP. This receiver exploits the advantages of two different VLP receiver types: photodiodes and imaging sensors. In this new receiver design a quadrant angular diversity aperture (QADA) receiver is combined with an off-the-shelf camera to form a robust new receiver called QADA-plus. Results are presented for QADA that show the impact of noise and luminaire geometry on angle of arrival estimation accuracy and positioning accuracy. Detailed discussions highlight other potential sources of error for the QADA receiver and explain how the two-stage QADA-plus can overcome these issues.

Keywords: visible light positioning; indoor positioning; angle of arrival; QADA; QADA-plus; quadrant photodiode

1. Introduction

Indoor positioning is an important new technology, with a wide variety of applications such as pedestrian navigation, asset tracking, and autonomous robot movement. There has been a lot research dedicated to finding an accurate and economical positioning system, with many potential approaches being explored [1,2]. One approach with huge potential is to use visible light positioning (VLP) [3–5]. In VLP, white LEDS are used for both indoor illumination and high-speed data transmission. VLP can take advantage of this technology by utilizing the LED lighting as positioning beacons that transmit their location using visible light communication (VLC). LEDs are fast becoming the standard choice for indoor lighting due to their energy efficiency and long lifespan, thus they could potentially be found in all buildings in the future. This makes VLP an attractive technology due its low infrastructure cost and its potential to achieve high levels of positioning accuracy.

The recent interest in VLP has resulted in an explosion in the number of papers describing a wide range of different novel indoor positioning systems [4,6,7]. Despite this, so far, no VLP system has emerged that is as useful and versatile as the Global Positioning System (GPS). To understand the challenges that VLP must meet, it is useful to consider the characteristics of GPS.

A GPS receiver works anywhere in the world as long as it can receive signals from enough satellite-mounted GPS transmitters [8]. To operate, a GPS receiver does not require any other source of information, such as access to the internet, or prior knowledge about its current location. Each GPS satellite transmits data about its position and also accurate time information based on the atomic clock carried on each satellite. Each GPS receiver must decode the transmitted information so that it knows the position of each satellite when the signal was transmitted. It must also measure the time difference of arrival of signals from each transmitter. By combining this with information about the satellite position and time, the receiver can estimate its distance from each transmitter and using trilateration attain its current position.

The fundamental challenge for VLP is to design a system, which like GPS, can combine the functions of data receiver and position estimation and so provide accurate position information without access to external databases or stored information. As we will show in the following literature survey, camera based receivers can provide accurate angle-of-arrival (AOA) information, which can be used for triangulation, but the rate at which they can receive data is very limited so they must rely on additional information, while photodiode (PD) based receivers can receive very high speed data, but cannot provide very accurate estimates of distance or angle-of-arrival. The aim of the QADA-plus is to combine the benefits of each receiver type.

A number of camera-based positioning systems have been described [9,10]. To receive data, most camera-based systems depend on the properties of the rolling shutters which are found in the cameras of typical mobile phones. One paper of interest is [11], which provides careful experimental results, and also discusses in detail many practical aspects of this type of system. They identify as a key limitation the very low data rate that can be supported by the rolling shutter approach. They overcome this by assuming that the receiver has access to a database containing the position of each transmitter, and so each luminaire need only transmit an identifying code. Because of the limited data rate of the rolling shutter approach, relatively few different codes can be used, and the system is not scalable. The paper however demonstrates that image-based systems can provide accurate positioning, with an experimentally average error of 7 cm within a 1 m $\times$ 1 m area illuminated by five beacon LEDs. Other papers have also demonstrated that camera-based systems can achieve accurate positioning, with an average error of 3.2 cm [10]. A number of papers have noted that the accuracy depends strongly on the number of beacons that are visible in the image [10,11].

A large number of systems have been described using PD receivers. Many of these are based on measurements of received signal strength (RSS). A disadvantage of RSS systems is that they usually require precise knowledge of the transmit power and the radiation pattern of each luminaire. In practice this information may not be known and/or may change with time as the efficiency of the LEDs in the luminaire reduce with time. The RSS measured at the receiver has also been shown to be sensitive to light reflected from walls [12] and to the precise waveform of the transmitted signal [13]. One way to mitigate the effect of unknown RSS is to use fingerprinting to measure the RSS at positions within the environment and use this stored information in the position calculations [14].

The use of AOA overcomes some of the limitations of RSS. In particular most AOA systems do not require knowledge of the transmitted optical power or the radiation pattern of each luminaire. However, AOA receivers do have to be able to determine the direction of arrival of the light. One way of achieving this is to have PDs with different orientations. Cubic and other structures have been described in the literature [15–17]. Another approach is to use an aperture receiver in which directionality is achieved by having different offsets between the aperture and the PD [18]. It has been shown theoretically [19] that, if it is assumed that there is perfect orientation and positioning of PDs and perfect matching of the receiver electronics, centimeter accuracy can be achieved by these receivers. However, these are unrealistic constraints for a practical system. The QADA structure reduces these constraints by using one aperture and using a quadrant PD with closely matched quadrants, but it does not completely solve the problem, and there is still significant discrepancy between the theoretical results and experimental measurements even under laboratory conditions and short transmission distances [20]. In fact, this is an example of a fundamental limitation of systems using a small number of PDs: the accuracy is strongly dependent on the precise value of the measured signal for each PD.

Time-based systems [21], like the time difference of arrival (TDOA) method used in GPS, are not useful in VLP as they require extremely accurate synchronization. Another approach is to merge information from different sensors, for example information from both a camera and accelerometer is used in [22].

Camera-based positioning is also used in other fields, particularly surveying and robot systems. Particularly relevant is the work on single camera systems using fiducial markers [23,24]. These visual markers are similar to QR codes, but they are specially designed for positioning. Because they may form a relatively small portion of an image and yet must still be both recognizable and decodable, they can only carry a limited number of bits of information. For example, the Apriltag version with 10 checkbits can only have 2221 distinct markers [24], so, like camera-based VLP systems, access to a lookup table is required.

In summary, although many different indoor positioning systems have been proposed, none so far matches the functionality of the GPS system.

In [25] we introduced the quadrant angular diversity aperture (QADA) receiver. This receiver was designed to have a compact, planar structure with low power requirements so that it could be easily incorporated into devices like mobile phones. We have demonstrated that QADA is capable of estimating the AOA of the incoming light [20], however we have also shown that it is extremely sensitive to fabrication imperfection and it is unlikely to achieve the accuracy that is implied by simulation results.

To overcome the challenges faced by QADA, we have developed QADA-plus [26]. This two-stage system provides an elegant solution by combining the QADA with a camera. Taking advantage of the strengths of both sensors, QADA-plus is able to perform well in a wide variety of indoor environments, making it an ideal VLP receiver. In Figure 1, a typical indoor scenario is shown where a person is receiving positioning information on a smart phone that has a QADA-plus. The LED luminaires serve two functions–room illumination and positioning beacons. Each luminaire is transmitting its coordinates, which is then decoded by the QADA and used, in combination with the camera data, to determine the position of the person holding the receiver. This is just one potential implementation of this new receiver design.

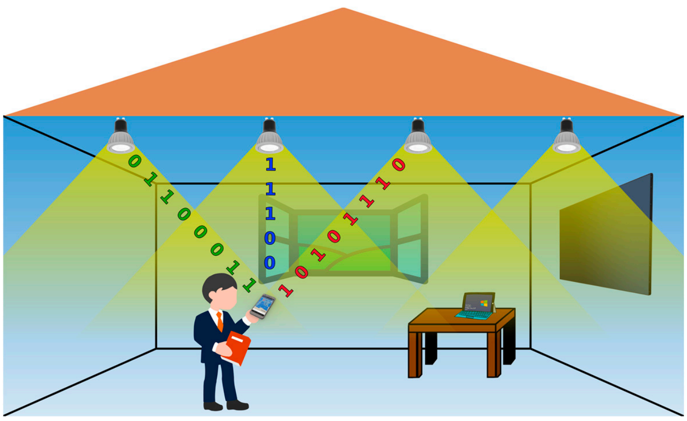

Figure 1. Typical indoor positioning scenario.

In this paper, we demonstrate the limitations of the QADA receiver by individually exploring several sources of error. At each stage we highlight the assumptions made in the simulation models and the other potential sources of error that will lead to further performance degradation.

The contributions in this paper are:

1. Detailed discussion of the potential sources of error for the QADA and how adopting the two-stage system will lead to better performance.
2. Description of reference points and their importance in precise indoor positioning.
3. In depth analysis of the impact of luminaire size and shape on the QADA receiver.
4. Triangulation results for the QADA that show how noise, luminaire shape and size and room dimensions impact on positioning accuracy.

2. Indoor Positioning with QADA and QADA-Plus

QADA-plus is a new form of two-stage receiver for VLP. A unique feature of this receiver is that it exploits the different advantages of PD-based receivers and camera-based receivers. This creates a hybrid receiver that is purpose designed for VLP. It consists of a QADA, which is ideal for receiving high-speed data with approximate AOA information, and a camera which captures high resolution images that are used to add accuracy to the estimated angles. Reference points are a further optional enhancement for use with QADA-plus that can improve accuracy.

2.1. QADA Design

This section details the design of QADA which is the first stage sensor in the QADA-plus receiver. QADA, shown in Figure 2, couples a quadrant PD with an aperture to create an angular diversity receiver that is compact and can be constructed from standard off-the-shelf components. A quadrant PD is made up of four individual PDs closely arranged in a 2×2 grid, with a small gap separating the quadrants. Unlike conventional applications, such as atomic force microscopy [27], that use quadrant PDs with laser light [28], our innovative use of an aperture means that QADA can be used with standard indoor illumination.

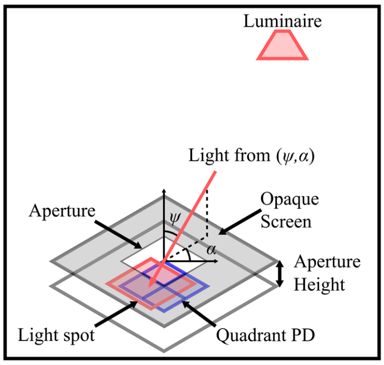

Figure 2. QADA receiver design.

The location of the centroid of the light spot that falls on the quadrant PD unambiguously determines the AOA. An important feature is the known aperture height, which is the vertical distance separating the aperture plane from the quadrant PD plane. This aperture height is selected to determine the field of view (FOV) of the QADA and, because it is a known value, it can be combined with the centroid of the light spot to estimate the incident and polar angles of the light.

An important advantage of using a square shape for the quadrant PD and the aperture is that the area of the light spot which overlaps the PD changes linearly as it passes over the PD. The aperture size matches the quadrant PD size exactly to maximize the received light. It is not possible to use an aperture that is larger than the quadrant PD as this would lead to ambiguity when estimating the AOA.

2.2. QADA-Plus

For many applications that require only approximate localization QADA alone may be adequate. Although theoretical results for QADA in ideal conditions [20,25,26] show promising results, in practice, factors such as minor changes to the aperture or partial blockages of the light path to the luminaire limit the accuracy that can be achieved. In [20], we demonstrated with a carefully controlled small-scale experiment that there was a large discrepancy between experimental and simulation results. This highlighted the limitations of the simulation results and also of the ability of the QADA to provide precise positioning. For applications that do require high accuracy, QADA can be improved by adding a second stage imaging sensor to become QADA-plus. QADA is a high speed but low pixel sensor, that can offer moderate accuracy, whilst a camera is a low speed, but high pixel sensor that offers high accuracy. For the two-stage system, the requirements for a highly calibrated and accurate QADA are much lower. An important requirement is that the QADA is sufficiently accurate to be able to identify the luminaires. The precise image co-ordinates of the identified LED beacons are used in a triangulation algorithm like the one we detailed in [26].

Figure 3 demonstrates how the two sensors work together in the QADA-plus receiver. LEDs installed in the ceiling of a room are transmitting information about their position in a local or global coordinate system, as shown in Figure 1. We call this transmitted information the beacon information packet (BIP). The transmitted signals are designed to be orthogonal and thus signals from multiple luminaires can simultaneously be separated by the QADA receiver. For each luminaire, QADA detects the angle of the incoming light and decodes the transmitted data. The position of each luminaire, along with the respective AOA, is then sent to a processing unit. While QADA is estimating the AOAs and decoding the data, a camera, with the same orientation as the QADA (as seen in Figure 4) captures an image of the luminaires on the ceiling. Using the AOAs, each luminaire that was detected by QADA is located in the image. The receiver now knows the identity and location of each luminaire and so long as sufficient luminaires are visible, triangulation from the high-resolution image occurs, providing an accurate position estimate in three-dimensions.

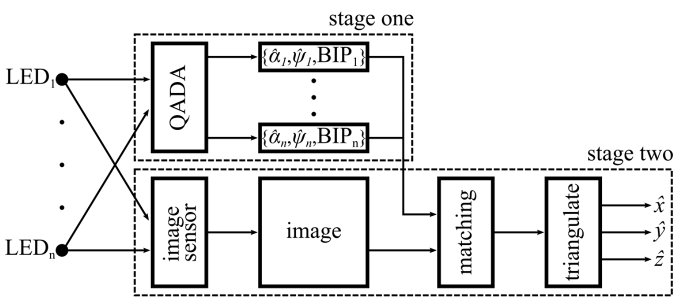

Figure 3. Block diagram showing the flow of information of QADA-plus.

Figure 4. QADA-plus in a typical smartphone. The inset shows the QADA sensor located next to the standard front-facing camera.

An example of a potential configuration of the two sensors is shown in Figure 4 where a QADA sensor is located next to the front-facing camera on a typical smartphone. This figure demonstrates an important future application for the QADA-plus. These cameras typically have a sufficient FOV and high pixel counts, making them ideal for accurate AOA estimation in the second stage. Another future configuration is a stand-alone widget that can be placed on assets or drones. For the purpose of asset and robot tracking, an additional uplink would be required to send the position back to the central control or monitoring unit. This uplink could be radio-frequency, infrared or VLC [29].

2.3. Reference Points

Reference points associated with luminaires, first described in [26], are a novel addition to camera-based VLP and are an important optional feature for systems using QADA-plus. A reference point is a visibly distinct location that can be detected by the imaging sensor. It is used to increase the precision when identifying the positions in the image that will be used for triangulation.

Potential reference point types may include: a single LED of a different wavelength that may or may not be visible to the human eye, a small mark on the luminaire frame or nearby to the luminaire, or a well-defined position in the luminaire, such as a corner. As a default, the reference point would be the centroid of the luminaire. Also, because the information about the reference point is transmitted by the luminaire, the particular reference point type and size that is chosen for a system can be optimized for the specific application.

In Figure 5, an image captured from the front-facing camera of a smartphone shows four batten luminaires demonstrating reference points. Batten luminaires, as well as linear lighting, are very commonly used in large commercial and industrial buildings. In this example, the reference point is a single red LED in the corner of each luminaire, however it would be possible to have more than one reference point on each luminaire. The overlay shows the information that is provided to the second stage from the QADA sensor. The estimated AOA is used to match the luminaires to the co-ordinates which have been transmitted in the BIPs and the imaging sensor can then detect the precise positions of the reference points to use in the triangulation algorithm. The number, type and location of the reference points may be globally defined for the system or can be transmitted in the BIP.

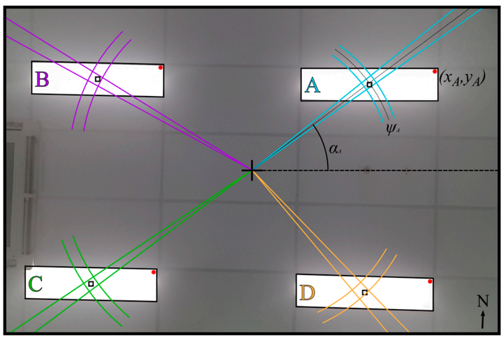

Figure 5. Image captured by smartphone camera showing four luminaires with a single red reference point each.

In many buildings the luminaires are large and sparsely spaced. It can be difficult to guarantee that enough luminaires will be captured in a single image frame to support triangulation. It can also be difficult to capture the entire luminaire in the frame, thus making it challenging to determine the centroid. In the case of large luminaires, there is the option of having multiple reference points for a single luminaire, thereby reducing the number of luminaires that must be visible to allow triangulation. This means that, so long as sufficient reference points are visible, partially obscured luminaires will still contribute to the positioning accuracy as there is no requirement that all of their reference points are visible. This is very advantageous as it also relaxes the need for a very large FOV for both the imaging sensor and the QADA.

3. QADA Triangulation Algorithm

To estimate the position of the receiver, a triangulation algorithm is needed. QADA estimates the AOA of the light from multiple luminaires simultaneously. As long as enough luminaires are in the FOV, it is possible to triangulate from this information.

Positioning accuracy is not just affected by the accuracy of the AOA estimates but it is also sensitive to the relative positions of the luminaires and the room dimensions as this will impact the geometric dilution of precision (DOP) [30].

The AOA is composed of two angles; the incident angle, ψ, and the polar angle, α. Figure 6 shows an indoor room scenario with four transmitting LEDs and one receiver. For this algorithm and the simulations in later sections, it is assumed that the receiver is pointing directly up towards the transmitters and thus the incident angle is equal to the emergence angle, ϕ. The transmitters are located at $(x_{L,n}, y_{L,n}, z_{L,n})$, where n is the LED index, and the receiver is located at (x_R, y_R, z_R). From the diagram, it can be seen that:

$$\begin{aligned} \delta x_n &= x_R - x_{L,n} \\ \delta y_n &= y_R - y_{L,n} \end{aligned} \tag{1}$$

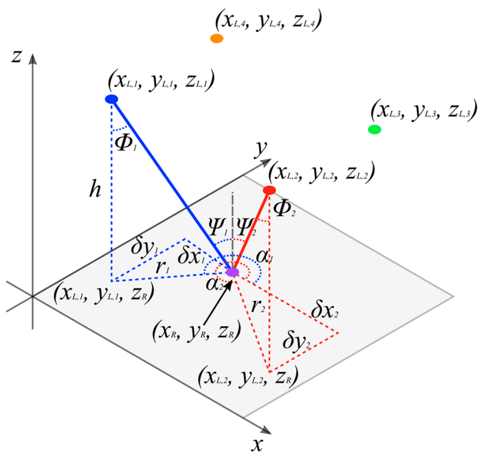

Figure 6. Co-ordinate system and angles used for triangulation algorithm.

The vertical distance from the transmitter to the receiver plane is h and the projection onto the receiver plane of the line from the nth transmitter to the receiver is defined as r_n. Using simple geometry, the relationship between these two variables is given by:

$$\begin{aligned} r_n &= h \tan \psi_n \\ &= (z_{L,n} - z_R) \tan \psi_n \end{aligned} \tag{2}$$

Thus, to find x_R, the relationship between r_n and δx_n can be used to give:

$$\begin{aligned} x_R &= x_{L,n} + (z_{L,n} - z_R) \tan \psi_n \cos \alpha_n \\ &= x_{L,n} + z_{L,n} \tan \psi_n \cos \alpha_n - z_R \tan \psi_n \cos \alpha_n \end{aligned} \tag{3}$$

The same process can be applied to find y_R. If N transmitters are present, an estimate of the position of the receiver can be found using linear least squares estimation:

$$\hat{\mathbf{x}} = \left(\mathbf{A}^T\mathbf{A}\right)^{-1}\mathbf{A}^T\mathbf{b} \tag{4}$$

where:

$$\mathbf{A} = \begin{bmatrix} 1 & 0 & \tan\psi_1\cos\alpha_1 \\ 0 & 1 & \tan\psi_1\sin\alpha_1 \\ \vdots & \vdots & \vdots \\ 1 & 0 & \tan\psi_N\cos\alpha_N \\ 0 & 1 & \tan\psi_N\sin\alpha_N \end{bmatrix}, \mathbf{x} = \begin{bmatrix} x_R \\ y_R \\ z_R \end{bmatrix}, \mathbf{b} = \begin{bmatrix} x_{L,1} + z_{L,1}\tan\psi_1\cos\alpha_1 \\ x_{L,1} + z_{L,1}\tan\psi_1\sin\alpha_1 \\ \vdots \\ x_{L,N} + z_{L,N}\tan\psi_N\cos\alpha_N \\ x_{L,N} + z_{L,N}\tan\psi_N\sin\alpha_N \end{bmatrix} \tag{5}$$

4. Analysis and Limitations of QADA

In this section, the QADA receiver is analyzed in detail and the limitations of the assumptions made are highlighted. The received optical power, P_R, is proportional to the transmitted optical power, P_T with the relationship $P_R = h_j P_T$, where h_j is the DC channel gain. In general, luminaires have diffusers that alter the radiation pattern of the LEDs. However, for this analysis the LED transmitters are assumed to have a Lambertian radiation pattern of order $m = 1$. Thus, the channel gain for the jth quadrant at time, t, is given by [31]:

$$h_j(t) = \frac{(m+1)A_j(t)}{2\pi d^2(t)}\cos^m(\phi(t))T_s(\psi(t))g(\psi(t))\cos(\psi(t)) \tag{6}$$

where d is the distance between the transmitter and the receiver, $A_j(t)$ is the area of quadrant j which the light spot overlaps, $T_s(\psi(t))$ is the signal transmission of the filter and $g(\psi(t))$ is the concentrator gain. We consider the case where the incident and emergence angles are equal, and the QADA does not have any optical filters or lenses, thus these values are set to 1. Therefore, the photocurrent, $i_j(t)$, in the jth quadrant at time, t, is:

$$i_j(t) = \frac{RP_T A_j(t)\cos^2(\psi(t))}{\pi d^2(t)} \tag{7}$$

where R is the responsivity of the PD.

Light Spot Centroid Estimation

To determine the centroid, $[x_1(t), y_1(t)]$, of the light spot, the ratio of the photocurrents from adjacent quadrant pairs is used. As the ratios depend on the relative values of the photocurrents and not the absolute values, QADA is insensitive to fluctuations in the power transmitted by the LEDs. From Equation (7), it can be seen that the photocurrent from each quadrant of the PD is proportional to the area of overlap with the light spot. This unrealistically assumes that the responsivity is uniform across the active area of the PD [32]. Thus, the ratios used to find the centroid are:

$$p_x = \frac{i_1(t) + i_4(t) + N_1(t) + N_4(t)}{i_2(t) + i_3(t) + N_2(t) + N_3(t)} \tag{8}$$

$$p_y = \frac{i_1(t) + i_2(t) + N_1(t) + N_2(t)}{i_3(t) + i_4(t) + N_3(t) + N_4(t)} \tag{9}$$

where $N_j(t)$ is the noise in the jth quadrant at time, t. This is shown in Figure 7 where the ratio of the left and right quadrant pairs is used to find $x_1(t)$ and the ratio of the top and bottom quadrant pairs is used to find $y_1(t)$. The dominant noise in the system is the shot noise due to background light. This is modelled as a white Gaussian process with zero mean and variance given by:

$$\sigma^2_{\text{shot}} = 2qRp_{\text{n}}A\Delta\lambda B \tag{10}$$

where q is the charge of an electron, p_n is the spectral irradiance, A is the area of a PD quadrant, $\Delta\lambda$ is the optical bandwidth and B is the electrical bandwidth.

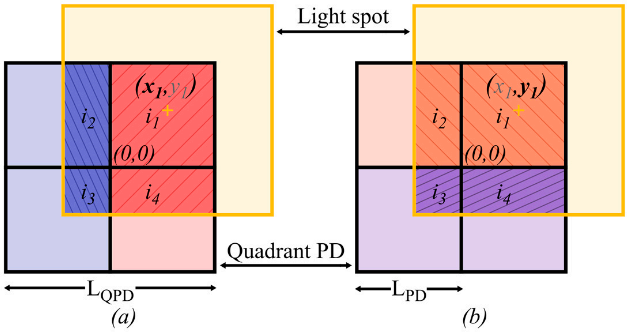

Figure 7. Light spot overlapping the quadrant PD. In (**a**), finding x_1 uses the ratio of the red and blue segments and in (**b**), finding y_1 use the ratio of the orange and purple segments.

It is important to note that the noise terms can be averaged out over many samples to reduce the errors, however manufacturing limitations will limit how well the photocurrents relate to the AOA. For example, Equations (8) and (9), assume that the individual PD quadrants are perfectly matched, which is unrealistic.

To estimate the centroid, the ratio functions are considered in the absence of noise, where they reduce to the ratio of the areas of overlap. If L_{PD} is the length of a single quadrant, then Equations (8) and (9) become:

$$p_x(t) = \frac{A_1(t) + A_4(t)}{A_2(t) + A_3(t)} = \begin{cases} \frac{L_{\text{PD}}+x_1(t)}{L_{\text{PD}}}, & -L_{\text{PD}} < x_1(t) \leq 0 \\ \frac{L_{\text{PD}}}{L_{\text{PD}}-x_1(t)}, & 0 < x_1(t) < L_{\text{PD}} \end{cases} \tag{11}$$

$$p_y(t) = \frac{A_1(t) + A_2(t)}{A_3(t) + A_4(t)} = \begin{cases} \frac{L_{\text{PD}}+y_1(t)}{L_{\text{PD}}}, & -L_{\text{PD}} < y_1(t) \leq 0 \\ \frac{L_{\text{PD}}}{L_{\text{PD}}-y_1(t)}, & 0 < y_1(t) < L_{\text{PD}} \end{cases} \tag{12}$$

As can be seen from Equation (11), the values of $x_1(t)$ and $y_1(t)$ do not depend on each other and thus can be estimated independently. With the dependence on L_{PD}, the assumption again is that all the quadrants of the PD are identical. Thus, any small manufacturing imperfection will impact the accuracy of the estimation.

For each quadrant of the PD, the received signals undergo low pass filtering to limit the bandwidth to B hertz and are then sampled at the Nyquist rate, $2B$. A matched filter is used to select the desired signal and reject orthogonal signals and the result is then averaged over M samples and substituted in Equations (8) and (9) to give an estimate at time $t = (k + M)/2B$. This process is shown in Figure 8. The estimate for $x_1(t)$ is expressed in Equation (13) and, using the same logic, a similar expression can be derived for $y_1(t)$.

$$\hat{x}_1\left[\frac{k+m}{2B}\right] = \begin{cases} L\left(p_x\left[\frac{k+M}{2B}\right] - 1\right), & -L < x_1\left[\frac{k+m}{2B}\right] \leq 0 \\ L - \frac{L}{p_x\left[\frac{k+M}{2B}\right]}, & 0 < x_1\left[\frac{k+m}{2B}\right] < L \end{cases} \tag{13}$$

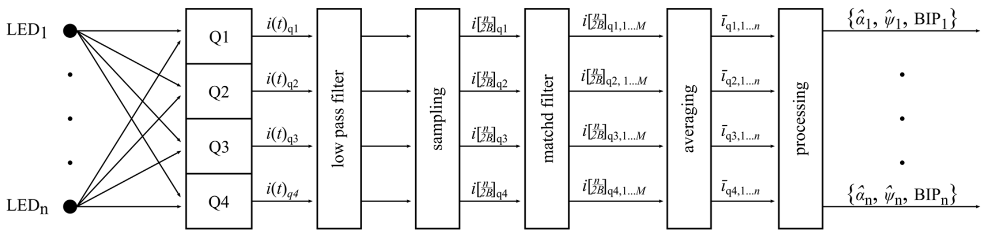

Figure 8. Digital signal processing path for QADA.

5. AOA Estimation for QADA

In this section, simulation results for AOA estimation are presented. It is important to note, that whilst the simulation parameters have been chosen to be realistic, the simulations do not take into account all sources of error. To be clear about the contributions of different sources of error to the limitation of QADA, we start by considering the case where the only source of error is noise. We assume the ideal case of a point source and a QADA with none of the limitations discussed in the previous section. Our previous experimental work in [20] demonstrates the limitations of assuming ideal cases in simulations. Next is an investigation on the impact of changing the size and shape of the LED transmitter. It is obvious that in the presence of multiple realistic sources of error, the performance of the receiver will be worse than the results presented below.

The parameters used in the simulations are shown in Table 1. The noise equivalent power is taken from the datasheet of a Hamamatsu quadrant PD [33] and the spectral irradiance is widely reported in the literature [31].

Table 1. Simulation Parameters.

Parameter	Value
Quadrant PD size	5 mm $\times$ 5 mm
Aperture height	2.5 mm
QADA FOV	90°
Responsivity	0.25 A/W
Electrical bandwidth	1 MHz
Optical bandwidth	300 nm
Noise Equivalent Power	1.9×10^{-14} W/$\sqrt{\text{Hz}}$
Spectral irradiance	6.2×10^{-6} W/(nm·cm)^2

5.1. *Angle of Arrival Accuracy for a Point Source*

The ability of the QADA receiver to estimate the incident and polar angles is first evaluated. Initially, the room configuration in Figure 9a is used where a single luminaire, transmitting 3 W of optical power, is located in the center of the ceiling of a room with dimensions 3.0 m $\times$ 3.0 m $\times$ 3.0 m. After low pass filtering, the transmitted signal is sampled at the Nyquist rate and averaged over 10 milliseconds, resulting in 20,000 samples used for a single estimate. The incident and polar angles are estimated for all positions in the room at a vertical distance of 1.5 m from the ceiling. We do not consider the effect of reflected light from the walls. This scenario represents an ideal case for indoor positioning with the receiver pointing directly up and the luminaires modelled as point sources.

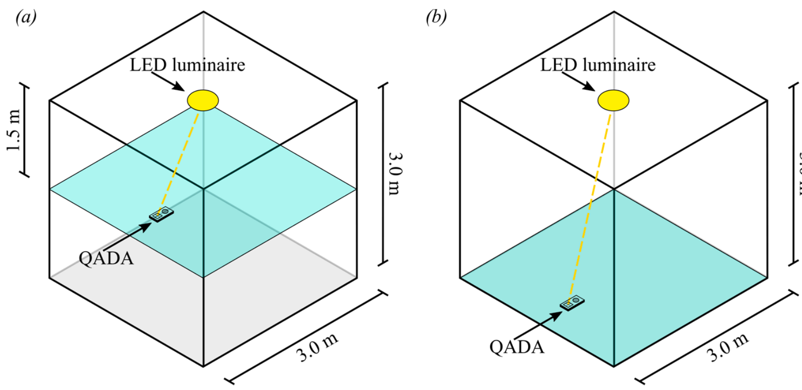

Figure 9. Two different room configurations used for the simulations. In (**a**) the vertical distance between the transmitter and the receiver is 1.5 m and in (**b**) the vertical distance between the transmitter and the receiver is 3.0 m.

The results shown in Figure 10 demonstrate the general trends of the root-mean-square-error (rMSE) for incident (a) and polar (b) angles. The values of the rMSE are very small only because a large number (20,000) of samples were used. It can be seen that the incident angle estimation is least accurate in the corners of the room and the polar angle estimation is worst in the center of the room. Also, from Figure 10b, it can be seen that the polar angles close to 45 + 90n° (where n is any integer) have lower rMSE than those closer to 0 + 90n°. This effect is much less noticeable than the large peak in the central values.

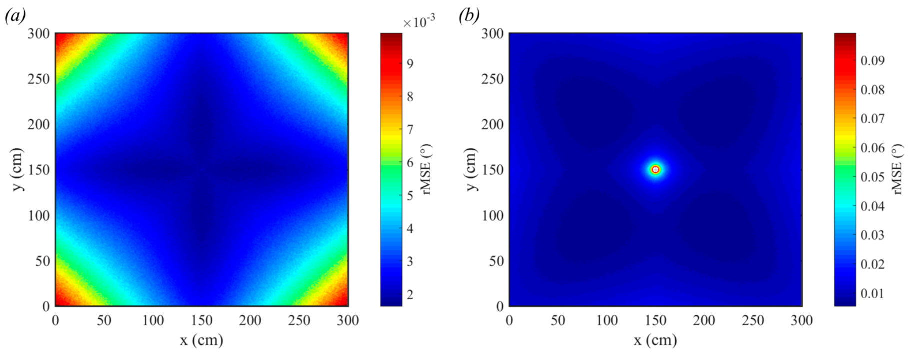

Figure 10. rMSE for incident angle detection (**a**) for polar angle detection (**b**). The transmitted power is 3 W, the vertical distance from the transmitter to the receiver is 1.5 m and each estimate is the average of 20,000 samples.

To demonstrate the sensitivity of QADA to reduced received optical power, the height was increased to 3.0 m and the transmitted power of the LED was reduced to 1 W. This room configuration is shown in Figure 9b. The results, in Figure 11, show that the rMSE has increased significantly for both incident (a) and polar angle (b) estimation. In particular, the polar angle estimation in the center of the room has worsened with an rMSE of almost 1.8°. Although the magnitude of the rMSE seem small, these simulations assume unrealistic ideal circumstances. The only source of error is the noise.

Figure 12 uses the same room configuration as used in Figure 11, however the results show the absolute error in AOA estimation. The absolute error in incident angle estimation is shown in Figure 12a and the absolute error in polar angle estimation is shown in Figure 12b. In Figure 12c we show a truncated version of Figure 12b where the errors greater than 1° have been removed to reveal additional detail. The incident angle maximum error is 0.13° and the mean error is 0.02°.

For polar angle, the maximum error is 11.78° and the mean error is 0.08°. In both cases, the minimum error is extremely close to zero. The polar angle is particularly inaccurate in the center of the room because, for these positions, small estimation errors in the centroid position have the potential to cause large errors in polar angle estimation. This data demonstrates that to achieve the greatest accuracy, the results must be averaged over a large number of samples.

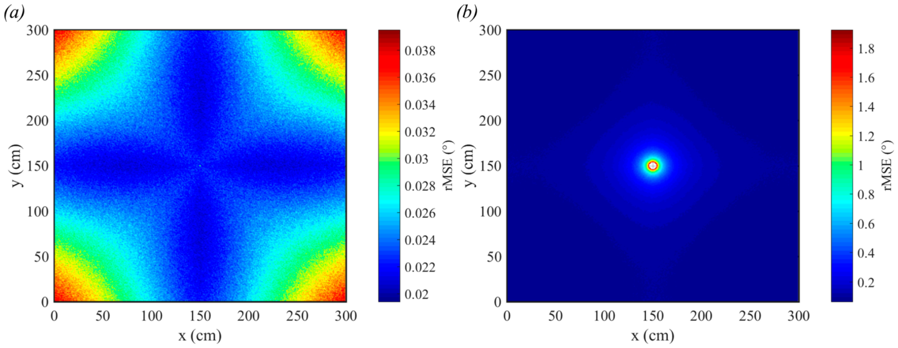

Figure 11. rMSE for incident angle detection (**a**) for polar angle detection (**b**). The transmitted power is 1 W, the vertical distance from the transmitter to the receiver is 3.0 m and each estimate is the average of 20,000 samples.

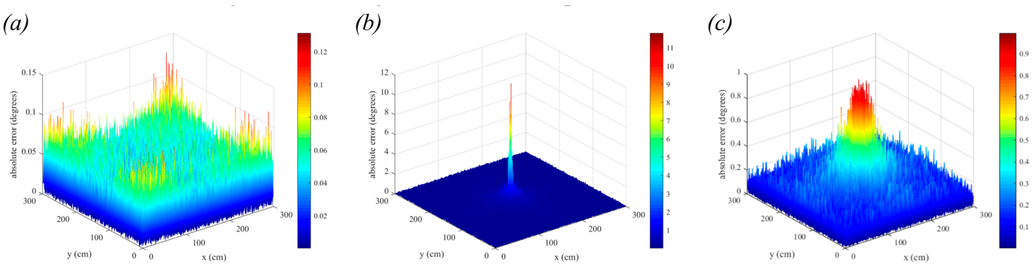

Figure 12. Single trial absolute error for incident angle detection (**a**) and polar angle detection (**b**). In (**c**), the large errors in the center of (**b**) have been removed to show additional detail. The transmitted power is 1 W, the vertical distance from the transmitter to the receiver is 3.0 m and each estimate is the average of 20,000 samples.

5.2. Impact of Luminaire Size and Shape on AOA Estimation

The previous simulations made the unrealistic assumption that the transmitting LED was modelled as a point source. The following results show a more realistic scenario where the transmitter is a LED luminaire that has a finite size and shape. We investigate the effect that changing the size and shape of this LED luminaire has on the ability of the QADA to estimate the AOA and how this reduces the accuracy that can be achieved. This reduction in accuracy is because the receiver has no knowledge of the luminaire geometry, thus, to be able to estimate the AOA it assumes the luminaire is a point source. Three different common luminaire shapes are compared: square, circular and rectangular. For the square shape, the effect of increasing the size of the luminaire is also shown. Each luminaire is modelled as an array of 2500 equally spaced Lambertian transmitters. We do not consider the impact of diffusers, though, in practice, diffusers are carefully designed to meet lighting requirements with minimum power usage [34]. The parameters used are the same as those in Table 1 and the room configuration is that shown in Figure 9a.

5.2.1. Varying Luminaire Size

Figure 13 shows the absolute errors for incident (a) and polar angle (b) estimation when a small square luminaire with side length 10 cm is used. For the incident angle, the errors in the outer edges of the room dominate, whilst for the polar angle the errors are greatest in the corners. In both cases, the maximum estimation errors are close to 0.25° (0.26° for incident angle and 0.24° for polar angle). The large errors in the extremities of the room are because the entire luminaire is not in the FOV of the QADA in these locations. This demonstrates one of the limitations of QADA.

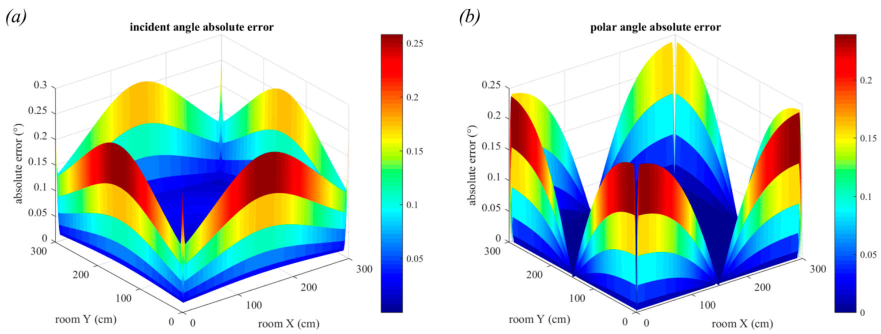

Figure 13. Absolute error in incident angle estimation (**a**), and in polar angle estimation (**b**), for a square luminaire with side length 10 cm.

In Figure 14a,b the outer edges of the room are omitted so that the smaller estimation errors in the central part of the room are clearer. In this region, the incident angle estimation is most accurate directly below the luminaire, whilst the polar angle is least accurate. The polar angle estimation experiences decreased estimation accuracy in the regions close to 0 + 90n°, whilst for all other parts of the room, the error is close to 0°. The mean incident angle error is 0.026°, whilst the mean polar angle error is close to 0°.

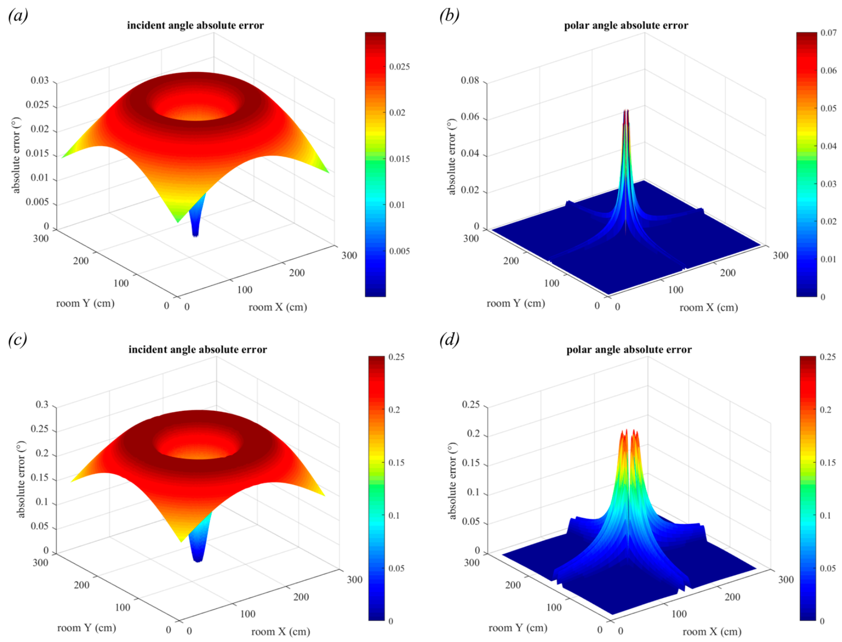

Figure 14. Absolute error in incident angle estimation and in polar angle estimation for a square luminaire with side length 10 cm, (**a**,**b**), and for a square luminaire with side length 30 cm, (**c**) and (**d**).

In Figure 14c,d the size of the square luminaire has been increased to 30 cm. Whilst the overall trend remains the same, the maximum estimation errors have increased to 0.86° for the incident angle and 0.68° for the polar angle. It can be seen that the maximum incident angle error is 0.26°, a tenfold increase from the smaller 10 cm luminaire, and the maximum polar angle error is 0.22°, also a very large increase. The mean errors are 0.22° for incident angle and 0.008° for polar angle. Again, the results show the effect of one source of error only. Thus, whilst the errors may seem small, the cumulative effect of all the errors must be considered. These results are primarily to highlight the trends and to demonstrate the degradation in performance as parameters are varied.

5.2.2. Varying Luminaire Shape

In this section, the figures show only the portions of the room where the receiver can see the entire luminaire in the FOV. The results for a circular luminaire with diameter 30 cm are shown in Figure 15. Both this figure and the corresponding subfigures (c) and (d) from Figure 14 are on the same scale, allowing for direct comparison. Interestingly, the results are very similar to those of the square luminaire with side length 30 cm. However, the circular luminaire does perform marginally better than the square luminaire. The maximum errors for incident angle estimation are 0.23° and for polar angle estimation are 0.21°. The mean errors in this region are 0.19° for incident angle and 0.006° for polar angle. The reason the circular luminaire performs better than the square luminaire is because the circular one has a smaller area than the square. Later, we will show the effect this small improvement has on positioning error.

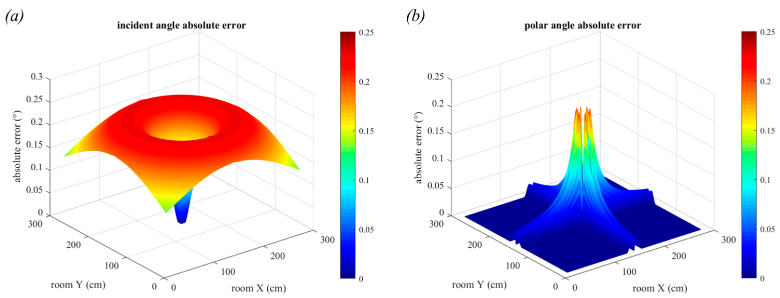

Figure 15. (**a**) Absolute error in incident angle estimation, and (**b**) in polar angle estimation for a circular luminaire with diameter 30 cm.

The dimensions that are used for the rectangular luminaire are 30 cm × 60 cm, with the long side aligned with the *x*-axis. The results for this luminaire are shown in Figure 16. It can be seen that they are significantly worse than those of the square and circular, with the maximum error in incident angle of 1° and for polar angle, the maximum error was 1.06°. The results are worse along the *x*-axis is because it is aligned with the longer side of the rectangle. The performance degradation seen with the rectangular luminaire is because it has fewer planes of symmetry than the square and the circular ones.

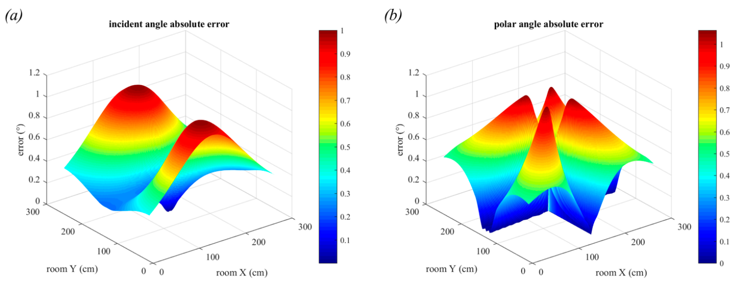

Figure 16. (**a**) Absolute error in incident angle estimation, and (**b**) in polar angle estimation for a rectangular light with dimensions 30 cm × 60 cm.

6. Triangulation Simulations Using QADA

The ultimate goal of QADA is not AOA estimation, but positioning, and thus this section details the effect that the errors in AOA estimation have on positioning accuracy. Positioning error is defined as the Euclidean distance from the estimated position to the true position. In the following simulations, the parameters used are in Table 1, the triangulation algorithm is from Section 3 and the room configuration is shown in Figure 17. In all three cases, the centroids of the luminaires are located at {(75, 75, 300), (75, 225, 300), (225, 75, 300), (225, 225, 300)} cm. These positions are chosen so that the luminaires are evenly distributed in the room. This is not entirely realistic as luminaires are often not evenly spaced. Again, we consider a best-case scenario and different configurations and receiver orientation would give worse results.

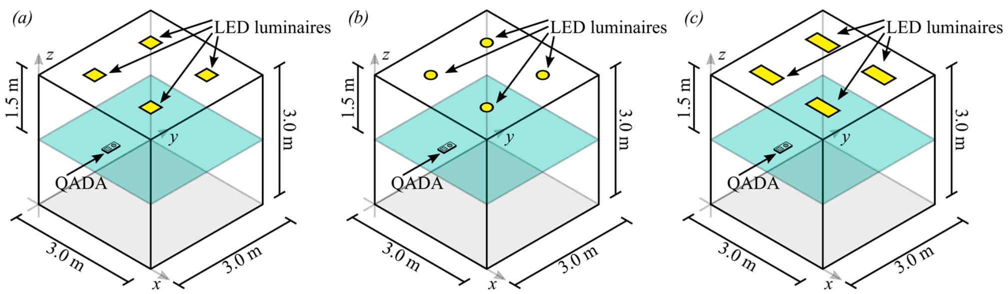

Figure 17. Room configurations for triangulation simulations. In (**a**), square luminaires with side length 30 cm are used, in (**b**), circular luminaires with diameter 30 cm are used and in (**c**), rectangular luminaires with dimensions 30 cm × 60 cm were used. In all cases, the centers of the luminaires are 75 cm from the edges of the room.

Measurements are taken for all positions on a plane that is 1.5 m below the luminaires. To ensure the entirety of each luminaire is in the FOV of the QADA in all positions, the aperture height is changed to 1.25 mm. We have previously shown in [25] that increasing the FOV of QADA will result in worse performance in the presence of noise.

6.1. Triangulation in the Absence of Noise

Initially, the simple case with no noise is considered, thus the only source of positioning error is the size and shape of the luminaire. Figure 18 shows the positioning errors for the scenarios in Figure 17a,b with the square and circular luminaires, respectively. There are many positioning applications that do not require three-dimensional positioning and thus in Figure 18a,b the errors in only the x-y plane are considered. The errors are much smaller if only two-dimensions are considered, with the maximum error of 0.53 cm for the square luminaires and 0.47 cm for the circular luminaires. In contrast, the maximum error in three-dimensions was 1.3 cm for the square luminaires and 1.24 cm for the circular luminaires. When only two-dimensions are considered, the largest errors are in the corners of the room, however in three-dimensions the largest error is in the center of the room. The corners have very similar errors in both cases, but the errors in the center of the room have greatly increased in three-dimensional positioning. This is caused by the contribution from the error in the estimation of the z co-ordinate which is large in the center of the room and small in the corners. It might appear from these results that QADA alone is capable of providing accurate positioning, however it should be noted that these results are only showing the impact of a single source of error.

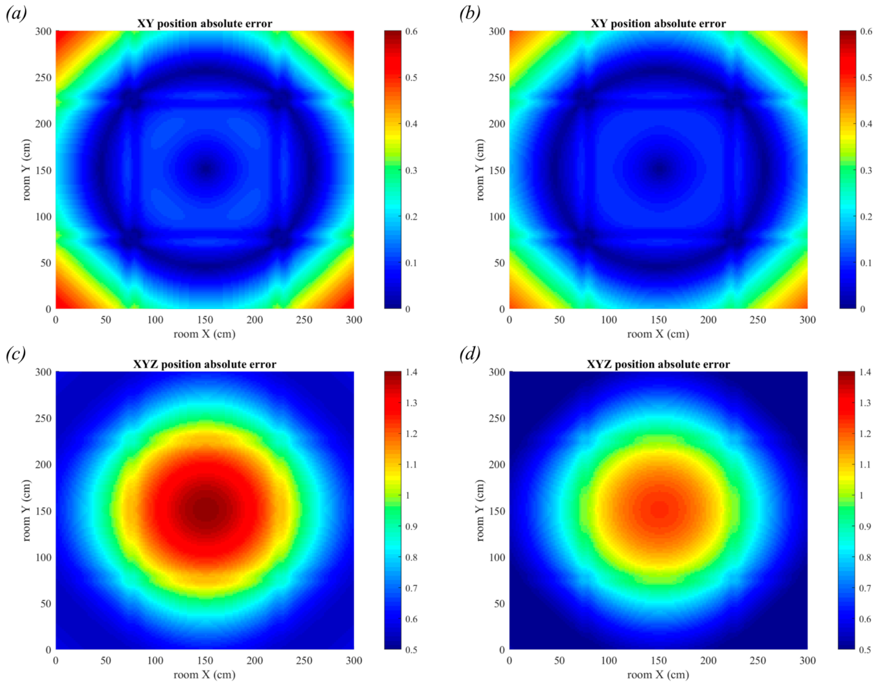

Figure 18. Positioning error for square luminaires with side length 30 cm, (**a**,**c**), and circular luminaires with diameter 30 cm, (**b**,**d**). Errors in two-dimensions are shown in (**a**,**b**) and errors in three-dimensions are shown in (**c**,**d**).

For comparison, the error when using rectangular luminaires is shown in Figure 19, using the configuration shown in Figure 17c.

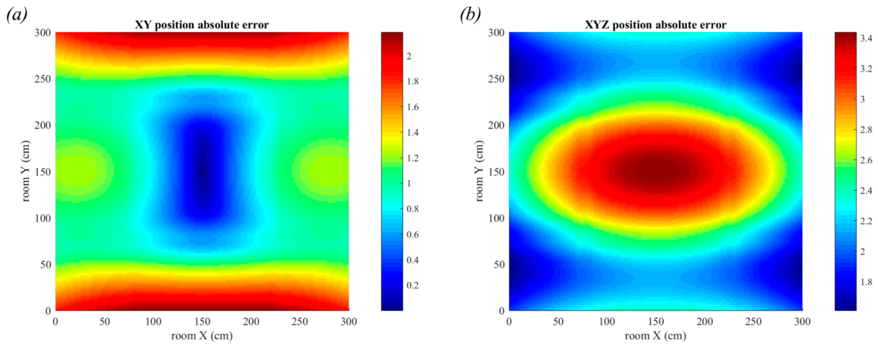

Figure 19. Positioning error for rectangular luminaires with dimensions 30 × 60 cm. Errors in two-dimensions are shown in (**a**) and errors in three-dimensions are shown in (**b**).

The large errors in AOA estimation have led to large errors in position estimation, as expected. The maximum error in two-dimensions is 2.18 cm and in three-dimensions is 3.43 cm. Unlike noise, these errors cannot be reduced by averaging over many samples. This is a particularly poor performance in two-dimensions, almost four times worse than using square or circular luminaires, and it suggests that rectangular luminaires are not ideal for use with the QADA receiver.

6.2. Triangulation in the Presence of Noise

The effect of noise on the positioning error is presented in this section. Initially, the transmitters are assumed to be point sources and all other room dimensions are the same as those in Figure 17. In reality, these room dimensions are very small compared to most indoor scenarios. The largest errors are in the edges of the room, as seen in Figure 20. In these positions, the light from three of the four luminaires will have travelled long distances, leading to worse AOA estimation. The maximum errors for two and three-dimensions are quite similar, however the mean in two-dimensions is lower at 0.14 cm compared to 0.21 cm for three-dimensions. It can also be seen that there is more variability in the errors for three-dimensions, particularly in the edges of the room.

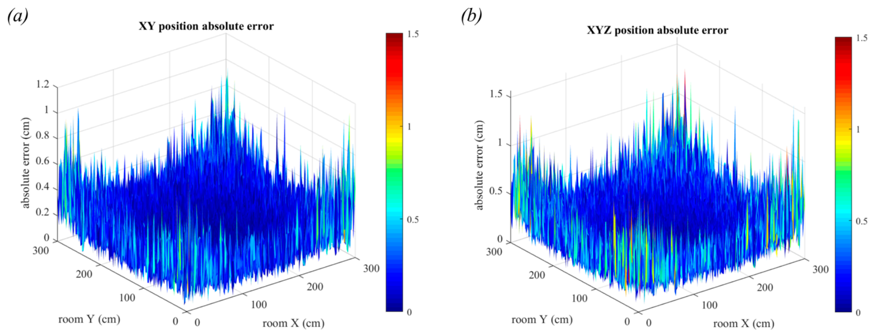

Figure 20. Positioning error in the presence of noise with point source transmitters. Errors in two-dimensions are shown in (**a**) and errors in three-dimensions are shown in (**b**). Each estimate is the average of 20,000 samples.

In Figure 21, the noise parameters remain the same, but the luminaires are no longer point sources. The room configuration used is shown in Figure 17a, with square luminaires of side length 30 cm.

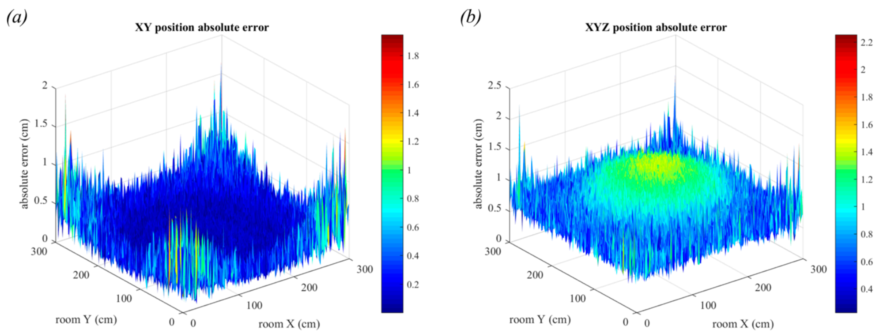

Figure 21. Positioning error in the presence of noise with square luminaires and a vertical distance of 1.5 m. Errors in two-dimensions are shown in (**a**) and errors in three-dimensions are shown in (**b**). Each estimate is the average of 20,000 samples.

In Figure 21a, the positioning error in two-dimensions is shown. The error has increased to a maximum of 1.9 cm and from the shape of the plot, it can be seen that the large central region is very flat, much like in Figure 18a. This shows the strong effect of having the large luminaires for this room configuration. In Figure 21b, this trend is more obvious with the large central area of increased error when compared to Figure 20b. This trend was previously seen in Figure 18c.

In Figure 22, the receiver position is changed to be 3 m below the ceiling and the room dimensions have changed to 6.0 m $\times$ 6.0 m. It can now be seen that the positioning error due to luminaire size is less evident and that the noise appears to be the dominant source of error. This is clearest when comparing Figure 21b with Figure 22b where the previously seen central trend is no longer visible. The reason for this is because when the room dimensions increase but the luminaire size remains the same, the ratio of the two values will have decreased and thus the overall impact of luminaire size is lessened. However, the increased distance the light has travelled results in a much lower received optical power, resulting in increased positioning error. The maximum error in two-dimensions is now 10.38 cm and the maximum error in three-dimensions has increased to 14.47 cm.

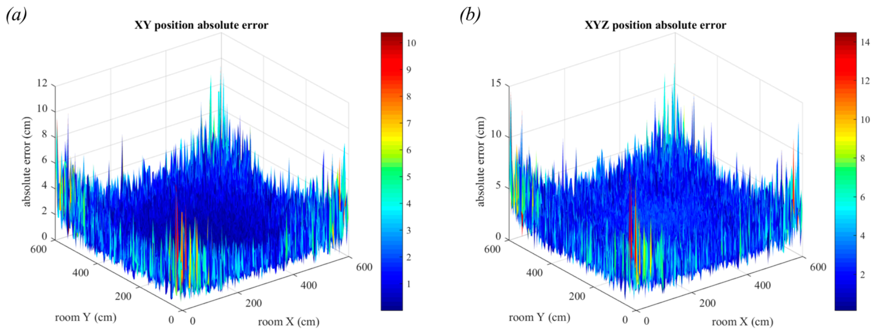

Figure 22. Positioning error in the presence of noise with square luminaires, room dimensions 6 m × 6 m and a vertical distance of 3 m. Errors in two-dimensions are shown in (**a**) and errors in three-dimensions are shown in (**b**). Each estimate is the average of 20,000 samples.

When the vertical distance between transmitter and receiver is increased, the performance degrades further due to the lower optical power received. In Figure 23, we show the 3-dimensional positioning errors for two additional vertical distances in the 6 m × 6 m room. In Figure 23a, the vertical distance is 4 m and in Figure 23b, the vertical distance is 5 m. These are reasonable distances to expect in large buildings with high ceilings. The maximum errors have now increased to 16.37 cm and 20.51 cm, respectively. Whilst these large errors are primarily in the corners of the room, these results demonstrate the progressive decline in QADA performance as the simulation parameters approach reality.

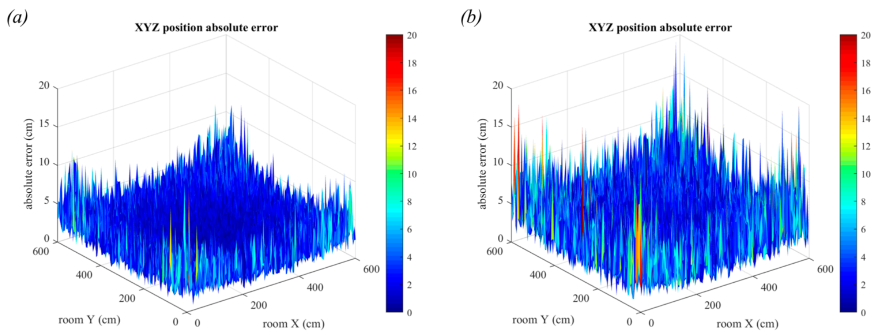

Figure 23. 3-dimensional positioning error in the presence of noise with square luminaires and room dimensions 6 m × 6 m. In (**a**) the vertical distance is 4 m and in (**b**) the vertical distance is 5 m. Each estimate is the average of 20,000 samples.

6.3. Triangulation with Fewer Samples

In the previous simulations, with the assumption of a perfectly calibrated and aligned receiver, it is clear that the noise is the dominant source of error, and the system is relying heavily on averaging over a large number of samples to achieve acceptable results. In many situations it may not be possible to average over many samples, such as power constrained systems that cannot sample at very high frequencies or when position update frequency requirements are high, limiting the time available for sampling. In Figure 24 we show the results when fewer samples are used to calculate the estimate.

In Figure 24a a single sample was used, and it can be seen that the errors are very large with a mean positioning error of 4.4 m. In Figure 24b, the estimate uses an average of 100 samples resulting in a mean positioning error of 45 cm and in Figure 24c, the estimate uses an average of 1000, resulting in a mean positioning error of 14.4 cm. These values can be compared to Figure 23b where 20,000 samples were used, giving a mean positioning error of 3.25 cm. An advantage of adopting a two-stage system is that the requirement to use a large number of samples is relaxed because the system does not rely on the QADA receiver for accuracy.

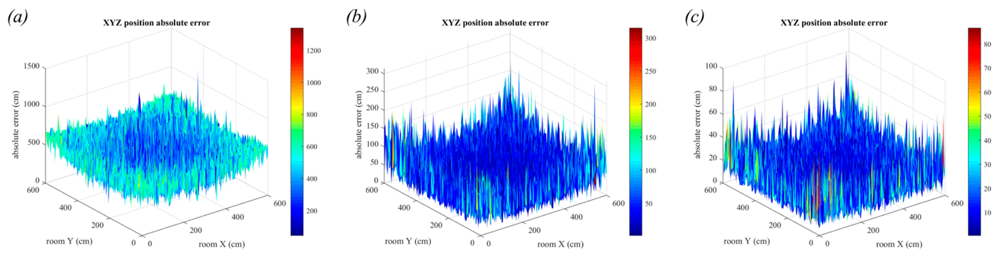

Figure 24. 3-dimensional positioning error in the presence of noise with square luminaires and room dimensions 6 m × 6 m × 5 m. Position estimates are calculated using (**a**) a single sample, (**b**) 100 samples and (**c**) 1000 samples. Note that these figures are on different scales.

Again, it is important to remember these results, along with all the results in this paper, are simulation only and unrealistically assume near ideal conditions. It was demonstrated that as the simulation model increased in complexity, with the addition of more potential sources of error, that the results degraded. It is reasonable to assume that if more potential sources of error were to be added to the simulation model, that the performance can only get worse. In our experimental work with the QADA receiver [20], we showed that our simulations underestimated the rMSE in incident angle estimation by up to a factor of two over very short distances.

7. Discussion and Conclusions

We have introduced the QADA-plus receiver, a two-stage receiver that has been optimized for VLP. This receiver consists of two sensors–a PD-based AOA detector and an imaging sensor. QADA-plus has the advantage of being compatible with modern consumer electronics due to its compact, planar structure. The unique feature of this receiver is that it combines the data from two different optical sensors, thereby taking advantage of the relative strengths of each sensor.

7.1. Accuracy of QADA as a Stand-Alone Sensor

The accuracy of PD based VLP systems is fundamentally limited by the small number of PDs and the resulting requirement for very accurate matching and alignment of components and very accurate measurement of the signal received by each PD. The QADA receiver has important advantages over some other PD receivers, including a planar structure, the use of a single aperture, and the use of a quadrant PD in which the properties of the PDs are closely matched. However, despite these advantages, it cannot overcome the fundamental limitation of PD based systems and we have previously shown that even in a careful experiment with transmission over a short distance there is significant discrepancy between measurement and simulation [20].

Two different factors limit the performance of a QADA: noise and systematic errors. Our detailed results demonstrate the potential accuracy under ideal conditions of the QADA receiver when used as a stand-alone sensor. We have presented extensive simulations using realistic parameter values showing that, by averaging over a number of measurements, the errors caused by noise alone can be made very small. An advantage of PD based systems is that they can be designed with relatively high bandwidth so very many samples can be taken within a short period of time. A disadvantage of averaging over a large number of samples is the computational cost and energy consumption.

We have provided results for one source of systematic error–the fact that typical luminaires are not point sources. Results are given for round, square and rectangular luminaires. Increasing the size of the luminaire is shown to increase the positioning error throughout the room, but it is particularly large near the walls where the entire luminaire is not within the FOV of the receiver. This highlights one limitation of PD based systems–their sensitivity to partial blocking of transmission from a luminaire. This will often occur in practice when a person or piece of equipment or furniture obscures part of the luminaire. The precise design of the diffuser of a luminaire will also significantly affect the radiation pattern. Luminaire manufacturers carefully design the diffuser to meet the illumination requirements with minimum power consumption.

In the simulated scenarios, the maximum error in three-dimensional positioning in the presence of noise was 20.51 cm using square luminaires. These results considered only the effect of luminaire geometry and noise, thus in practice, QADA is unlikely to achieve this level of accuracy.

7.2. Other Sources of QADA Error

There are also many other potential sources of error. These include limitations in the manufacturing of the QADA, changes to the QADA with time and use such as PD ageing [35] and responsivity variation with temperature, the properties of real luminaires, the orientation of the receiver and the locations of the luminaires.

The AOA estimation in the QADA is based on the ratio of the photocurrents from the four quadrants of the PD and assumes that each photocurrent is directly proportional to the illuminated area of that quadrant. This depends on perfect alignment of the aperture and the PD, perfect uniformity of response across the entire surface of all four PD quadrants, and perfect matching of the output circuits for each quadrant. While some of these effects may be mitigated by a calibration step at the production stage, they may be subject to change with time and variations in temperature which calibration cannot correct. The balance may also be affected by dirt on the surface of the aperture and small changes to the surface such as scratches. In the simulations we used an ideal scenario, in which the luminaires were evenly spaced, and the receiver was pointing upwards. It is well known that in less ideal situations DOP significantly reduces the accuracy that can be achieved. The QADA, like other positioning systems, shares this limitation. The layout of luminaires in buildings is determined by lighting requirements, aesthetics and infrastructure design and in many cases will not be ideal. Also, any tilting of the receiver will affect which luminaires are within its FOV.

7.3. Reference Points

We have also introduced the concept of reference points; visibly distinct features associated with luminaires for use with QADA-plus. While the importance of reference points may not be immediately obvious–they offer multiple important practical advantages. Their measured position does not depend on the size and radiation pattern of a luminaire, therefore removing the problem of partial obstruction of luminaires. There can be multiple reference points per luminaire–so fewer luminaires need to be within the FOV of the receiver. The size and shape of reference points can be designed to optimize their identification by the camera part of the QADA-plus. For example, it may be advantageous to choose shapes for which there are well known image processing algorithms, such as circles. The use of reference points depends on the ability of the QADA-plus to both receive a significant amount of data from each luminaire and to process an image to identify a small reference point. Reference points allow for flexible implementations and increased accuracy, especially in challenging environments such as buildings with large sparsely located luminaires.

7.4. Image Sensor Stage of QADA-Plus

The detailed requirements for the camera used for the image processing stage of the QADA are an area for further study, but it is clear that these will be less stringent than for cameras currently used for VLP and also for the fiducial marker systems used in robotics. There is no requirement for a rolling shutter in the QADA-plus—although a rolling shutter camera can be used. The image resolution required may be less than for fiducial marker systems because only the position, not the detailed structure of the reference points must be determined. While the QADA-plus is also subject to DOP, the triangulation is based on much more accurate AOA estimates, so the position estimates are also much more accurate. Thus, we can confidently assume that the experimental results found in other studies will be matched by the QADA-plus.

7.5. QADA-Plus

We have shown that in practice the QADA alone will provide limited positioning accuracy but despite this in situations where accuracy is not paramount, it may be adequate. It does have the benefit of being low power, very compact and offers reasonable accuracy. However, when increased accuracy and flexibility in implementation is required, the option is available to move to the two-stage QADA-plus that uses both a QADA and an imaging sensor.

In the two-stage QADA-plus, the accuracy is now related to the camera quality. A common use case is indoor pedestrian navigation, where the front facing camera on a smartphone makes an ideal second stage imaging sensor. Such cameras are high resolution and have been shown to offer good positioning accuracy [36]. In this case the positioning update rate is tied to the maximum frame rate of the camera which is typically around 30 fps. This is more than adequate for indoor pedestrian navigation. However, it may not be suitable for faster moving objects such as drones working in future factories. For more specialized applications, like drones, a better imaging sensor may be warranted to offer improved positioning accuracy and faster updates. Importantly though, with QADA-plus, the need for high frame rates is tied only to the need for fast position updates and not to the communications aspects of the system. Thus, for standard consumer needs, it is possible to use common off-the-shelf components to make a relatively cheap VLP receiver.

The QADA-plus is a promising new receiver design which by combining a PD based sensor and a camera-based sensor builds on the advantages of each. It has the potential to provide an indoor position system which like the outdoor GPS is accurate, ubiquitous and does not require access to other sources of information or prior knowledge about its location.

8. Patents

J. Armstrong, A. Neild, S. Cincotta, Visible light positioning receiver arrangement and two stage positioning method, 2018902351, 2018.

Author Contributions: Conceptualization, J.A. and A.N.; methodology, J.A., A.N. and S.C.; software, S.C. and C.H.; formal analysis, J.A. and S.C.; data curation, S.C.; writing—original draft preparation, J.A., A.N. and S.C.; writing—review and editing, J.A., A.N. and S.C.; visualization, S.C.; validation, C.H.; supervision, J.A. and A.N.; project administration, J.A. and A.N.; funding acquisition, J.A. and A.N.

Funding: This research was funded by the Australian Research Council's (ARC) Discovery funding schemes (DP150100003 and DP180100872) and an Australian Government Research Training Program (RTP) Scholarship.

Conflicts of Interest: The authors declare no conflict of interest.

References

1. Liu, H.; Darabi, H.; Banerjee, P.; Liu, J. Survey of Wireless Indoor Positioning Techniques and Systems. *IEEE Trans. Syst. Man Cybern. Part C* **2007**, *37*, 1067–1080. [CrossRef]
2. Dwiyasa, F.; Lim, M.H. A survey of problems and approaches in wireless-based indoor positioning. In Proceedings of the 2016 International Conference on Indoor Positioning and Indoor Navigation (IPIN), Madrid, Spain, 4–7 October 2016; pp. 1–7.
3. Jang, B.; Kim, H. Indoor Positioning Technologies without Offline Fingerprinting Map: A Survey. *IEEE Commun. Surv. Tutor.* **2018**, *21*, 508–525. [CrossRef]
4. Luo, J.; Fan, L.; Li, H. Indoor Positioning Systems Based on Visible Light Communication: State of the Art. *IEEE Commun. Surv. Tutor.* **2017**, *19*, 2871–2893. [CrossRef]
5. Do, T.-H.; Yoo, M. An in-Depth Survey of Visible Light Communication Based Positioning Systems. *Sensors* **2016**, *16*, 678. [CrossRef] [PubMed]
6. Mautz, R.; Tilch, S. Survey of optical indoor positioning systems. In Proceedings of the 2011 International Conference on Indoor Positioning and Indoor Navigation, Guimarães, Portugal, 21–23 September 2011; pp. 1–7.
7. Keskin, M.F.; Sezer, A.D.; Gezici, S. Localization via Visible Light Systems. *Proc. IEEE* **2018**, *106*, 1063–1088. [CrossRef]
8. Retscher, G.; Kealy, A. Ubiquitous Positioning Technologies for Modern Intelligent Navigation Systems. *J. Navig.* **2006**, *59*, 91–103. [CrossRef]
9. Bergen, M.H.; Schaal, F.S.; Klukas, R.; Cheng, J.; Holzman, J.F. Toward the implementation of a universal angle-based optical indoor positioning system. *Front. Optoelectron.* **2018**, *11*, 116–127. [CrossRef]
10. Zhu, B.; Cheng, J.; Wang, Y.; Yan, J.; Wang, J. Three-Dimensional VLC Positioning Based on Angle Difference of Arrival with Arbitrary Tilting Angle of Receiver. *IEEE J. Sel. Areas Commun.* **2018**, *36*, 8–22. [CrossRef]
11. Kuo, Y.-S.; Pannuto, P.; Hsiao, K.-J.; Dutta, P. Luxapose: Indoor positioning with mobile phones and visible light. In Proceedings of the Annual International Conference on Mobile Computing and Networking, MOBICOM, Maui, HI, USA, 7–11 September 2014; pp. 447–458.
12. Plets, D.; Eryildirim, A.; Bastiaens, S.; Stevens, N.; Martens, L.; Joseph, W. A performance comparison of different cost functions for RSS-based visible light positioning under the presence of reflections. In Proceedings of the 4th ACM Workshop on Visible Light Communication Systems at the 23rd Annual International Conference on Mobile Computing and Networking, Snowbird, UT, USA, 16 October 2017; pp. 37–41.
13. Bastiaens, S.; Plets, D.; Martens, L.; Joseph, W. Impact of Nonideal LED Modulation on RSS-based VLP Performance. In Proceedings of the 2018 IEEE 29th Annual International Symposium on Personal, Indoor and Mobile Radio Communications (PIMRC), Bologna, Italy, 9–12 September 2018; pp. 1–5.
14. Bastiaens, S.; Plets, D.; Martens, L.; Joseph, W. Response Adaptive Modelling for Reducing the Storage and Computation of RSS-Based VLP. In Proceedings of the 2018 International Conference on Indoor Positioning and Indoor Navigation (IPIN), Nantes, France, 24–27 September 2018; pp. 1–8.
15. Wei, L.; Zhang, H.; Yu, B.; Song, J.; Guan, Y. Cubic-Receiver-Based Indoor Optical Wireless Location System. *IEEE Photonics J.* **2016**, *8*, 1–7. [CrossRef]
16. Yasir, M.; Ho, S.W.; Vellambi, B.N. Indoor Position Tracking Using Multiple Optical Receivers. *J. Lightw. Technol.* **2016**, *34*, 1166–1176. [CrossRef]
17. Yang, S.H.; Kim, H.S.; Son, Y.H.; Han, S.K. Three-Dimensional Visible Light Indoor Localization Using AOA and RSS with Multiple Optical Receivers. *J. Lightw. Technol.* **2014**, *32*, 2480–2485. [CrossRef]
18. Wang, T.Q.; He, C.; Armstrong, J. Performance Analysis of Aperture-Based Receivers for MIMO IM/DD Visible Light Communications. *J. Lightw. Technol.* **2017**, *35*, 1513–1523. [CrossRef]
19. Steendam, H.; Wang, T.Q.; Armstrong, J. Theoretical Lower Bound for Indoor Visible Light Positioning Using Received Signal Strength Measurements and an Aperture-Based Receiver. *J. Lightw. Technol.* **2017**, *35*, 309–319. [CrossRef]
20. Cincotta, S.; He, C.; Neild, A.; Armstrong, J. High angular resolution visible light positioning using a quadrant photodiode angular diversity aperture receiver (QADA). *Opt. Express* **2018**, *26*, 9230–9242. [CrossRef] [PubMed]

21. Wang, T.Q.; Sekercioglu, Y.A.; Neild, A.; Armstrong, J. Position Accuracy of Time-of-Arrival Based Ranging Using Visible Light with Application in Indoor Localization Systems. *J. Lightw. Technol.* **2013**, *31*, 3302–3308. [CrossRef]
22. Huynh, P.; Yoo, M. VLC-Based Positioning System for an Indoor Environment Using an Image Sensor and an Accelerometer Sensor. *Sensors* **2016**, *16*, 783. [CrossRef] [PubMed]
23. Wang, J.; Olson, E. AprilTag 2: Efficient and robust fiducial detection. In Proceedings of the 2016 IEEE/RSJ International Conference on Intelligent Robots and Systems (IROS), Daejeon, Korea, 9–14 October 2016; pp. 4193–4198.
24. Olson, E. AprilTag: A robust and flexible visual fiducial system. In Proceedings of the 2011 IEEE International Conference on Robotics and Automation, Shanghai, China, 9–13 May 2011; pp. 3400–3407.
25. Cincotta, S.; Neild, A.; He, C.; Armstrong, J. Visible Light Positioning Using an Aperture and a Quadrant Photodiode. In Proceedings of the 2017 IEEE Globecom Workshops (GC Wkshps), Singapore, 4–8 December 2017; pp. 1–6.
26. Cincotta, S.; He, C.; Neild, A.; Armstrong, J. QADA-PLUS: A Novel Two-Stage Receiver for Visible Light Positioning. In Proceedings of the 2018 International Conference on Indoor Positioning and Indoor Navigation (IPIN), Nantes, France, 24–27 September 2018; pp. 1–5.
27. Alexander, S.; Hellemans, L.; Marti, O.; Schneir, J.; Elings, V.; Hansma, P.K.; Longmire, M.; Gurley, J. An atomic-resolution atomic-force microscope implemented using an optical lever. *J. Appl. Phys.* **1989**, *65*, 164–167. [CrossRef]
28. Li, Q.; Wu, J.; Chen, Y.; Wang, J.; Gao, S.; Wu, Z. High Precision Position Measurement Method for Laguerre-Gaussian Beams Using a Quadrant Detector. *Sensors* **2018**, *18*, 4007. [CrossRef] [PubMed]
29. Armstrong, J.; Sekercioglu, Y.A.; Neild, A. Visible light positioning: A roadmap for international standardization. *IEEE Commun. Mag.* **2013**, *51*, 68–73. [CrossRef]
30. Bergen, M.H.; Arafa, A.; Jin, X.; Klukas, R.; Holzman, J.F. Characteristics of Angular Precision and Dilution of Precision for Optical Wireless Positioning. *J. Lightw. Technol.* **2015**, *33*, 4253–4260. [CrossRef]
31. Kahn, J.M.; Barry, J.R. Wireless infrared communications. *Proc. IEEE* **1997**, *85*, 265–298. [CrossRef]
32. Barranco, G.F.; Tröbs, M.; Müller, V.; Gerberding, O.; Seifert, F.; Heinzel, G. Spatially resolved photodiode response for simulating precise interferometers. *Appl. Opt.* **2016**, *55*, 6688–6693. [CrossRef] [PubMed]
33. Hamamatsu Photonics. Multi-Element Photodiodes for Surface Mounting, S5980 Datasheet. 2017. Available online: https://www.hamamatsu.com/resources/pdf/ssd/s5980_etc_kpin1012e.pdf (accessed on 24 February 2019).
34. Cree. LED Luminaire Design Guide. 2016. Available online: https://www.cree.com/led-components/media/documents/LED_Luminaire_Design_Guide.pdf (accessed on 24 February 2019).
35. Jones, T.C.E. The long term stability of the response of silicon photodiodes. In Proceedings of the IEE Colloquium on Developments in Near Infra-Red Visible Ultraviolet Detectors, London, UK, 7 November 1991; pp. 6/1–6/3.
36. Arafa, A.; Jin, X.; Bergen, M.H.; Klukas, R.; Holzman, J.F. Characterization of Image Receivers for Optical Wireless Location Technology. *IEEE Photonics Technol. Lett.* **2015**, *27*, 1923–1926. [CrossRef]

Chapter 8

Luminaire Reference Points in Visible Light Positioning using Hybrid Imaging Photodiode Receivers

8.1 Overview

In Chapter 6, the concept of luminaire reference points (LRP) was introduced. Typically, in imaging sensor based VLP, the assumption is made that the centroid of the luminaire will be used for triangulation [105], [131], [132], [218]. However, this can be challenging to implement in practice. An obvious problem occurs when the luminaire is at the edge of the FOV and not captured entirely in the image. This results in either discarding this luminaire entirely from the data set and thus not being able to use it for triangulation, or inaccurately determining the centroid. For the case of large luminaires, this has the potential to result in very inaccurate position estimations. Another problem, related to the first, is that it can be difficult to capture a sufficient number of luminaires in the FOV to be able to triangulate. This is especially true if luminaires are large and spaced far apart, or if partial luminaires in the image are discarded because the centroid is not clear. These issues can all be overcome by using LRPs instead of centroids.

An LRP is any identifiable feature associated with the luminaire that can be detected in an image and is located at a known position. LRPs can take the form of small, inconspicuous marks on the luminaire frame, or a single LED having a subtly different wavelength. The location of the LRPs can easily be transmitted by the luminaires, which is decoded by the PD-based receiver. Thus, and most importantly, it would be possible to co-locate multiple LRPs on a single luminaire. Now, the requirement to have three luminaires in the FOV is reduced to the requirement to have a single luminaire with three LRPs. This is much easier to achieve and reduces the FOV requirements on both the QADA and the camera.

In this work, the GDOP [159], [237] is used to investigate the effect of co-locating multiple LRPs on a single luminaire. The geometry of the beacon locations used for triangulation will impose limits on the accuracy of the position estimate. If the geometry is not ideal, as is likely the case when using LRPs, this will reduce the potential accuracy that can be achieved. However, there are many indoor scenarios where it is unlikely there will be three luminaires in the FOV, thus using LRPs makes it possible to triangulate without major infrastructure changes. Another important consideration is the linearity of the imaging sensor. This work assumes linearity, however in reality, bright objects can saturate the sensor and lead to errors in determining the position of the LRPs.

This paper presents two examples of challenging environments for VLP; corridors that are typically long and narrow with low illumination requirements resulting in a single row of sparsely installed luminaires, and large rooms that utilise large square luminaires installed far apart. The impact of these LRP geometries are presented, showing that in all cases it is possible to achieve good positioning accuracy with low FOV requirements.

8.2 Publication

> S. Cincotta, A. Neild, and J. Armstrong, "Luminaire Reference Points (LRP) in Visible Light Positioning using Hybrid Imaging-Photodiode (HIP) Receivers," in *2019 International Conference on Indoor Positioning and Indoor Navigation (IPIN)*, Pisa, Italy, 2019, pp. 1–8.

(HIP) Receivers," in 2019 International Conference on Indoor Positioning and Indoor Navigation (IPIN), 2019

The references are [19] [25] [17] [18] [150] [238] [41] [220] [192] [131] [209] [105] [123] [148] [151] [213] [239] [240] [241] [237] [159] [242] [243] [244] [245] [246]

2018 International Conference on Indoor Positioning and Indoor Navigation (IPIN), 24-27 September 2018, Nantes, France

QADA-PLUS: a novel two-stage receiver for visible light positioning

Stefanie Cincotta, Cuiwei He, Adrian Neild and Jean Armstrong
Monash University
Melbourne, Australia
{Stefanie.Cincotta, Cuiwei.He, Adrian.Neild, Jean.Armstrong}@monash.edu

Abstract*— In this paper, we introduce a new two-stage receiver structure for visible light positioning (VLP) and a particular implementation of the new structure called the QADA-PLUS receiver. By using two sensors, one a photodiode (PD) based sensor and the other an image-based sensor, the new structure exploits the strengths of both technologies while avoiding their weaknesses. The QADA-PLUS uses a quadrant angular diversity aperture receiver (QADA) for the PD-based stage. The QADA has a very compact, planar structure suitable for incorporation in a smartphone or other small device and has been shown to provide good angular diversity in a proof-of-concept laboratory experiment. The QADA is also, unlike typical image sensors, able to reliably demodulate high frequency visible light signals. In this paper extensive simulation results for a range of typical indoor scenarios and realistic parameters show that the QADA has the potential to accurately estimate the polar and incident angle of light transmitted by LED luminaires. The average absolute error in estimation of incident angle was 0.0006° and for polar angle estimation was 0.005°. A limitation of these simulations is that it is assumed that the luminaires can be modelled as point sources and that the dimensions of the QADA are very precisely known. Incorporation of the QADA in the new two-stage QADA-PLUS receiver removes these limitations in two ways – the image-based receiver provides very accurate angle-of-arrival estimates and the use of visible reference points means that the QADA-PLUS is compatible with luminaires of any shape.

Keywords—visible light positioning, quadrant photodiode, aperture, QADA, QADA-PLUS

I. Introduction

Recently, because of the widespread introduction of LED based indoor lighting, there has been significant and increasing interest in the use of visible light communications (VLC) for indoor positioning [1], [2]. Unlike conventional lighting, LEDs can be modulated at high rates. Receivers, using photodiodes (PDs) or imaging sensors, detect the signals and determine the receiver position. A major advantage of visible light positioning (VLP) is that it takes advantage of existing lighting infrastructure and so reduces the cost of installation dramatically [1]. Additionally, unlike radio frequency (RF) based methods, it is not subject to significant multipath propagation issues [3].

This work was supported by the Australian Research Council's (ARC) Discovery funding schemes (DP150100003 and DP180100872) and an Australian Government Research Training Program (RTP) Scholarship.

978-1-5090-1629-7/18/$31.00 ©2016 Crown

There are many different approaches to VLP each with their own strengths and weaknesses. One of the most intuitive approaches is to use the received signal strength (RSS) to determine the distance from the transmitter to the receiver [4]–[6]. However, without very accurate knowledge of the transmitted power and the optical channel, it is difficult to accurately estimate this distance. Alternative well-known methods use time-of-arrival (TOA) or time-difference-of-arrival (TDOA) [7], [8]. Whilst the latter works well for GPS, it is not practical for VLP due to the expensive synchronized clocks that are required and the very small time differences that would need to be accurately measured.

Another alternative is to estimate the angle-of-arrival (AOA) of the received light. This is possible because there is typically a line-of-sight (LOS) path available from the LED beacons to the receiver. AOA estimation requires an angular diversity optical receiver. This can be implemented using either imaging sensors [9]–[11] or PDs [12]–[15]. Imaging sensors generally have high resolutions making them well suited to accurate AOA estimation, but because of frame rate limitations, they are not able to demodulate high-frequency signals. This is a major limitation because to avoid adverse biological effects [16], modulation of LEDs at low frequencies must be avoided. A number of innovative workarounds have been proposed which depend on the rolling shutter mechanism of typical low cost digital cameras [17] but these systems can only provide rough positioning and can demodulate only relatively low data rate signals.

In the past, a number of PD-based receivers have achieved angular diversity by having PDs facing in different directions [13], [15]. These three-dimensional PD structures have been shown to provide good angular diversity, however, they are not well suited to integration into modern consumer electronics due to the awkward protrusion they create. The quadrant PD angular diversity aperture (QADA) receiver solves this problem by combining an aperture with a quadrant PD [18], [19]. We have previously demonstrated that this achieves good angular diversity within a compact and planar structure.

In this paper, we present a completely new approach and describe an all-new hybrid two-stage receiver, called QADA-PLUS. The new receiver has two distinct sensors: one a PD-based sensor and the other an imaging sensor. In this way, we build on the strengths and avoid the weaknesses of each type of sensor. In the system described in this paper, the first stage uses the QADA receiver to demodulate the signals and identify the LED beacons. The second stage captures a still image and

2018 International Conference on Indoor Positioning and Indoor Navigation (IPIN), 24-27 September 2018, Nantes, France

combines this with the information from the first stage to achieve accurate positioning. We also describe how, by associating precise visible reference points with each luminaire, the performance can be further improved.

The significant contributions of this paper include

1. The first publication of the all new two-stage positioning receiver that provides high accuracy.
2. The use of reference point or points to identify precise position(s) associated with each luminaire[1].
3. A detailed analysis of QADA in two dimensions, including angular diversity analysis

Section II provides a detailed description of each of the two stages of the system and the use of reference points. In Section III the results of simulations are presented that demonstrate the suitability of the QADA receiver for stage one. Section IV is a discussion on realistic implementations and Section VI contains the conclusions.

II. System Description

Fig. 1 shows the overall structure of a positioning system using the new QADA-PLUS two-stage receiver. Each LED beacon transmits an optical signal which contains information about its position. In this paper, we call the position information message transmitted by the n^{th} LED beacon the Beacon Information packet (BIP_n). The BIP message contains information about the positions of the reference point, or points, on the luminaire. Reference points are specific points on the luminaire that can be identified by an image sensor. We discuss the use of reference points in detail in a later section.

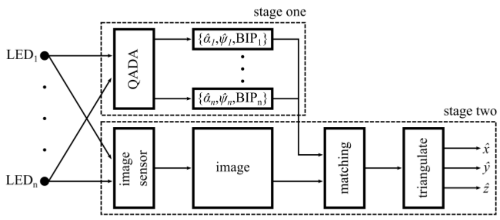

Fig. 1. Block diagram showing the overall structure of the receiver and the flow of information between stage one and stage two.

Light from each transmitter is received by both the PD-based sensor and the image sensor. The PD-based sensor, which in this paper is a QADA, demodulates the signals transmitted by each LED beacon and decodes the BIP messages for all of the transmitters within range. We assume that the LED beacons transmit orthogonal signals so that the signals from each can be readily separated at the receiver. For example, time-division-multiplexed or frequency-division-multiplexed signals could be used. The PD-based sensor simultaneously provides approximate estimates of the incident angle, ψ, and the polar angle, α, of all LED beacons in the field-of-view (FOV). At the same time, the image-based sensor takes a high-resolution image that includes the luminaires. The outputs of the two sensors are then used in the matching stage. The approximate incident angle and polar angle of the LED beacon from the first stage allows each luminaire to be unambiguously identified in the image. This, in combination with the position information contained in the BIP message, allows the precise positions of the reference points in the image plane to be very accurately determined. By using the AOA information from three or more reference points, well-known triangulation algorithms can be used to calculate the x, y, and z coordinates of the receiver. This method is more accurate than using a single-stage QADA receiver.

A. Stage one – QADA

The QADA receiver, in Fig. 2, consists of a quadrant PD, shown in blue, positioned directly below a transparent aperture. A quadrant PD is a type of segmented PD that consists of four discrete PDs arranged in a 2 x 2 array. The PDs are separated by a very narrow gap. Segmented PDs are available in varying shapes, sizes and number of segments and are typically used in laser light applications such as beam centering [20], [21] where they are capable of providing position information in two dimensions. In these applications, an aperture is not required. The combination of an aperture with a quadrant PD in the form of the QADA and its potential in indoor positioning applications has only been very recently described [18].

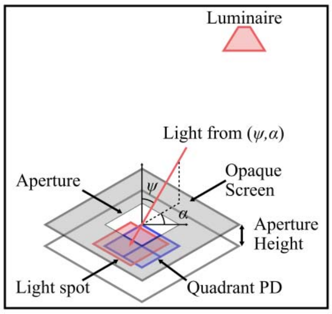

Fig. 2. QADA receiver structure.

The aperture plane is separated from the quadrant PD plane by a known vertical distance, h. We call this distance the aperture height. In Fig. 2, the light from an LED luminaire passes through the aperture and forms a light spot, shown in red, on the quadrant PD. The light spot shape and size match that of the aperture. The position of this light spot is unique for a given AOA provided that the aperture is no larger than the quadrant PD and the dimensions of the light beacon are much smaller than the distance from the beacon to the receiver.

We use a square aperture and quadrant PD so that the position of the light spot maintains a linear relationship as it passes over the quadrant PD [18]. We choose an aperture size that matches the quadrant PD size as we have previously shown that this maximizes the signal-to-noise ratio (SNR) [18].

[1] We use the term 'luminaire' as it is the technical term for the light fitting. Luminaires can be made up of one, or multiple, LEDs, of which some, or all, will be transmitting signals. We refer to the LEDs that are transmitting signals as the LED beacons.

2018 International Conference on Indoor Positioning and Indoor Navigation (IPIN), 24-27 September 2018, Nantes, France

First, we analyze how the position information for one beacon is determined, and then we will show how the use of orthogonal signals allows simultaneous calculation of the positions of multiple beacons.

The ratio of photocurrents in adjacent quadrant pairs is used to determine the position of the light spot centroid. In Fig. 3, the light spot, shown in yellow, overlaps the quadrant PD. The colors in the overlap areas represent the quadrant pairs used in the ratio function. In Fig. 3 (a), we determine the x coordinate of the centroid of the spot by using the ratios between the left and right quadrant pairs and in Fig. 3 (b), we determine the y coordinate of the centroid by using the ratios between the top and bottom quadrant pairs. The x and y coordinates of the centroid are estimated independently and then used, in combination with the known aperture height, to estimate the incident and polar angles of the incoming light.

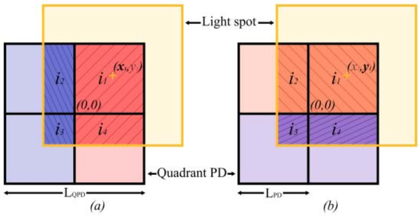

Fig. 3. Light spot overlapping the quadrant PD

These ratios are expressed as

$$p_x(t) = \frac{i_1(t) + i_4(t) + N_1(t) + N_4(t)}{i_2(t) + i_3(t) + N_2(t) + N_3(t)} \quad (1)$$

$$p_y(t) = \frac{i_1(t) + i_2(t) + N_1(t) + N_2(t)}{i_3(t) + i_4(t) + N_3(t) + N_4(t)} \quad (2)$$

where $i_j(t)$ and $N_j(t)$ are the photocurrent and noise generated by the j^{th} quadrant of the PD.

The LEDs are assumed to have a radiation pattern that is Lambertian with an order of $m = 1$. We can express the channel gain for the j^{th} quadrant at time, t, as [22]

$$h_c(t) = \frac{(m+1)A_j(t)}{2\pi d^2(t)} \cos^m(\phi(t)) T_s(\psi(t)) g(\psi(t)) \cos(\psi(t)) \quad (3)$$

where d is the distance between the transmitter and the receiver, ϕ is the emergence angle, ψ is the incidence angle, $T_s(\psi(t))$ is the filter transmission and $g(\psi(t))$ is the concentrator gain. The QADA does not use any optical filters[2], lenses, or concentrators, thus the photocurrent for the j^{th} quadrant at time, t, is given by

$$i_j(t) = \frac{RP_T A_j(t) \cos^2(\psi(t))}{\pi d^2(t)} \quad (4)$$

where R is the responsivity of the PD, P_T is the transmitted optical power and $A_j(t)$ is the area of quadrant j which the light spot overlaps.

From (4), it is clear that the photocurrent is directly proportional to the area of overlap. If we exclude the noise terms from the above functions, we can simplify them to a function of the overlap area. We define L_{PD} as the length of a single quadrant, shown in Fig. 3 (b), and $[x_1(t), y_1(t)]$ as the centroid of the light spot at time, t .Thus, in the absence of noise, the ratios in (1) and (2), can be expressed as:

$$p_x(t) = \frac{A_1(t) + A_4(t)}{A_2(t) + A_3(t)} = \begin{cases} \dfrac{L_{PD} + x_1(t)}{L_{PD}}, & -L_{PD} < x_1(t) \le 0 \\ \dfrac{L_{PD}}{L_{PD} - x_1(t)}, & 0 < x_1(t) < L_{PD} \end{cases} \quad (5)$$

$$p_y(t) = \frac{A_1(t) + A_2(t)}{A_3(t) + A_4(t)} = \begin{cases} \dfrac{L_{PD} + y_1(t)}{L_{PD}}, & -L_{PD} < y_1(t) \le 0 \\ \dfrac{L_{PD}}{L_{PD} - y_1(t)}, & 0 < y_1(t) < L_{PD} \end{cases} \quad (6)$$

We can now rearrange (5) and use the result to derive an estimate for $x_1(t)$. The received signal undergoes low pass filtering to limit the bandwidth to B hertz, before sampling at the Nyquist rate, $2B$, and matched filtering to select the desired signal and reject any orthogonal signals received from other beacons [23]. We then average over M values to find the estimate at time $t = (k+M)/2B$, which can be expressed as

$$\hat{x}_1\left[\frac{k+M}{2B}\right] = \begin{cases} \dfrac{1}{M}\displaystyle\sum_{n=k}^{k+M-1} L_{PD}\left(p_x\left[\frac{n}{2B}\right] - 1\right), & -L_{PD} < x_1\left[\frac{k+M}{2B}\right] \le 0 \\ \dfrac{1}{M}\displaystyle\sum_{n=k}^{k+M-1} L_{PD} - \dfrac{L_{PD}}{p_x\left[\frac{n}{2B}\right]}, & 0 < x_1\left[\frac{k+M}{2B}\right] < L_{PD} \end{cases} \quad (7)$$

The block diagram showing this process is shown in Fig. 4

We can derive a similar estimate for $y_1(t)$. As can be seen in (7), the estimate for $x_1(t)$ depends only on the value of L_{PD} and p_x. It does not depend on the value of $y_1(t)$. However, the photocurrent, $i_j(t)$, depends on the values of $x_1(t)$ and $y_1(t)$. Thus, the SNR is reduced because of the reduced area of overlap.

2 Optical filters operate in the optical domain before the PD and are used to selectively transmit different wavelengths of light, whilst electrical filters operate in the electrical domain after the PD and remove unwanted electrical frequencies.

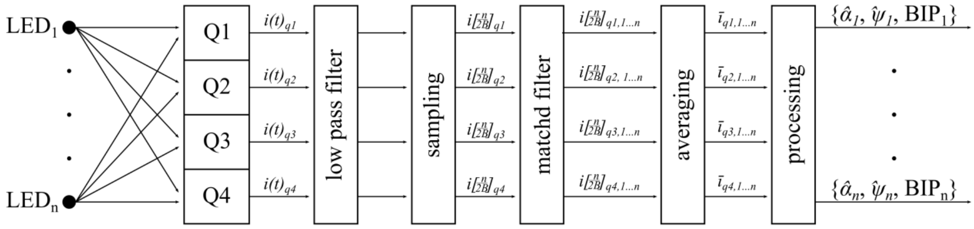

Fig. 4 Digital signal processing path for QADA

The noise in optical receivers is typically a combination of both the shot noise and the thermal noise [22]. The shot noise due to background illumination is the dominant noise source. It is modeled as a white Gaussian process. The variance of the shot noise for an isotropic receiver, expressed in (8), is the product of the single-sided noise power density and the electrical bandwidth, B .

$$\sigma_{shot}^2 = 2qRp_n A\Delta\lambda B \tag{8}$$

where q is the charge of an electron, p_n is the spectral irradiance, A is the area of the PD quadrant and $\Delta\lambda$ is the optical bandwidth.

The thermal noise is calculated using the noise equivalent power (NEP). Like the shot noise, it is the product of the spectral density and the electrical bandwidth.

$$\sigma_{thermal}^2 = \left(NEP \times R\right)^2 B \tag{9}$$

QADA is a well suited AOA detector for stage one. Using a small 5 mm square quadrant PD, its compact planar structure means that it can be easily incorporated into a smartphone and it provides sufficiently accurate AOA data for input to stage two.

B. Stage two – Image sensor

An image sensors, such as cameras typically found in a smartphone, can provide very high angular resolution as they typically have a large number of pixels. Position accuracy in the sub-decimeter range has been shown to be possible using high megapixel cameras [11], [24], [25]. However, demodulation of transmitted data is difficult without high frame rates or complex algorithms [26]–[28]. In QADA-PLUS, this is avoided by using a PD-based AOA detector to demodulate the signals and identify the LED beacons. This information from stage one, consisting of an AOA estimate and BIP message, is combined with the information gathered in stage two to estimate the position with very high accuracy. As the location of the luminaires is approximately known, the computational complexity of the image processing is significantly reduced.

We use photogrammetry to determine the position of the receiver. After the LED beacons have been identified and the BIP messages, stating the position of the reference points within a local (or global) coordinate system, has been decoded in stage one, the reference points are located in the image plane and, finally, a triangulation algorithm is used.

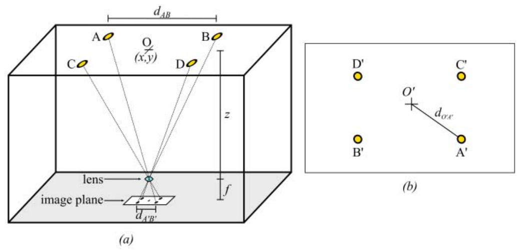

Fig. 5. (a) Room with image of ceiling captured and (b) image plane

In Fig. 5, the camera has captured an image of the ceiling showing four LED beacons. In Fig. 5 (a), the focal length of the camera, f , is a known value. The distance between the LEDs, A and B, can be easily determined in both the image and room coordinates. To determine the position in the room, first we must determine the height, z , using the ratio of the distance between two beacons: $z : f = d_{AB} : d_{A'B'}$. From this relationship, we obtain

$$\hat{z} = f\,\frac{\sqrt{\left(x_A - x_B\right)^2 + \left(y_A - y_B\right)^2}}{\sqrt{\left(x_{A'} - x_{B'}\right)^2 + \left(y_{A'} - y_{B'}\right)^2}} \tag{10}$$

We then repeat the calculation in (10) for all possible combinations of LED beacons and use the mean of these values to estimate the height. Once the height is known, we calculate an estimate for $\hat{x}$ and $\hat{y}$, using

$$\frac{z}{f} = \frac{d_{OA}}{d_{O'A'}} = \frac{d_{OB}}{d_{O'B'}} = \frac{d_{OC}}{d_{O'C'}} = \frac{d_{OD}}{d_{O'D'}} \tag{11}$$

The distance from the origin in the image plane, O' , to each beacon, shown in Fig. 5 (b), can be determined using image processing, whilst the corresponding origin in room coordinates, O , is the (x, y) location of the receiver. From (11), we get

$$\begin{aligned}
\left(d_{OA}^2 - d_{OB}^2 - x_A^2 + x_B^2 - y_A^2 + y_B^2\right)/2 &= x(x_B - x_A) + y(y_B - y_A) \\
\left(d_{OB}^2 - d_{OC}^2 - x_B^2 + x_C^2 - y_B^2 + y_C^2\right)/2 &= x(x_C - x_B) + y(y_C - y_B) \\
\left(d_{OC}^2 - d_{OD}^2 - x_C^2 + x_D^2 - y_C^2 + y_D^2\right)/2 &= x(x_D - x_C) + y(y_D - y_C)
\end{aligned} \tag{12}$$

This overdetermined set of equations can easily be solved using linear least squares regression. In reality, the receiver may be tilted at arbitrary angles and thus additional algorithms are needed to compensate for these rotations.

C. Reference Points

In this section, we describe the use of visible reference points. The use of these in conjunction with the new two-stage receiver has two major advantages – it makes the new receiver more accurate and it makes it compatible with any shape of luminaire. In this paper we use the term ‘reference points’, these play a similar role to anchor nodes or landmarks in other positioning systems.

In principle, reference points can be any specific position within the luminaire as long as they can be unambiguously identified from the image taken in the second stage. For example, a reference point could be a given corner of the luminaire or a single colored LED. The form of the reference point can either be defined for the entire system or, can be transmitted as part of the BIP message. For example, a system could be built where every positioning luminaire has one red LED which is the reference point for that luminaire, or a more versatile system could be built where the BIP messages convey both the type and position of the reference point in each luminaire.

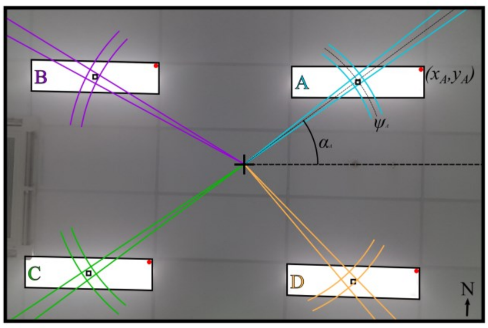

Fig. 6. Example image captured by smartphone camera with overlay showing the information provided by stage one.

Fig. 6 shows a practical example of the use of reference points. It shows an image of a ceiling on which there are four separate batten luminaires. It was captured using a front-facing smartphone camera. Batten luminaires are often used in commercial and industrial settings and consist of many LEDs in a linear array. In our new system some, or all, of the LEDs can be used to transmit positioning information. In this example, we assume a LED in the center of each luminaire is used as the beacon LED. The overlay demonstrates how the incident and polar angle estimates, from stage one, are used to locate the LED beacons and, by extension, the luminaires, in the image plane. For example, the LED beacon in luminaire A is estimated to have an incident angle of ψ_1 and a polar angle of α_1. The colored lines represent the uncertainty in the estimation and thus the intersection of the blue lines should contain the LED beacon. This information is then matched with the BIP message that was decoded by the QADA. So now the second stage knows from the BIP the precise position of the reference point in each luminaire and its position on the image, shown as a red dot. These values are then used in (11) to calculate the receiver position.

Although we do not analyze it in detail in this paper, the concept of reference points can be extended to the use of multiple reference points within one luminaire. This would be particularly useful for large area luminaires such as the batten luminaire as fewer LED beacons are required to support triangulation.

III. Simulation Results

In this section, we investigate the performance of the QADA as the position of the receiver and the height of the ceiling is varied. We start with a room with dimensions $3\,\text{m} \times 3\,\text{m} \times 2.4\,\text{m}$ and a single LED installed in the center of the ceiling, shown in Fig. 7.

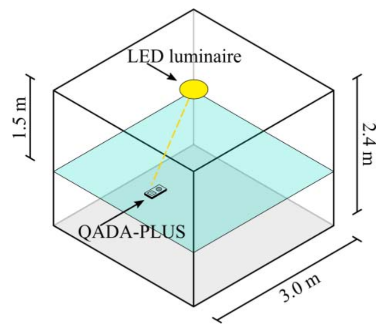

Fig. 7. Schematic of the room with dimensions 3 m x 3 m x 2.4 m that is used in the initial simulation. A single LED is located at the center of the ceiling.

We first assume that the receiver is located at a vertical distance of 1.5 m from the ceiling and that the optical power of the LED beacon is 3 W. For simplicity, we model the LED beacon as a point source. The transmitted signal is sampled at the Nyquist rate and the samples are averaged over 0.01 seconds. This allows for rapid position updates. The rest of the simulation parameters can be found in Table 1.

Table 1. Simulation parameters

Parameter	Value
Quadrant PD size	5 mm × 5 mm
Aperture height	2.5 mm
Responsivity	0.25 A/W
Electrical bandwidth	1 MHz
Optical bandwidth	300 nm
Noise Equivalent Power	1.9×10^{-14} W/$\sqrt{\text{Hz}}$
Spectral irradiance	6.2×10^{-6} W/(nm.cm^2)

A. Angular Diversity of QADA

First, we analyze the angular diversity of the QADA receiver. In Fig. 8, the channel gains of the QADA receiver are

2018 International Conference on Indoor Positioning and Indoor Navigation (IPIN), 24-27 September 2018, Nantes, France

presented for all possible receiver positions using the indoor scenario described in Fig. 7. Each subplot in Fig. 8 shows the channel gains between the LED beacon and a single quadrant as a function of the QADA receiver's position. We can see that, when the QADA receiver is located in the center of the room, the channel gains of the four quadrants are relatively large, but have very similar values. However, when the QADA receiver is located close to the corner of the room, the similarity between these four channel gains is significantly reduced. An important feature is that the relationship between these four channel gains is different at every point so the gains, and consequently the photocurrents, uniquely determine the position.

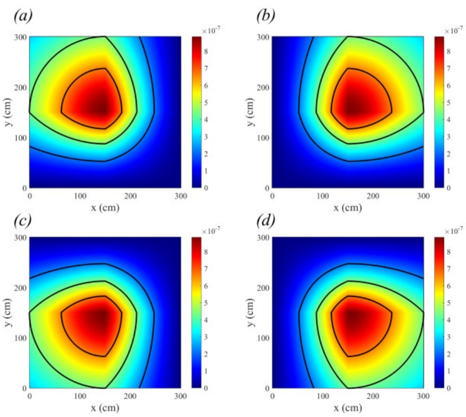

Fig. 8. Channel gain plot for all positions in the room. Each plot represents the channel gain for a single quadrant of the PD.

B. AOA estimation

We now investigate how the accuracy of AOA estimation varies as a function of receiver position. Fig. 9 shows the rMSE and the absolute error in AOA estimation. In Fig. 9 (a) it can be seen that the absolute errors in the estimation of the incident angle are very small for all positions; the largest absolute error in incident angle estimation is only 8.2×10^{-4} degrees. In the corners, where the incident angles are largest, the performance is worst. This is due to the low signal power resulting from lower area of overlap of the light spot and the dependence on d^{-2} and $\cos(\psi)^2$, as expressed in (4). In Fig. 9 (b), it can be seen that the absolute errors in polar angle estimation are also very small for the majority of positions, with most errors below 1×10^{-3} degrees. This is similar in magnitude to the errors in Fig. 9 (a). The largest absolute error in estimation for the polar angle is 0.0117 degrees which is directly below the luminaire. This is because small errors in the estimation of $x_1(t)$ and $y_1(t)$ in these positions can result in large errors in the polar angle estimation.

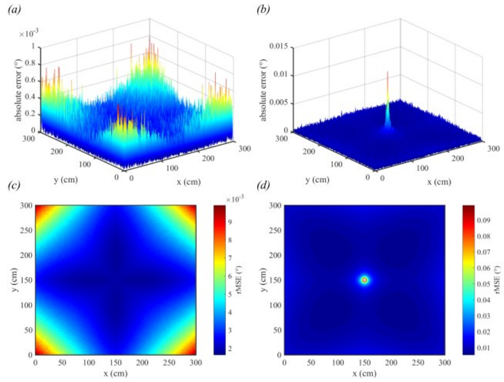

Fig. 9. Absolute error in (a) incident angle and (b) polar angle estimation. rMSE for (c) incident angle and (d) polar angle. For all plots, the receiver is 150 cm below the ceiling and the transmitted power is 3 W.

In Fig. 9 (c) and (d) we look at the root mean square error (rMSE) for incident and polar angle estimation. In general, the rMSE are very small for all positions, but in both plots, we can see that the error is greater at the extremities, as expected. Also, for the polar angle, the central values are also high as we saw in Fig. 9 (b). For clarity, the center values in Fig. 9 (d) have been truncated and thus, the true maximum value was 0.2892°. This is still a very small value. Additionally, the rMSE for the polar angle is smallest when closest to $45°\pm90n°$, where n is any integer. We can extrapolate this data to any LED in any position in the room as it encompasses the entire FOV of the QADA.

To investigate how sensitive the performance of the QADA is to variation in the parameters, we now change the vertical height to 3 m and the transmitted optical power to 1 W. This causes a significant reduction in received optical power. The results are shown in Fig. 10. The overall trends are very similar, however, the magnitude of the absolute error and rMSE are greater. In Fig. 10 (a) we can see that the absolute error for incident angle in the center is worse and in Fig. 10 (b) that a larger portion of the center has a relatively large error than in Fig. 9 (b).

In Fig. 10 (c) and (d) we again look at the rMSE for incident and polar angle estimation. It is important to note that because the height of the room has been increased, the range of incident angles represented is smaller. The rMSE for incident angle are again very small, whilst the rMSE for polar angles have increased but are still small. Again, we have cropped the central values for clarity. It can be seen that the circle of cropped values in the center is larger than Fig. 9 (d). The QADA has difficulty estimating angles when it is directly below the luminaire and these difficulties become more evident as the SNR decreases. The similarities in channel gain for all four quadrants, and hence the lack of angular diversity, at these positions, is a reason for this limitation.

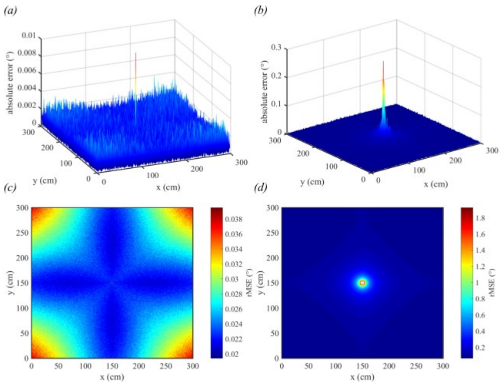

Fig. 10. Absolute error in (a) incident angle and (b) polar angle estimation. rMSE for (c) incident angle and (d) polar angle. For all plots, the receiver is 300 cm below the ceiling and the transmitted power is 1 W

C. Impact of varying height

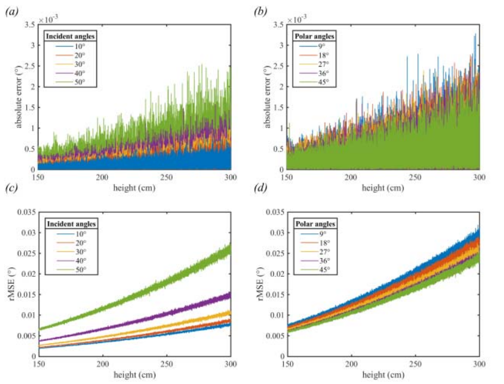

Fig. 11. Absolute error in (a) incident angle and (b) polar angle estimation and rMSE for (c) incident angle and (d) polar angle. Height is varying from 150 cm to 300 cm

We further analyze the impact of increasing the vertical distance, h, between the transmitter and receiver. In Fig. 11, for all angles and heights, the absolute errors and rMSE are small. In Fig. 11 (a) and (c) we keep the polar angle fixed at 45° and vary the incident angle between 10° and 50°. In general, the performance degrades as the height increases for all incident angles due to the reduced optical power received. Larger incident angles are impacted more than smaller incident angles due to the lower SNR.

The rMSE and error in polar angle estimation are shown in Fig. 11 (b) and (d). The incident angle is fixed at 25° and we show polar angles in the first 45° only. These can be extrapolated to other polar angles because of the repeating pattern visible in Fig. 9 (d). The estimation of polar angle is impacted in a similar way to the estimation of incident angle with the worst performance occurring at the largest distance between transmitter and receiver. Also, consistent with Fig. 9, the polar angle 45°performs best.

D. Impact of varying power

We now vary the transmitted power and fix the height at 1.5 m. The power received by QADA is directly proportional to the power transmitted by the LED beacon. The results are shown in Fig. 12. As transmitted power increases, the performance improves, as we expect. The general trends are very similar to the previous example with the varying vertical height, albeit inverted. Interestingly, there is a rapid improvement in performance between 0.5 W and 1 W, with diminishing returns thereafter.

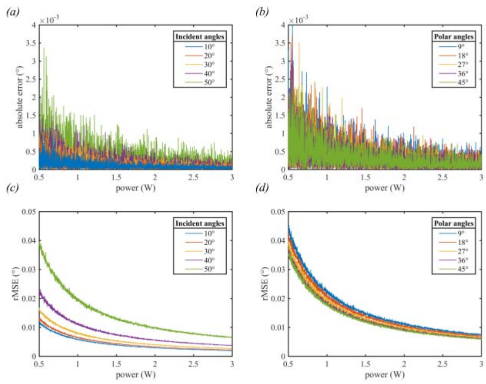

Fig. 12. Absolute error in (a) incident angle and (b) polar angle estimation and rMSE for (c) incident angle and (d) polar angle. Power is varying from 0.5 W to 1 W.

IV. Discussion

The important advantage of this new two-stage hybrid system is that it exploits the strengths of each individual method. In the previous section, it was shown that in ideal circumstances the QADA alone gives excellent estimates of angle of arrival, however, in practice, many factors may degrade the performance, including dust on the aperture, very high ceilings, dimmed luminaires or manufacturing imperfections. By moving to a two-stage system, we relax the requirements for accuracy in the QADA and create a system that is likely to be very robust in most or all realistic applications. The use of visible reference points enables the new two-stage receiver to be used for any shape of luminaire.

The performance of the second, image-based, stage depends very much on the specifications of the camera. As an example, we consider the front-facing camera of a current flagship smartphone. Current flagship smartphones have front cameras with resolution in the range of 7-8 MP, a maximum frame rate of 30 fps, and a wide FOV. Although the back cameras traditionally have higher resolution, it is likely that it will be the front camera that has the luminaires within its FOV, as the user will typically be looking at the screen. If we assume a maximum indoor movement speed of 10 km/hr, which equates to 2.78 m/s, and also assume that images are captured

2018 International Conference on Indoor Positioning and Indoor Navigation (IPIN), 24-27 September 2018, Nantes, France

every 0.033 seconds (30 fps), then the position will have only changed by a maximum of 9 cm between estimates. In most indoor applications the receiver position will change much more slowly or even be stationary for long periods of time. So, the accuracy and speed of the new system is likely to be more than adequate for the majority of future applications.

This completely new receiver design opens up many important areas for future study. Questions to be answered include: How can image processing algorithms be optimized for use in the QADA-PLUS receiver, and what accuracy can they achieve? How does the accuracy depend on the position of the LED beacon within the luminaire? What is the optimum type and position of visible reference point? And can multiple reference points within one luminaire improve performance?

V. CONCLUSION

In this paper, we have introduced a new two-stage receiver structure for visible light positioning. The new structure uses two sensors, one of which is a PD-based sensor and the other is an image-based sensor. We describe how this combination exploits both the ability of PDs to receive and demodulate high frequency signals and the ability of image-based sensors to provide very accurate positioning information. The paper also introduces the use of visible reference points in VLP. These are highly localized features which can be readily identified within an image. Potential reference points are a single colored LED within the luminaire, or a specific corner of the luminaire. The use of precise reference points allows very accurate positioning even when the LED beacons are distributed rather than point sources. Extensive simulation results are presented for the case where the PD-based sensor is a QADA. We have shown that, for a range of practical scenarios, the QADA has excellent angular diversity and can provide very accurate AOA estimation. For the case of a high ceiling and low transmitted power, the majority of errors in estimation of incident and polar angle were below 0.003° and 0.02°, respectively. The QADA sensor has the very important practical advantage over other angular diversity receivers that it has compact planar structure. This advantage is shared by the QADA-PLUS which is the new two-stage structure where a QADA is used in the first stage.

REFERENCES

[1] J. Armstrong, Y. A. Sekercioglu, and A. Neild, “Visible light positioning: a roadmap for international standardization,” *IEEE Commun. Mag.*, vol. 51, no. 12, pp. 68–73, Dec. 2013.

[2] J. Luo, L. Fan, and H. Li, “Indoor Positioning Systems Based on Visible Light Communication: State of the Art,” *IEEE Commun. Surv. Tutor.*, vol. 19, no. 4, pp. 2871–2893, Fourthquarter 2017.

[3] H. Liu, H. Darabi, P. Banerjee, and J. Liu, “Survey of Wireless Indoor Positioning Techniques and Systems,” *IEEE Trans. Syst. Man Cybern. Part C Appl. Rev.*, vol. 37, no. 6, pp. 1067–1080, Nov. 2007.

[4] H. Zheng, Z. Xu, C. Yu, and M. Gurusamy, “A 3-D high accuracy positioning system based on visible light communication with novel positioning algorithm,” *Opt. Commun.*, vol. 396, no. Supplement C, pp. 160–168, Aug. 2017.

[5] W. Gu, M. Aminikashani, P. Deng, and M. Kavehrad, “Impact of Multipath Reflections on the Performance of Indoor Visible Light Positioning Systems,” *J. Light. Technol.*, vol. 34, no. 10, pp. 2578–2587, May 2016.

[6] H. Steendam, T. Q. Wang, and J. Armstrong, “Theoretical Lower Bound for Indoor Visible Light Positioning Using Received Signal Strength Measurements and an Aperture-Based Receiver,” *J. Light. Technol.*, vol. PP, no. 99, pp. 1–1, 2016.

[7] T. Q. Wang, Y. A. Sekercioglu, A. Neild, and J. Armstrong, “Position Accuracy of Time-of-Arrival Based Ranging Using Visible Light With Application in Indoor Localization Systems,” *J. Light. Technol.*, vol. 31, no. 20, pp. 3302–3308, Oct. 2013.

[8] T.-H. Do and M. Yoo, “TDOA-based indoor positioning using visible light,” *Photonic Netw. Commun.*, vol. 27, no. 2, pp. 80–88, Apr. 2014.

[9] J. Y. Kim, S. H. Yang, Y. H. Son, and S. K. Han, “High-resolution indoor positioning using light emitting diode visible light and camera image sensor,” *IET Optoelectron.*, vol. 10, no. 5, pp. 184–192, 2016.

[10] M. H. Bergen, X. Jin, D. Guerrero, H. A. L. F. Chaves, N. V. Fredeen, and J. F. Holzman, “Design and Implementation of an Optical Receiver for Angle-of-Arrival-Based Positioning,” *J. Light. Technol.*, vol. 35, no. 18, pp. 3877–3885, Sep. 2017.

[11] Y.-S. Kuo, P. Pannuto, K.-J. Hsiao, and P. Dutta, “Luxapose: indoor positioning with mobile phones and visible light,” in *Proceedings of the Annual International Conference on Mobile Computing and Networking, MOBICOM*, Maui; United States, 2014, pp. 447–458.

[12] S. H. Yang, H. S. Kim, Y. H. Son, and S. K. Han, “Three-Dimensional Visible Light Indoor Localization Using AOA and RSS With Multiple Optical Receivers,” *J. Light. Technol.*, vol. 32, no. 14, pp. 2480–2485, Jul. 2014.

[13] L. Wei, H. Zhang, B. Yu, J. Song, and Y. Guan, “Cubic-Receiver-Based Indoor Optical Wireless Location System,” *IEEE Photonics J.*, vol. 8, no. 1, pp. 1–7, Feb. 2016.

[14] H. Steendam, “A 3D Positioning Algorithm for AOA-Based VLP with an Aperture-Based Receiver,” *IEEE J. Sel. Areas Commun.*, vol. 36, no. 1, pp. 23–33, Jan. 2018.

[15] A. Arafa, S. Dalmiya, R. Klukas, and J. F. Holzman, “Angle-of-arrival reception for optical wireless location technology,” *Opt. Express*, vol. 23, no. 6, pp. 7755–7766, Mar. 2015.

[16] “IEEE Recommended Practices for Modulating Current in High-Brightness LEDs for Mitigating Health Risks to Viewers,” *IEEE Std 1789-2015*, pp. 1–80, Jun. 2015.

[17] R. Zhang, W. D. Zhong, Q. Kemao, and S. Zhang, “A Single LED Positioning System Based on Circle Projection,” *IEEE Photonics J.*, vol. 9, no. 4, pp. 1–9, Aug. 2017.

[18] S. Cincotta, C. He, A. Neild, and J. Armstrong, “High angular resolution visible light positioning using a quadrant photodiode angular diversity aperture receiver (QADA),” *Opt. Express*, vol. 26, no. 7, pp. 9230–9242, Apr. 2018.

[19] S. Cincotta, A. Neild, C. He, and J. Armstrong, “Visible Light Positioning Using an Aperture and a Quadrant Photodiode,” in *2017 IEEE Globecom Workshops (GC Wkshps)*, 2017, pp. 1–6.

[20] A. M. Nugrowati, W. G. Stam, and J. P. Woerdman, “Position measurement of non-integer OAM beams with structurally invariant propagation,” *Opt. Express*, vol. 20, no. 25, pp. 27429–27441, Dec. 2012.

[21] J. H. G. Huisstede, K. O. van der Werf, M. L. Bennink, and V. Subramaniam, “Force detection in optical tweezers using backscattered light,” *Opt. Express*, vol. 13, no. 4, pp. 1113–1123, Feb. 2005.

[22] J. M. Kahn and J. R. Barry, “Wireless infrared communications,” *Proc. IEEE*, vol. 85, no. 2, pp. 265–298, Feb. 1997.

[23] J. Proakis, M. Salehi, and G. Bauch, *Contemporary Communication Systems using MATLAB*, 3rd edition. Stamford, USA: Cengage Learning, 2013.

[24] P. Huynh and M. Yoo, “VLC-Based Positioning System for an Indoor Environment Using an Image Sensor and an Accelerometer Sensor,” *Sensors*, vol. 16, no. 6, p. 783, May 2016.

[25] R. Zhang, W. D. Zhong, K. Qian, and D. Wu, “Image Sensor Based Visible Light Positioning System With Improved Positioning Algorithm,” *IEEE Access*, vol. 5, pp. 6087–6094, 2017.

[26] M. H. Bergen *et al.*, “Design and optimization of indoor optical wireless positioning systems,” in *Photonic Instrumentation Engineering III*, 2016, vol. 9754, p. 97540A.

[27] C. Danakis, M. Afgani, G. Povey, I. Underwood, and H. Haas, “Using a CMOS camera sensor for visible light communication,” in *2012 IEEE Globecom Workshops*, 2012, pp. 1244–1248.

[28] Y. Nakazawa, H. Makino, K. Nishimori, D. Wakatsuki, and H. Komagata, “Indoor positioning using a high-speed, fish-eye lens-equipped camera in Visible Light Communication,” in *International Conference on Indoor Positioning and Indoor Navigation*, 2013, pp. 1–8.

Chapter 9

Conclusions and Future Work

9.1 Overview

The research presented in this thesis contributes to the area of VLP, with the design and analysis of a novel receiver that is ideal for an accurate and robust IPS using AOA techniques. This thesis contains publications from peer-reviewed journals and conferences. The publications can be classified into three major topics: the PD-based QADA receiver, the hybrid QADA-plus receiver and luminaire reference points. This chapter presents an outline of the contributions and conclusions from each publication as well a discussion on potential future work.

9.1.1 Quadrant Angular Diversity Aperture Receiver

The first group of publications explore the QADA receiver. The QADA is created from the combination of a quadrant PD and an aperture. This is a novel receiver structure for VLP that is shown to have good AOA detection capabilities whilst maintaining a compact, planar form factor.

This first publication on the QADA receiver was:

> S. Cincotta, A. Neild, C. He, and J. Armstrong, 'Visible Light Positioning Using an Aperture and a Quadrant Photodiode', in *2017 IEEE Globecom Workshops (GC Wkshps)*, 2017, pp. 1–6

In this paper, the receiver structure was described in detail and the algorithm for light spot detection was derived. The impact of noise on the receiver was analysed and simulation results were presented that showed the accuracy of incident angle detection. Receiver design parameters were explored with simulation results presented for varying PD size and aperture height.

The second publication on the QADA receiver was:

> S. Cincotta, C. He, A. Neild, and J. Armstrong, 'High angular resolution visible light positioning using a quadrant photodiode angular diversity aperture receiver (QADA)', *Opt. Express*, OE, vol. 26, no. 7, pp. 9230–9242, Apr. 2018

This paper analysed the QADA receiver further with both simulation and experimental results. An adapted light spot detection algorithm was presented that can be used for the case where the aperture is smaller than the quadrant PD. An experiment was performed on an optical bench using a prototype QADA receiver and a single LED. The experimental results for incident angle estimation were shown to closely match the simulation results, demonstrating the suitability of the QADA for AOA detection.

9.1.2 QADA-plus

The following publications relate to the QADA-plus receiver. In this hybrid receiver structure, a QADA is combined with a camera to improve the overall accuracy and robustness of the receiver. This is a novel approach to receiver design in VLP that benefits from the advantages of the two different receiver types, whilst overcoming the challenges they individually face.

The first publication on the QADA-plus receiver was:

> S. Cincotta, C. He, A. Neild, and J. Armstrong, 'QADA-PLUS: A Novel Two-Stage Receiver for Visible Light Positioning', in *2018 International Conference on Indoor Positioning and Indoor Navigation (IPIN)*, 2018, pp. 1–8

This paper introduced the hybrid receiver design and derived a positioning algorithm for use with this receiver. The analysis and results of this paper focused on factors that affect a QADA receiver alone but did not impact a hybrid receiver like QADA-plus. Thus, these results demonstrate how a hybrid receiver design can overcome difficulties in using a PD-based receiver alone.

In the analysis, the angular diversity of the QADA receiver was discussed and demonstrated with channel gains plots of the four PD quadrants. Simulation results were presented that demonstrated the impact on AOA estimation for varying height and transmitted power. These results highlighted the deficiencies of using a QADA in non-ideal scenarios. This paper was also the first discussion on the important new concept of reference points.

The second publication on the QADA-plus receiver was:

> S. Cincotta, C. He, A. Neild, and J. Armstrong, 'Indoor Visible Light Positioning: Overcoming the Practical Limitations of the Quadrant Angular Diversity Aperture Receiver (QADA) by Using the Two-Stage QADA-Plus Receiver', *Sensors*, vol. 19, no. 4, p. 956, Jan. 2019

This publication further demonstrated the importance of hybrid receivers with an in depth exploration of the challenges of using PD-based receivers like QADA. Detailed discussion was presented on the potential sources of error for the QADA and several of these sources were explored in simulation. The results showed the impact on AOA estimation and positioning accuracy, in both two and three dimensions. The derivation of the positioning algorithm used in the simulations was also presented. The results demonstrated the impact of realistic luminaire geometry on AOA and position estimation, highlighting the non-negligible effect of this unavoidable problem. Also, results were presented that showed the impact of noise and number of samples used.

9.1.3 Luminaire Reference Points

The following publication focuses on reference points. LRP are identifiable features in an image that can be used in positioning algorithms. Using LRPs, has many advantages. One important advantage is the ability to co-locate multiple LRP on a single luminaire. This reduces the FOV requirements for the receiver and also makes it possible to position in environments where the luminaires are large and installed far apart.

The publication on luminaire reference points was:

> S. Cincotta, A. Neild, and J. Armstrong, 'Luminaire Reference Points (LRP) in Visible Light Positioning using Hybrid Imaging-Photodiode (HIP) Receivers', in *2019 International Conference on Indoor Positioning and Indoor Navigation (IPIN)*, 2019, pp. 1–8

Whilst reference points were introduced and discussed in the previous publications, the following paper provided a deeper analysis and focus on the topic. In this paper, LRPs were analysed using the GDOP. We showed that some luminaire layouts and geometries, such as in most corridors, were very challenging for VLP due to FOV limitations. We then showed that by using multiple LRPs on a single luminaire, this FOV requirement was much less. Simulation results were presented for various LRP layouts that showed the effect of the GDOP.

9.2 Future Work

The research into AOA receiver design for VLP presented in this thesis provides numerous avenues for further work. This section presents several important options for future investigation.

In the work that was presented in this thesis, the scenario where the receiver does not experience tilt was investigated in depth. There are many indoor positioning applications where this is a reasonable assumption. This includes any scenario where the receiver is affixed to a vehicle or object in a static orientation; examples of this are trollies or forklifts. However, there are also many applications where the receiver will experience arbitrary tilt. In particular, all handheld applications, such as pedestrian navigation. Thus, it would be most useful to develop the system further for these applications.

Another interesting avenue for further research is the camera stage of the QADA-plus receiver. Much of the analysis and simulations results in this thesis focused on characterising the QADA receiver. Whilst it was clear that there were advantages to adopting a hybrid receiver structure, it would be valuable to investigate the camera stage in more depth. Although there is already a significant body of research on camera-based VLP systems, there are some aspects that are unique to the QADA-plus receiver that would be important to investigate. In particular, development of image processing algorithms, especially in conjunction with optimisation of reference points. The size, shape and form of the reference points are important to consider as there is a need to satisfy both the receiver functionality as well consumer acceptance of the aesthetic.

Finally, to confirm the theoretical and simulation results, the QADA-plus receiver should be experimentally validated. The experimental results presented in this thesis demonstrated the

AOA estimation of the QADA receiver. However, the experiment was constrained by resources at the time and consisted of a prototype QADA and an optical bench. It would be good to extend the experiment further, comparing QADA and QADA-plus in a full-scale room. These experimental results would be important in quantifying the gains that are to be had when using a hybrid receiver. They would also be valuable for demonstrating the real world potential of the system.

Bibliography

[1] N. Samama, "A Brief History of Navigation and Positioning," in *Global Positioning*, 1st ed., New Jersey: John Wiley & Sons, Ltd, 2008, pp. 1–27.

[2] N. Islam and R. Want, "Smartphones: Past, Present, and Future," *IEEE Pervasive Computing*, vol. 13, no. 4, pp. 89–92, Oct. 2014.

[3] N. E. Klepeis *et al.*, "The National Human Activity Pattern Survey (NHAPS): A resource for assessing exposure to environmental pollutants," *Journal of Exposure Science & Environmental Epidemiology*, vol. 11, no. 3, pp. 231–252, Jul. 2001.

[4] P. Enge and P. Misra, "Special Issue on Global Positioning System," *Proceedings of the IEEE*, vol. 87, no. 1, pp. 3–15, Jan. 1999.

[5] F. van Diggelen and P. Enge, "The World's first GPS MOOC and Worldwide Laboratory using Smartphones," in *Proceedings of the 28th International Technical Meeting of the Satellite Division of The Institute of Navigation (ION GNSS+ 2015)*, Sep. 2015, pp. 361–369.

[6] BeiDou Navigation Satellite System, [Online]. Available: http://en.beidou.gov.cn/ (visited on 02/02/2020).

[7] Galileo is the European global satellite-based navigation system, [Online]. Available: https://www.gsa.europa.eu/european-gnss/galileo/galileo-european-global-satellite-based-navigation-system (visited on 02/02/2020).

[8] Glonass Constellation Status, [Online]. Available: https://www.glonass-iac.ru/en/GLONASS/ (visited on 02/02/2020).

[9] GPS: The Global Positioning System, [Online]. Available: https://www.gps.gov/ (visited on 02/02/2020).

[10] N. Samama, "Applications of Modern Geographical Positioning System," in *Global Positioning*, 1st ed., New Jersey: John Wiley & Sons, Ltd, 2008, pp. 345–378.

[11] P. Connolly, "Indoor Location in Retail: Where is the Money? | ABI Research," ABI Research, Sep. 13, 2016.

[12] D. Lymberopoulos and J. Liu, “The Microsoft Indoor Localization Competition: Experiences and Lessons Learned,” *IEEE Signal Processing Magazine*, vol. 34, no. 5, pp. 125–140, Sep. 2017.

[13] G. M. Mendoza-Silva, J. Torres-Sospedra, and J. Huerta, “A Meta-Review of Indoor Positioning Systems,” *Sensors*, vol. 19, no. 20, p. 4507, Jan. 2019.

[14] V. Renaudin *et al.*, “Evaluating Indoor Positioning Systems in a Shopping Mall: The Lessons Learned From the IPIN 2018 Competition,” *IEEE Access*, vol. 7, pp. 148 594–148 628, 2019.

[15] C. Gong, “Visible Light Communication and Positioning: Present and Future,” *Electronics*, vol. 8, no. 7, p. 788, Jul. 2019.

[16] M. Kavehrad, M. I. S. Chowdhury, and Z. Zhou, “Indoor Positioning Methods Using VLC LEDs,” in *Short-Range Optical Wireless*, John Wiley & Sons, Ltd, 2015, pp. 225–262.

[17] J. Luo, L. Fan, and H. Li, “Indoor Positioning Systems Based on Visible Light Communication: State of the Art,” *IEEE Communications Surveys Tutorials*, vol. 19, no. 4, pp. 2871–2893, Fourthquarter 2017.

[18] Y. Zhuang *et al.*, “A Survey of Positioning Systems Using Visible LED Lights,” *IEEE Communications Surveys Tutorials*, vol. 20, no. 3, pp. 1963–1988, Thirdquarter 2018.

[19] J. Armstrong, Y. A. Sekercioglu, and A. Neild, “Visible light positioning: A roadmap for international standardization,” *IEEE Communications Magazine*, vol. 51, no. 12, pp. 68–73, Dec. 2013.

[20] A. Arafa, X. Jin, and R. Klukas, “Wireless Indoor Optical Positioning With a Differential Photosensor,” *IEEE Photonics Technology Letters*, vol. 24, no. 12, pp. 1027–1029, Jun. 2012.

[21] L. Wei, H. Zhang, B. Yu, J. Song, and Y. Guan, “Cubic-Receiver-Based Indoor Optical Wireless Location System,” *IEEE Photonics Journal*, vol. 8, no. 1, pp. 1–7, Feb. 2016.

[22] W. Xu, J. Wang, H. Shen, H. Zhang, and X. You, “Indoor Positioning for Multiphotodiode Device Using Visible-Light Communications,” *IEEE Photonics Journal*, vol. 8, no. 1, pp. 1–11, Feb. 2016.

[23] S. H. Yang, H. S. Kim, Y. H. Son, and S. K. Han, “Three-Dimensional Visible Light Indoor Localization Using AOA and RSS With Multiple Optical Receivers,” *Journal of Lightwave Technology*, vol. 32, no. 14, pp. 2480–2485, Jul. 2014.

[24] M. Yasir, S. W. Ho, and B. N. Vellambi, “Indoor Position Tracking Using Visible Light,” in *Vehicular Technology Conference (VTC Fall), 2015 IEEE 82nd*, Sep. 2015, pp. 1–5.

[25] B. Jang and H. Kim, “Indoor Positioning Technologies Without Offline Fingerprinting Map: A Survey,” *IEEE Communications Surveys Tutorials*, vol. 21, no. 1, pp. 508–525, Firstquarter 2019.

[26] Z. B. Tariq, D. M. Cheema, M. Z. Kamran, and I. H. Naqvi, “Non-GPS Positioning Systems: A Survey,” *ACM Computing Surveys*, vol. 50, no. 4, pp. 1–34, Aug. 30, 2017.

[27] A. Yassin *et al.*, “Recent Advances in Indoor Localization: A Survey on Theoretical Approaches and Applications,” *IEEE Communications Surveys Tutorials*, vol. 19, no. 2, pp. 1327–1346, Secondquarter 2017.

[28] F. Zafari, A. Gkelias, and K. K. Leung, “A Survey of Indoor Localization Systems and Technologies,” *IEEE Communications Surveys Tutorials*, vol. 21, no. 3, pp. 2568–2599, Thirdquarter 2019.

[29] A. F. G. Ferreira, D. M. A. Fernandes, A. P. Catarino, and J. L. Monteiro, “Localization and Positioning Systems for Emergency Responders: A Survey,” *IEEE Communications Surveys Tutorials*, vol. 19, no. 4, pp. 2836–2870, Fourthquarter 2017.

[30] Locating you in an emergency – what you need to know about E112, [Online]. Available: https://www.gsa.europa.eu/newsroom/news/locating-you-emergency-what-you-need-know-about-e112 (visited on 02/02/2020).

[31] Z. Yang and A. Ganz, “Egocentric Landmark-Based Indoor Guidance System for the Visually Impaired,” *International Journal of E-Health and Medical Communications (IJEHMC)*, vol. 8, no. 3, pp. 55–69, 2017.

[32] S. Holm, “Airborne ultrasound data communications: The core of an indoor positioning system,” in *IEEE Ultrasonics Symposium, 2005.*, vol. 3, Sep. 2005, pp. 1801–1804.

[33] A. Martinelli, S. Jayousi, S. Caputo, and L. Mucchi, “UWB Positioning for Industrial Applications: The Galvanic Plating Case Study,” in *2019 International Conference on Indoor Positioning and Indoor Navigation (IPIN)*, Sep. 2019, pp. 1–7.

[34] T. Smieszek, G. Lazzari, and M. Salathé, “Assessing the Dynamics and Control of Droplet- and Aerosol-Transmitted Influenza Using an Indoor Positioning System,” *Scientific Reports*, vol. 9, no. 1, pp. 1–10, Feb. 18, 2019.

[35] L. Wirola, T. A. Laine, and J. Syrjärinne, “Mass-market requirements for indoor positioning and indoor navigation,” in *2010 International Conference on Indoor Positioning and Indoor Navigation*, Sep. 2010, pp. 1–7.

[36] Y. Gu, A. Lo, and I. Niemegeers, "A survey of indoor positioning systems for wireless personal networks," *IEEE Communications Surveys Tutorials*, vol. 11, no. 1, pp. 13–32, Firstquarter 2009.

[37] A. Basiri *et al.*, "Indoor location based services challenges, requirements and usability of current solutions," *Computer Science Review*, vol. 24, pp. 1–12, May 2017.

[38] J. A. López-Pastor, A. J. Ruiz-Ruiz, A. S. Martínez-Sala, and J. Luis Gómez-Tornero, "Evaluation of an indoor positioning system for added-value services in a mall," in *2019 International Conference on Indoor Positioning and Indoor Navigation (IPIN)*, Sep. 2019, pp. 1–8.

[39] F. Alsehly, T. Arslan, and Z. Sevak, "Indoor positioning with floor determination in multi story buildings," in *2011 International Conference on Indoor Positioning and Indoor Navigation*, Sep. 2011, pp. 1–7.

[40] C. Yang and H.-r. Shao, "WiFi-based indoor positioning," *IEEE Communications Magazine*, vol. 53, no. 3, pp. 150–157, Mar. 2015.

[41] B. Zhu, J. Cheng, Y. Wang, J. Yan, and J. Wang, "Three-Dimensional VLC Positioning Based on Angle Difference of Arrival With Arbitrary Tilting Angle of Receiver," *IEEE Journal on Selected Areas in Communications*, vol. 36, no. 1, pp. 8–22, Jan. 2018.

[42] The Realities of Installing iBeacon to Scale - BKM TECH, [Online]. Available: https://www.brooklynmuseum.org/community/blogosphere/2015/02/04/the-realities-of-installing-ibeacon-to-scale/ (visited on 02/02/2020).

[43] A. Pérez-Navarro *et al.*, "1 - Challenges of Fingerprinting in Indoor Positioning and Navigation," in *Intelligent Data-Centric Systems, Geographical and Fingerprinting Data to Create Systems for Indoor Positioning and Indoor/Outdoor Navigation*, J. Conesa, A. Pérez-Navarro, J. Torres-Sospedra, and R. Montoliu, Eds., Academic Press, Jan. 1, 2019, pp. 1–20.

[44] K. Georgiou, T. Constambeys, C. Laoudias, L. Petrou, G. Chatzimilioudis, and D. Zeinalipour-Yazti, "Anyplace: A Crowdsourced Indoor Information Service," in *2015 16th IEEE International Conference on Mobile Data Management*, Pittsburgh, PA, USA, Jun. 2015, pp. 291–294.

[45] M. Kwak, C. Hamm, S. Park, and T. T. Kwon, "Magnetic Field based Indoor Localization System: A Crowdsourcing Approach," in *2019 International Conference on Indoor Positioning and Indoor Navigation (IPIN)*, Sep. 2019, pp. 1–8.

[46] E. Worrell *et al.*, "Emerging Energy-Efficient Technologies for Industry," *Energy Engineering*, vol. 99, no. 2, pp. 36–55, 2002.

[47] M. M. Ardestani, C. Ferrigno, M. Moazen, and M. A. Wimmer, "From normal to fast walking: Impact of cadence and stride length on lower extremity joint moments," *Gait & Posture*, vol. 46, pp. 118–125, May 1, 2016.

[48] A. Karaagac, J. Haxhibeqiri, M. Ridolfi, W. Joseph, I. Moerman, and J. Hoebeke, "Evaluation of accurate indoor localization systems in industrial environments," in *2017 22nd IEEE International Conference on Emerging Technologies and Factory Automation (ETFA)*, Sep. 2017, pp. 1–8.

[49] D. Plets, A. Eryildirim, S. Bastiaens, N. Stevens, L. Martens, and W. Joseph, "A performance comparison of different cost functions for RSS-based visible light positioning under the presence of reflections," in *Proceedings of the 4th ACM Workshop on Visible Light Communication Systems at the 23rd Annual International Conference on Mobile Computing and Networking*, ACM Press, 2017, pp. 37–41.

[50] M. Deffenbaugh, J. Bellingham, and H. Schmidt, "The relationship between spherical and hyperbolic positioning," in *OCEANS 96 MTS/IEEE Conference Proceedings. The Coastal Ocean - Prospects for the 21st Century*, vol. 2, Sep. 1996, 590–595 vol.2.

[51] S. He and S.-H. G. Chan, "Wi-Fi Fingerprint-Based Indoor Positioning: Recent Advances and Comparisons," *IEEE Communications Surveys Tutorials*, vol. 18, no. 1, pp. 466–490, Firstquarter 2016.

[52] "IEEE Standard for Information technology—Telecommunications and information exchange between systems Local and metropolitan area networks—Specific requirements - Part 11: Wireless LAN Medium Access Control (MAC) and Physical Layer (PHY) Specifications," *IEEE Std 802.11-2016 (Revision of IEEE Std 802.11-2012)*, pp. 1–3534, Dec. 2016.

[53] R. Faragher and R. Harle, "Location Fingerprinting With Bluetooth Low Energy Beacons," *IEEE Journal on Selected Areas in Communications*, vol. 33, no. 11, pp. 2418–2428, Nov. 2015.

[54] K. Kaemarungsi and P. Krishnamurthy, "Properties of indoor received signal strength for WLAN location fingerprinting," in *The First Annual International Conference on Mobile and Ubiquitous Systems: Networking and Services, 2004. MOBIQUITOUS 2004.*, Aug. 2004, pp. 14–23.

[55] iBeacon - Apple Developer, [Online]. Available: https://developer.apple.com/ibeacon/ (visited on 02/02/2020).

[56] S. Gezici *et al.*, "Localization via ultra-wideband radios: A look at positioning aspects for future sensor networks," *IEEE Signal Processing Magazine*, vol. 22, no. 4, pp. 70–84, Jul. 2005.

[57] S. Gezici and H. V. Poor, "Position Estimation via Ultra-Wide-Band Signals," *Proceedings of the IEEE*, vol. 97, no. 2, pp. 386–403, Feb. 2009.

[58] F. Mazhar, M. G. Khan, and B. Sällberg, "Precise Indoor Positioning Using UWB: A Review of Methods, Algorithms and Implementations," *Wireless Personal Communications*, vol. 97, no. 3, pp. 4467–4491, Dec. 1, 2017.

[59] D. Vecchia, P. Corbalán, T. Istomin, and G. P. Picco, "TALLA: Large-scale TDoA Localization with Ultra-wideband Radios," in *2019 International Conference on Indoor Positioning and Indoor Navigation (IPIN)*, Sep. 2019, pp. 1–8.

[60] Decawave, [Online]. Available: https://www.decawave.com/ (visited on 02/02/2020).

[61] Ultra Wideband information, [Online]. Available: https://support.apple.com/en-au/guide/iphone/iph771fd0aad/ios (visited on 02/02/2020).

[62] A. Mandal, C. Lopes, T. Givargis, A. Haghighat, R. Jurdak, and P. Baldi, "Beep: 3D indoor positioning using audible sound," in *Second IEEE Consumer Communications and Networking Conference, 2005. CCNC. 2005*, Jan. 2005, pp. 348–353.

[63] N. B. Priyantha, A. Chakraborty, and H. Balakrishnan, "The Cricket location-support system," in *Proceedings of the 6th Annual International Conference on Mobile Computing and Networking*, ser. MobiCom '00, Boston, Massachusetts, USA: Association for Computing Machinery, Aug. 1, 2000, pp. 32–43.

[64] J. Ureña *et al.*, "Acoustic Local Positioning With Encoded Emission Beacons," *Proceedings of the IEEE*, vol. 106, no. 6, pp. 1042–1062, Jun. 2018.

[65] B. Li, T. Gallagher, A. G. Dempster, and C. Rizos, "How feasible is the use of magnetic field alone for indoor positioning?" In *2012 International Conference on Indoor Positioning and Indoor Navigation (IPIN)*, Nov. 2012, pp. 1–9.

[66] J. Blankenbach and A. Norrdine, "Position estimation using artificial generated magnetic fields," in *2010 International Conference on Indoor Positioning and Indoor Navigation*, Sep. 2010, pp. 1–5.

[67] G. De Angelis *et al.*, "An Indoor AC Magnetic Positioning System," *IEEE Transactions on Instrumentation and Measurement*, vol. 64, no. 5, pp. 1267–1275, May 2015.

[68] V. Pasku *et al.*, "Magnetic Field Based Positioning Systems," *IEEE Communications Surveys Tutorials*, vol. 3, no. 19, pp. 2003–2017, Thirdquarter 2017.

[69] R. Harle, "A Survey of Indoor Inertial Positioning Systems for Pedestrians," *IEEE Communications Surveys Tutorials*, vol. 15, no. 3, pp. 1281–1293, Thirdquarter 2013.

[70] X. Tong *et al.*, "A Double-Step Unscented Kalman Filter and HMM-Based Zero-Velocity Update for Pedestrian Dead Reckoning Using MEMS Sensors," *IEEE Transactions on Industrial Electronics*, vol. 67, no. 1, pp. 581–591, Jan. 2020.

[71] A. R. Jimenez Ruiz, F. Seco Granja, J. C. Prieto Honorato, and J. I. Guevara Rosas, "Accurate Pedestrian Indoor Navigation by Tightly Coupling Foot-Mounted IMU and RFID Measurements," *IEEE Transactions on Instrumentation and Measurement*, vol. 61, no. 1, pp. 178–189, Jan. 2012.

[72] T. Akiyama, M. Sugimoto, and H. Hashizume, "Time-of-arrival-based smartphone localization using visible light communication," in *2017 International Conference on Indoor Positioning and Indoor Navigation (IPIN)*, Sep. 2017, pp. 1–7.

[73] L. Bai, Y. Yang, C. Guo, C. Feng, and X. Xu, "Camera Assisted Received Signal Strength Ratio Algorithm for Indoor Visible Light Positioning," *IEEE Communications Letters*, vol. 23, no. 11, pp. 2022–2025, Nov. 2019.

[74] S. Li and R. Rashidzadeh, "Hybrid indoor location positioning system," *IET Wireless Sensor Systems*, vol. 9, no. 5, pp. 257–264, 2019.

[75] Y. Shu, C. Bo, G. Shen, C. Zhao, L. Li, and F. Zhao, "Magicol: Indoor Localization Using Pervasive Magnetic Field and Opportunistic WiFi Sensing," *IEEE Journal on Selected Areas in Communications*, vol. 33, no. 7, pp. 1443–1457, Jul. 2015.

[76] Q. Liang, J. Lin, and M. Liu, "Towards Robust Visible Light Positioning Under LED Shortage by Visual-inertial Fusion," in *2019 International Conference on Indoor Positioning and Indoor Navigation (IPIN)*, Sep. 2019, pp. 1–8.

[77] Z. Li, A. Yang, H. Lv, L. Feng, and W. Song, "Fusion of Visible Light Indoor Positioning and Inertial Navigation Based on Particle Filter," *IEEE Photonics Journal*, vol. 9, no. 5, pp. 1–13, Oct. 2017.

[78] T. D. Vy, T. L. N. Nguyen, and Y. Shin, “A Smartphone Indoor Localization Using Inertial Sensors and Single Wi-Fi Access Point,” in *2019 International Conference on Indoor Positioning and Indoor Navigation (IPIN)*, Sep. 2019, pp. 1–7.

[79] E. Aitenbichler and M. Muhlhauser, “An IR local positioning system for smart items and devices,” in *23rd International Conference on Distributed Computing Systems Workshops, 2003. Proceedings.*, May 2003, pp. 334–339.

[80] E. Martín-Gorostiza, M. A. García-Garrido, D. Pizarro, P. Torres, M. O. Miguel, and D. Salido-Monzú, “Infrared and Camera Fusion Sensor for Indoor Positioning,” in *2019 International Conference on Indoor Positioning and Indoor Navigation (IPIN)*, Sep. 2019, pp. 1–8.

[81] L. Ni, Y. Liu, Y. C. Lau, and A. Patil, “LANDMARC: Indoor location sensing using active RFID,” in *Proceedings of the First IEEE International Conference on Pervasive Computing and Communications, 2003. (PerCom 2003).*, Mar. 2003, pp. 407–415.

[82] S. S. Saab and Z. S. Nakad, “A Standalone RFID Indoor Positioning System Using Passive Tags,” *IEEE Transactions on Industrial Electronics*, vol. 58, no. 5, pp. 1961–1970, May 2011.

[83] T. Alhmiedat, “An adaptive indoor positioning algorithm for ZigBee WSN,” in *Fifth International Conference on the Innovative Computing Technology (INTECH 2015)*, May 2015, pp. 51–55.

[84] F. Wen, H. Wymeersch, B. Peng, W. P. Tay, H. C. So, and D. Yang, “A survey on 5G massive MIMO localization,” *Digital Signal Processing*, Special Issue on Source Localization in Massive MIMO, vol. 94, pp. 21–28, Nov. 1, 2019.

[85] Estimote, [Online]. Available: http://estimote.com/ (visited on 02/02/2020).

[86] Home | Pozyx, [Online]. Available: https://www.pozyx.io/ (visited on 02/02/2020).

[87] IndoorAtlas, [Online]. Available: http://www.indooratlas.com/ (visited on 02/02/2020).

[88] LED Based Indoor Positioning System, [Online]. Available: http://www.lighting.philips.com.au/systems/themes/led-based-indoor-positioning (visited on 02/02/2020).

[89] Solutions for Real-Time Locating Systems (RTLS) by infsoft, [Online]. Available: https://www.infsoft.com/ (visited on 02/02/2020).

[90] J. Kostak. Real-time location system (RTLS) for indoor tracking, [Online]. Available: https://www.sewio.net/ (visited on 02/02/2020).

[91] Gatwick installs 2000 indoor navigation beacons enabling augmented reality wayfinding – a world first for an airport, [Online]. Available: http://www.mediacentre.gatwickairport.com/press-releases/2017/17_05_25_beacons.aspx (visited on 02/02/2020).

[92] MLBAM completes initial iBeacon installations, [Online]. Available: https://www.mlb.com/news/mlb-advanced-media-completes-initial-ibeacon-installations/c-67782508 (visited on 02/02/2020).

[93] G. Gruman. Beacons are harder to deploy than you think, [Online]. Available: https://www.infoworld.com/article/2983166/beacons-are-harder-to-deploy-than-you-think.html (visited on 02/02/2020).

[94] M. Aminikashani, W. Gu, and M. Kavehrad, "Indoor location estimation with optical-based orthogonal frequency division multiplexing communications," *Optical Engineering*, vol. 55, no. 5, pp. 056 116–056 116, 2016.

[95] W. Gu, M. Aminikashani, and M. Kavehrad, "Indoor visible light positioning system with multipath reflection analysis," in *2016 IEEE International Conference on Consumer Electronics (ICCE)*, Jan. 2016, pp. 89–92.

[96] C. Amini, A. Taherpour, T. Khattab, and S. Gazor, "Theoretical accuracy analysis of indoor visible light communication positioning system based on time-of-arrival," in *2016 IEEE Canadian Conference on Electrical and Computer Engineering (CCECE)*, May 2016, pp. 1–5.

[97] I. Demirel and S. Gezici, "Accuracy Limits of Distance Estimation in Visible Light Systems with RGB LEDs," in *2019 IEEE 30th Annual International Symposium on Personal, Indoor and Mobile Radio Communications (PIMRC)*, Sep. 2019, pp. 1–6.

[98] E. Gonendik and S. Gezici, "Fundamental Limits on RSS Based Range Estimation in Visible Light Positioning Systems," *IEEE Communications Letters*, vol. 19, no. 12, pp. 2138–2141, Dec. 2015.

[99] M. F. Keskin, E. Gonendik, and S. Gezici, "Improved Lower Bounds for Ranging in Synchronous Visible Light Positioning Systems," *Journal of Lightwave Technology*, vol. 34, no. 23, pp. 5496–5504, Dec. 2016.

[100] A. Sahin, Y. S. Eroglu, I. Guvenc, N. Pala, and M. Yuksel, "Accuracy of AOA-Based and RSS-Based 3D Localization for Visible Light Communications," in *2015 IEEE 82nd Vehicular Technology Conference (VTC2015-Fall)*, Sep. 2015, pp. 1–5.

[101] H. Steendam, T. Q. Wang, and J. Armstrong, "Cramer-Rao bound for AOA-based VLP with an aperture-based receiver," in *2017 IEEE International Conference on Communications (ICC)*, May 2017, pp. 1–6.

[102] H. Steendam, T. Q. Wang, and J. Armstrong, "Theoretical Lower Bound for Indoor Visible Light Positioning Using Received Signal Strength Measurements and an Aperture-Based Receiver," *Journal of Lightwave Technology*, vol. 35, no. 2, pp. 309–319, Jan. 2017.

[103] X. Sun, Y. Zou, J. Duan, and A. Shi, "The positioning accuracy analysis of AOA-based indoor visible light communication system," in *2015 International Conference on Optoelectronics and Microelectronics (ICOM)*, Jul. 2015, pp. 186–190.

[104] T. Q. Wang, Y. A. Sekercioglu, A. Neild, and J. Armstrong, "Position Accuracy of Time-of-Arrival Based Ranging Using Visible Light With Application in Indoor Localization Systems," *Journal of Lightwave Technology*, vol. 31, no. 20, pp. 3302–3308, Oct. 2013.

[105] R. Zhang, W. D. Zhong, K. Qian, and D. Wu, "Image Sensor Based Visible Light Positioning System With Improved Positioning Algorithm," *IEEE Access*, vol. 5, pp. 6087–6094, 2017.

[106] X. Zhang, J. Duan, Y. Fu, and A. Shi, "Theoretical Accuracy Analysis of Indoor Visible Light Communication Positioning System Based on Received Signal Strength Indicator," *Journal of Lightwave Technology*, vol. 32, no. 21, pp. 4180–4186, Nov. 2014.

[107] T.-H. Do and M. Yoo, "An in-Depth Survey of Visible Light Communication Based Positioning Systems," *Sensors (Basel, Switzerland)*, vol. 16, no. 5, May 12, 2016.

[108] E. W. Lam and T. D. C. Little, "Visible light positioning: Moving from 2D planes to 3D spaces [Invited]," *Chinese Optics Letters*, vol. 17, no. 3, p. 030 604, Mar. 10, 2019.

[109] G. B. Prince and T. D. C. Little, "Two-Phase Framework for Indoor Positioning Systems Using Visible Light †," *Sensors*, vol. 18, no. 6, p. 1917, Jun. 12, 2018.

[110] K. Yan, H. Zhou, H. Xiao, and X. Zhang, "Current status of indoor positioning system based on visible light," in *2015 15th International Conference on Control, Automation and Systems (ICCAS)*, Oct. 2015, pp. 565–569.

[111] E. W. Lam and T. D. C. Little, "Visible Light Positioning for Location-Based Services in Industry 4.0," in *2019 16th International Symposium on Wireless Communication Systems (ISWCS)*, Aug. 2019, pp. 345–350.

[112] I. Ahmed, H. Karvonen, T. Kumpuniemi, and M. Katz, "Wireless Communications for the Hospital of the Future: Requirements, Challenges and Solutions," *International Journal of Wireless Information Networks*, Oct. 28, 2019.

[113] J. Torlach, "Radio-Frequency Energy - Hazards & Safeguards," Department of Minerals and Energy.

[114] Y. Hu *et al.*, "A Visible Light Based Indoor Positioning System," Jun. 1, 2015. arXiv: 1505.05977.

[115] X. Liu, H. Makino, and K. Mase, "Improved Indoor Location Estimation Using Fluorescent Light Communication System with a Nine-Channel Receiver," *IEICE TRANSACTIONS on Communications*, vol. E93-B, no. 11, pp. 2936–2944, Nov. 1, 2010.

[116] C. Zhang, S. Zhou, and X. Zhang, "Visible Light Localization Using Incumbent Light Fixtures: Demo Abstract," in *Proceedings of the 14th ACM Conference on Embedded Network Sensor Systems CD-ROM - SenSys '16*, Stanford, CA, USA: ACM Press, 2016, pp. 304–305.

[117] R. D. Dupuis and M. R. Krames, "History, Development, and Applications of High-Brightness Visible Light-Emitting Diodes," *Journal of Lightwave Technology*, vol. 26, no. 9, pp. 1154–1171, May 2008.

[118] R. and Markets. (May 15, 2019). Asia-Pacific $58 Billion LED Lighting Market to 2024 - Growing Popularity of Smart LED Lighting, [Online]. Available: http://www.globenewswire.com/news-release/2019/05/15/1824590/0/en/Asia-Pacific-58-Billion-LED-Lighting-Market-to-2024-Growing-Popularity-of-Smart-LED-Lighting.html (visited on 01/29/2020).

[119] D. A. Steigerwald *et al.*, "Illumination with solid state lighting technology," *IEEE Journal of Selected Topics in Quantum Electronics*, vol. 8, no. 2, pp. 310–320, Mar. 2002.

[120] S. Rajbhandari *et al.*, "A review of gallium nitride LEDs for multi-gigabit-per-second visible light data communications," *Semiconductor Science and Technology*, vol. 32, no. 2, p. 023 001, 2017.

[121] H. Elgala, R. Mesleh, and H. Haas, "Indoor optical wireless communication: Potential and state-of-the-art," *IEEE Communications Magazine*, vol. 49, no. 9, pp. 56–62, Sep. 2011.

[122] H. Haas, C. Chen, and D. O'Brien, "A guide to wireless networking by light," *Progress in Quantum Electronics*, vol. 55, pp. 88–111, Sep. 2017.

[123] H. Haas, L. Yin, Y. Wang, and C. Chen, "What is LiFi?" *Journal of Lightwave Technology*, vol. 34, no. 6, pp. 1533–1544, Mar. 2016.

[124] D. Karunatilaka, F. Zafar, V. Kalavally, and R. Parthiban, "LED Based Indoor Visible Light Communications: State of the Art," *IEEE Communications Surveys Tutorials*, vol. 17, no. 3, pp. 1649–1678, Thirdquarter 2015.

[125] D. C. O'Brien, L. Zeng, H. Le-Minh, G. Faulkner, J. W. Walewski, and S. Randel, "Visible light communications: Challenges and possibilities," in *2008 IEEE 19th International Symposium on Personal, Indoor and Mobile Radio Communications*, Sep. 2008, pp. 1–5.

[126] Y. Tanaka, T. Komine, S. Haruyama, and M. Nakagawa, "Indoor visible communication utilizing plural white LEDs as lighting," in *12th IEEE International Symposium on Personal, Indoor and Mobile Radio Communications. PIMRC 2001. Proceedings*, vol. 2, Oct. 2001.

[127] S. Kitsinelis, L. Arexis-Boisson, Y. Zhang, and G. Zissis, "LED Flicker: A Drawback or an Opportunity?" *Optics and Photonics Journal*, vol. 03, no. 01, p. 63, Mar. 22, 2013.

[128] "IEEE Recommended Practices for Modulating Current in High-Brightness LEDs for Mitigating Health Risks to Viewers," *IEEE Std 1789-2015*, pp. 1–80, Jun. 2015.

[129] G. Cossu, A. M. Khalid, P. Choudhury, R. Corsini, and E. Ciaramella, "3.4 Gbit/s visible optical wireless transmission based on RGB LED," *Optics Express*, vol. 20, no. 26, B501–B506, Dec. 10, 2012.

[130] A. T. Hussein, M. T. Alresheedi, and J. M. H. Elmirghani, "20 Gb/s Mobile Indoor Visible Light Communication System Employing Beam Steering and Computer Generated Holograms," *Journal of Lightwave Technology*, vol. 33, no. 24, pp. 5242–5260, Dec. 2015.

[131] Y.-S. Kuo, P. Pannuto, K.-J. Hsiao, and P. Dutta, "Luxapose: Indoor positioning with mobile phones and visible light," in *Proceedings of the Annual International Conference on Mobile Computing and Networking, MOBICOM*, Maui; United States: ACM Press, 2014, pp. 447–458.

[132] R. Qv, L. Feng, A. Yang, P. Guo, B. Lin, and H. Huang, "A High Efficient Code for Visible Light Positioning System Based on Image Sensor," *IEEE Access*, vol. 7, pp. 77 762–77 770, 2019.

[133] C. Xie, W. Guan, Y. Wu, L. Fang, and Y. Cai, "The LED-ID Detection and Recognition Method Based on Visible Light Positioning Using Proximity Method," *IEEE Photonics Journal*, vol. 10, no. 2, pp. 1–16, Apr. 2018.

[134] S. D. Lausnay, L. D. Strycker, J. P. Goemaere, B. Nauwelaers, and N. Stevens, "A survey on multiple access Visible Light Positioning," in *2016 IEEE International Conference on Emerging Technologies and Innovative Business Practices for the Transformation of Societies (EmergiTech)*, Aug. 2016, pp. 38–42.

[135] Y. Gong, Z. Shi, and Y. Wang, "Indoor visual positioning system using LED and mobile phone," in *Selected Papers of the Photoelectronic Technology Committee Conferences Held November 2015*, vol. 9796, International Society for Optics and Photonics, Jan. 26, 2016, 97961N.

[136] M. Yasir, S. W. Ho, and B. N. Vellambi, "Indoor Position Tracking Using Multiple Optical Receivers," *Journal of Lightwave Technology*, vol. 34, no. 4, pp. 1166–1176, Feb. 2016.

[137] B. Lin, X. Tang, Z. Ghassemlooy, C. Lin, and Y. Li, "Experimental Demonstration of an Indoor VLC Positioning System Based on OFDMA," *IEEE Photonics Journal*, vol. 9, no. 2, pp. 1–9, Apr. 2017.

[138] S. Pergoloni, Z. Mohamadi, A. M. Vegni, Z. Ghassemlooy, and M. Biagi, "Visible Light indoor positioning through colored LEDs," in *2017 IEEE International Conference on Communications Workshops (ICC Workshops)*, May 2017, pp. 150–155.

[139] A. A. Saed, M. Yasir, S. W. Ho, and C. W. Sung, "Coding for uncoordinated multiple access in visible light positioning systems," in *2016 10th International Conference on Signal Processing and Communication Systems (ICSPCS)*, Dec. 2016, pp. 1–7.

[140] Y. Xu *et al.*, "Accuracy analysis and improvement of visible light positioning based on VLC system using orthogonal frequency division multiple access," *Optics Express*, vol. 25, no. 26, pp. 32 618–32 630, Dec. 25, 2017.

[141] M. Yasir, A. A. Saed, and S. W. Ho, "Uncoordinated multiple access scheme for VLC systems with positioning capability," in *2016 Australian Communications Theory Workshop (AusCTW)*, Jan. 2016, pp. 118–123.

[142] N. Wu, L. Feng, and A. Yang, "Localization Accuracy Improvement of a Visible Light Positioning System Based on the Linear Illumination of LED Sources," *IEEE Photonics Journal*, vol. 9, no. 5, pp. 1–11, Oct. 2017.

[143] What to expect from smartphone cameras in 2020, [Online]. Available: https://www.androidauthority.com/smartphone-cameras-2020-1066830/ (visited on 02/02/2020).

[144] Phantom Ultrahigh-Speed, [Online]. Available: https://www.phantomhighspeed.com/products/cameras/ultrahighspeed (visited on 02/02/2020).

[145] M. Rátosi and G. Simon, "Towards Robust VLC Beacon Identification in Camera Based Localization Systems," in *2019 International Conference on Indoor Positioning and Indoor Navigation (IPIN)*, Sep. 2019, pp. 1–8.

[146] P. Chavez-Burbano, V. Guerra, J. Rabadan, and R. Perez-Jimenez, "Optical Camera Communication system for three-dimensional indoor localization," *Optik*, vol. 192, p. 162 870, Sep. 1, 2019.

[147] J. Gao, F. Yang, and X. Ma, "Indoor positioning system based on visible light communication with gray-coded identification," in *2017 13th International Wireless Communications and Mobile Computing Conference (IWCMC)*, Jun. 2017, pp. 899–903.

[148] H.-Y. Lee, H.-M. Lin, Y.-L. Wei, H.-I. Wu, H.-M. Tsai, and K. C.-J. Lin, "RollingLight: Enabling Line-of-Sight Light-to-Camera Communications," in *Proceedings of the 13th Annual International Conference on Mobile Systems, Applications, and Services*, ser. MobiSys '15, New York, NY, USA: ACM, 2015, pp. 167–180.

[149] P. Liu, R. Jiang, R. Bai, T. Mao, J. Quan, and Z. Wang, "High-Accuracy Three-Dimensional Visible Light Positioning Systems Using Image Sensor," in *2018 IEEE 87th Vehicular Technology Conference (VTC Spring)*, Jun. 2018, pp. 1–5.

[150] S. Cincotta, C. He, A. Neild, and J. Armstrong, "Indoor Visible Light Positioning: Overcoming the Practical Limitations of the Quadrant Angular Diversity Aperture Receiver (QADA) by Using the Two-Stage QADA-Plus Receiver," *Sensors*, vol. 19, no. 4, p. 956, Jan. 2019.

[151] S. Cincotta, C. He, A. Neild, and J. Armstrong, "QADA-PLUS: A Novel Two-Stage Receiver for Visible Light Positioning," in *2018 International Conference on Indoor Positioning and Indoor Navigation (IPIN)*, Sep. 2018, pp. 1–8.

[152] W. Gu, M. Aminikashani, P. Deng, and M. Kavehrad, "Impact of Multipath Reflections on the Performance of Indoor Visible Light Positioning Systems," *Journal of Lightwave Technology*, vol. 34, no. 10, pp. 2578–2587, May 2016.

[153] J. M. Kahn and J. R. Barry, "Wireless infrared communications," *Proceedings of the IEEE*, vol. 85, no. 2, pp. 265–298, Feb. 1997.

[154] S. Hranilovic, *Wireless Optical Communication Systems*. Springer Science & Business Media, Jan. 16, 2006.

[155] S. B. Alexander, *Optical Communication Receiver Design*. SPIE Optical Engineering Press, 1997.

[156] B. Technologies. High Performance Diffusers, [Online]. Available: http://www.lightingaustralia.com.au/uploads/420/bright-view-data-sheets-2011-10-06-2.pdf (visited on 02/02/2020).

[157] P.-L. Chen *et al.*, "The illumination uniformity study of diffuser plates for reflective LED desk lighting," in *The 9th IEEE International Conference on Nano/Micro Engineered and Molecular Systems (NEMS)*, Apr. 2014, pp. 525–529.

[158] C.-W. Chiang, Y.-K. Hsu, and J.-W. Pan, "Design and demonstration of high efficiency anti-glare LED luminaires for indoor lighting," *Optics Express*, vol. 23, no. 3, A15–A26, Feb. 9, 2015.

[159] M. H. Bergen, A. Arafa, X. Jin, R. Klukas, and J. F. Holzman, "Characteristics of Angular Precision and Dilution of Precision for Optical Wireless Positioning," *Journal of Lightwave Technology*, vol. 33, no. 20, pp. 4253–4260, Oct. 2015.

[160] M. H. Bergen, F. S. Schaal, R. Klukas, J. Cheng, and J. F. Holzman, "Toward the implementation of a universal angle-based optical indoor positioning system," *Frontiers of Optoelectronics*, vol. 11, no. 2, pp. 116–127, Jun. 1, 2018.

[161] D. Plets *et al.*, "Three-dimensional Visible Light Positioning: An Experimental Assessment of the Importance of the LEDs' Locations," in *2019 International Conference on Indoor Positioning and Indoor Navigation (IPIN)*, Sep. 2019, pp. 1–6.

[162] S. Cincotta, A. Neild, and J. Armstrong, "Luminaire Reference Points (LRP) in Visible Light Positioning using Hybrid Imaging-Photodiode (HIP) Receivers," in *2019 International Conference on Indoor Positioning and Indoor Navigation (IPIN)*, Sep. 2019, pp. 1–8.

[163] R. Amsters, E. Demeester, P. Slaets, D. Holm, J. Joly, and N. Stevens, "Towards Automated Calibration of Visible Light Positioning Systems," in *2019 International Conference on Indoor Positioning and Indoor Navigation (IPIN)*, Sep. 2019, pp. 1–8.

[164] D. Gualda, J. Ureña, J. Alcalá, and C. Santos, "Calibration of Beacons for Indoor Environments based on a Digital Map and Heuristic Information," *Sensors*, vol. 19, no. 3, p. 670, Jan. 2019.

[165] T. C. E. Jones, "The long term stability of the response of silicon photodiodes," in *IEE Colloquium on Developments in near Infra-Red Visible Ultraviolet Detectors*, Nov. 1991, pp. 6/1–6/3.

[166] D. Li, C. Gong, and Z. Xu, "A RSSI-based indoor visible light positioning approach," in *2016 10th International Symposium on Communication Systems, Networks and Digital Signal Processing (CSNDSP)*, Jul. 2016, pp. 1–6.

[167] J. M. Menéndez and H. Steendam, "Influence of the aperture-based receiver orientation on RSS-based VLP performance," in *2017 International Conference on Indoor Positioning and Indoor Navigation (IPIN)*, Sep. 2017, pp. 1–7.

[168] N. Stevens, D. Plets, and L. D. Strycker, "Monte Carlo algorithm for the evaluation of the distance estimation variance in RSS-based visible light positioning," in *2017 20th International Symposium on Wireless Personal Multimedia Communications (WPMC)*, Dec. 2017, pp. 212–216.

[169] Z. Zheng, L. Liu, and W. Hu, "Accuracy of Ranging Based on DMT Visible Light Communication for Indoor Positioning," *IEEE Photonics Technology Letters*, vol. PP, no. 99, pp. 1–1, 2017.

[170] P. Du *et al.*, "Experimental Demonstration of 3D Visible Light Positioning Using Received Signal Strength With Low-Complexity Trilateration Assisted by Deep Learning Technique," *IEEE Access*, vol. 7, pp. 93 986–93 997, 2019.

[171] P. Luo *et al.*, "Experimental demonstration of an indoor visible light communication positioning system using dual-tone multi-frequency technique," in *2014 3rd International Workshop in Optical Wireless Communications (IWOW)*, Sep. 2014, pp. 55–59.

[172] L. Li, P. Hu, C. Peng, G. Shen, and F. Zhao, "Epsilon: A Visible Light Based Positioning System," in *Proceedings of the 11th USENIX Symposium on Networked Systems Design and Implementation*, Apr. 2014, pp. 331–343.

[173] F. Alam, B. Parr, and S. Mander, "Visible Light Positioning Based on Calibrated Propagation Model," *IEEE Sensors Letters*, vol. 3, no. 2, pp. 1–4, Feb. 2019.

[174] S. Bastiaens, D. Plets, L. Martens, and W. Joseph, "Response Adaptive Modelling for Reducing the Storage and Computation of RSS-Based VLP," in *2018 International Conference on Indoor Positioning and Indoor Navigation (IPIN)*, Sep. 2018, pp. 1–8.

[175] H. Q. Tran and C. Ha, "Improved Visible Light-Based Indoor Positioning System Using Machine Learning Classification and Regression," *Applied Sciences*, vol. 9, no. 6, p. 1048, Jan. 2019.

[176] T.-H. Do and M. Yoo, "TDOA-based indoor positioning using visible light," *Photonic Network Communications*, vol. 27, no. 2, pp. 80–88, Apr. 1, 2014.

[177] P. Du, S. Zhang, C. Chen, A. Alphones, and W.-D. Zhong, "Demonstration of a Low-Complexity Indoor Visible Light Positioning System Using an Enhanced TDOA Scheme," *IEEE Photonics Journal*, vol. 10, no. 4, pp. 1–10, Aug. 2018.

[178] S. Y. Jung, S. Hann, and C. S. Park, "TDOA-based optical wireless indoor localization using LED ceiling lamps," *IEEE Transactions on Consumer Electronics*, vol. 57, no. 4, pp. 1592–1597, Nov. 2011.

[179] A. Naz, H. M. Asif, T. Umer, and B. S. Kim, "PDOA based Indoor Positioning using Visible Light Communication," *IEEE Access*, vol. 6, pp. 7557–7564, 2018.

[180] S. Hamidi-Rad, K. Lyons, and N. Goela, "Infrastructure-less indoor localization using light fingerprints," in *2017 IEEE International Conference on Acoustics, Speech and Signal Processing (ICASSP)*, Mar. 2017, pp. 5995–5999.

[181] H. Q. Tran and C. Ha, "Fingerprint-Based Indoor Positioning System Using Visible Light Communication—A Novel Method for Multipath Reflections," *Electronics*, vol. 8, no. 1, p. 63, Jan. 2019.

[182] A. M. Vegni and M. Biagi, "An indoor localization algorithm in a small-cell LED-based lighting system," in *2012 International Conference on Indoor Positioning and Indoor Navigation (IPIN)*, Sydney, Nov. 2012, pp. 1–7.

[183] M. T. Taylor and S. Hranilovic, "Angular diversity approach to indoor positioning using visible light," in *2013 IEEE Globecom Workshops (GC Wkshps)*, Dec. 2013, pp. 1093–1098.

[184] L. Yin, X. Wu, and H. Haas, "Indoor Visible Light Positioning with Angle Diversity Transmitter," IEEE, Sep. 2015, pp. 1–5.

[185] S. H. Yang, E. M. Jeong, and S. K. Han, "Indoor positioning based on received optical power difference by angle of arrival," *Electronics Letters*, vol. 50, no. 1, pp. 49–51, Jan. 2014.

[186] X. Yu, J. Wang, and H. Lu, "Single light-emitting diode-based high-accuracy indoor positioning system using symmetrical optical receiver," *Optical Engineering*, vol. 57, no. 10, p. 106 104, Oct. 2018.

[187] B. Zhu, Z. Zhu, Y. Wang, and J. Cheng, "Optimal Optical Omnidirectional Angle-of-Arrival Estimator With Complementary Photodiodes," *Journal of Lightwave Technology*, vol. 37, no. 13, pp. 2932–2945, Jul. 2019.

[188] T. Q. Wang, C. He, and J. Armstrong, "Angular diversity for indoor MIMO optical wireless communications," in *2015 IEEE International Conference on Communications (ICC)*, Jun. 2015, pp. 5066–5071.

[189] C. He, S. Cincotta, M. M. A. Mohammed, and J. Armstrong, "Angular Diversity Aperture (ADA) Receivers for Indoor Multiple-Input Multiple-Output (MIMO) Visible Light Communications (VLC)," *IEEE Access*, vol. 7, pp. 145 282–145 301, 2019.

[190] T. Q. Wang, C. He, and J. Armstrong, "Performance Analysis of Aperture-Based Receivers for MIMO IM/DD Visible Light Communications," *Journal of Lightwave Technology*, vol. 35, no. 9, pp. 1513–1523, May 2017.

[191] S. Bastiaens and H. Steendam, "Coarse estimation of the incident angle for VLP with an aperture-based receiver," in *2017 14th Workshop on Positioning, Navigation and Communications (WPNC)*, Oct. 2017, pp. 1–6.

[192] H. Steendam, "A 3D Positioning Algorithm for AOA-Based VLP with an Aperture-Based Receiver," *IEEE Journal on Selected Areas in Communications*, vol. 36, no. 1, pp. 23–33, Jan. 2018.

[193] Z. Li, "Indoor Positioning System Using Visible Light Communication and Smartphone With Rolling Shutter Camera," UC Riverside, 2016.

[194] M. Halpern, Y. Zhu, and V. J. Reddi, "Mobile CPU's rise to power: Quantifying the impact of generational mobile CPU design trends on performance, energy, and user satisfaction," in *2016 IEEE International Symposium on High Performance Computer Architecture (HPCA)*, Mar. 2016, pp. 64–76.

[195] H. Hosseinianfar, A. Chizari, and J. A. Salehi, "GOPA: Geometrical Optics Positioning Algorithm," in *2019 IEEE International Conference on Consumer Electronics (ICCE)*, Jan. 2019, pp. 1–6.

[196] J. Gancarz, H. Elgala, and T. D. Little, "Impact of lighting requirements on VLC systems," *IEEE Communications Magazine*, vol. 51, no. 12, pp. 34–41, Dec. 2013.

[197] T. Komine and M. Nakagawa, "Fundamental analysis for visible-light communication system using LED lights," *IEEE Transactions on Consumer Electronics*, vol. 50, no. 1, pp. 100–107, Feb. 2004.

[198] W. Gu, W. Zhang, M. Kavehrad, and L. Feng, "Three-dimensional light positioning algorithm with filtering techniques for indoor environments," *Optical Engineering*, vol. 53, no. 10, p. 107 107, 2014.

[199] K. Panta and J. Armstrong, "Indoor localisation using white LEDs," *Electronics Letters*, vol. 48, no. 4, pp. 228–230, Feb. 2012.

[200] G. del Campo-Jimenez, J. M. Perandones, and F. J. Lopez-Hernandez, "A VLC-based beacon location system for mobile applications," in *2013 International Conference on Localization and GNSS (ICL-GNSS)*, Jun. 2013, pp. 1–4.

[201] S. Alexander *et al.*, "An atomic-resolution atomic-force microscope implemented using an optical lever," *Journal of Applied Physics*, vol. 65, no. 1, pp. 164–167, Jan. 1989.

[202] S. Keen, J. Leach, G. Gibson, and M. J. Padgett, "Comparison of a high-speed camera and a quadrant detector for measuring displacements in optical tweezers," *Journal of Optics A: Pure and Applied Optics*, vol. 9, no. 8, S264, 2007.

[203] S. Lakämper, A. Lamprecht, I. A. T. Schaap, and J. Dual, "Direct 2D measurement of time-averaged forces and pressure amplitudes in acoustophoretic devices using optical trapping," *Lab on a Chip*, vol. 15, no. 1, pp. 290–300, Dec. 3, 2014.

[204] "Quadrant and Bi-Cell Silicon Photodiode Amplifier Module," OSI Optoelectronics.

[205] Ray, Sidney F., *Applied Photographic Optics*, 2nd edition. Oxford: Focal Press, 1994.

[206] S.-Y. Jung, D.-H. Kwon, S.-H. Yang, and S.-K. Han, "Inter-cell interference mitigation in multi-cellular visible light communications," *Optics Express*, vol. 24, no. 8, pp. 8512–8526, Apr. 18, 2016.

[207] H. Zheng, Z. Xu, C. Yu, and M. Gurusamy, "A 3-D high accuracy positioning system based on visible light communication with novel positioning algorithm," *Optics Communications*, vol. 396, pp. 160–168, Supplement C Aug. 1, 2017.

[208] A. Arafa, S. Dalmiya, R. Klukas, and J. F. Holzman, "Angle-of-arrival reception for optical wireless location technology," *Optics Express*, vol. 23, no. 6, pp. 7755–7766, Mar. 23, 2015.

[209] M. H. Bergen, X. Jin, D. Guerrero, H. A. L. F. Chaves, N. V. Fredeen, and J. F. Holzman, "Design and Implementation of an Optical Receiver for Angle-of-Arrival-Based Positioning," *Journal of Lightwave Technology*, vol. 35, no. 18, pp. 3877–3885, Sep. 2017.

[210] P. Huynh and M. Yoo, "VLC-Based Positioning System for an Indoor Environment Using an Image Sensor and an Accelerometer Sensor," *Sensors*, vol. 16, no. 6, p. 783, May 28, 2016.

[211] H. Steendam, T. Q. Wang, and J. Armstrong, "Cramer-Rao bound for indoor visible light positioning using an aperture-based angular-diversity receiver," in *2016 IEEE International Conference on Communications (ICC)*, May 2016, pp. 1–6.

[212] I. Gőzse, "Optical Indoor Positioning System Based on TFT Technology," *Sensors (Basel, Switzerland)*, vol. 16, no. 1, p. 19, Dec. 24, 2015.

[213] S. Cincotta, A. Neild, C. He, and J. Armstrong, "Visible Light Positioning Using an Aperture and a Quadrant Photodiode," in *2017 IEEE Globecom Workshops (GC Wkshps)*, Dec. 2017, pp. 1–6.

[214] J. H. G. Huisstede, K. O. van der Werf, M. L. Bennink, and V. Subramaniam, "Force detection in optical tweezers using backscattered light," *Optics Express*, vol. 13, no. 4, pp. 1113–1123, Feb. 21, 2005.

[215] A. M. Nugrowati, W. G. Stam, and J. P. Woerdman, "Position measurement of non-integer OAM beams with structurally invariant propagation," *Optics Express*, vol. 20, no. 25, pp. 27 429–27 441, Dec. 3, 2012.

[216] A. Haapalinna, P. Kärhä, and E. Ikonen, "Spectral reflectance of silicon photodiodes," *Applied Optics*, vol. 37, no. 4, pp. 729–732, Feb. 1, 1998.

[217] H. Liu, H. Darabi, P. Banerjee, and J. Liu, "Survey of Wireless Indoor Positioning Techniques and Systems," *IEEE Transactions on Systems, Man, and Cybernetics, Part C (Applications and Reviews)*, vol. 37, no. 6, pp. 1067–1080, Nov. 2007.

[218] J. Y. Kim, S. H. Yang, Y. H. Son, and S. K. Han, "High-resolution indoor positioning using light emitting diode visible light and camera image sensor," *IET Optoelectronics*, vol. 10, no. 5, pp. 184–192, 2016.

[219] R. Zhang, W. D. Zhong, Q. Kemao, and S. Zhang, "A Single LED Positioning System Based on Circle Projection," *IEEE Photonics Journal*, vol. 9, no. 4, pp. 1–9, Aug. 2017.

[220] S. Cincotta, C. He, A. Neild, and J. Armstrong, "High angular resolution visible light positioning using a quadrant photodiode angular diversity aperture receiver (QADA)," *Optics Express*, vol. 26, no. 7, pp. 9230–9242, Apr. 2, 2018.

[221] J. Proakis, M. Salehi, and G. Bauch, *Contemporary Communication Systems Using MATLAB*, 3rd edition. Stamford, USA: Cengage Learning, 2013.

[222] M. H. Bergen *et al.*, "Design and optimization of indoor optical wireless positioning systems," in *Photonic Instrumentation Engineering III*, vol. 9754, International Society for Optics and Photonics, Mar. 16, 2016, 97540A.

[223] C. Danakis, M. Afgani, G. Povey, I. Underwood, and H. Haas, "Using a CMOS camera sensor for visible light communication," in *2012 IEEE Globecom Workshops*, Dec. 2012, pp. 1244–1248.

[224] Y. Nakazawa, H. Makino, K. Nishimori, D. Wakatsuki, and H. Komagata, "Indoor positioning using a high-speed, fish-eye lens-equipped camera in Visible Light Communication," in *International Conference on Indoor Positioning and Indoor Navigation*, Oct. 2013, pp. 1–8.

[225] F. Dwiyasa and M. H. Lim, "A survey of problems and approaches in wireless-based indoor positioning," in *2016 International Conference on Indoor Positioning and Indoor Navigation (IPIN)*, Oct. 2016, pp. 1–7.

[226] R. Mautz and S. Tilch, "Survey of optical indoor positioning systems," in *2011 International Conference on Indoor Positioning and Indoor Navigation*, Sep. 2011, pp. 1–7.

[227] M. F. Keskin, A. D. Sezer, and S. Gezici, "Localization via Visible Light Systems," *Proceedings of the IEEE*, vol. 106, no. 6, pp. 1063–1088, Jun. 2018.

[228] G. Retscher and A. Kealy, "Ubiquitous Positioning Technologies for Modern Intelligent Navigation Systems," *The Journal of Navigation*, vol. 59, no. 1, pp. 91–103, Jan. 2006.

[229] S. Bastiaens, D. Plets, L. Martens, and W. Joseph, "Impact of Nonideal LED Modulation on RSS-based VLP Performance," in *2018 IEEE 29th Annual International Symposium on Personal, Indoor and Mobile Radio Communications (PIMRC)*, Sep. 2018, pp. 1–5.

[230] J. Wang and E. Olson, "AprilTag 2: Efficient and robust fiducial detection," in *2016 IEEE/RSJ International Conference on Intelligent Robots and Systems (IROS)*, Oct. 2016, pp. 4193–4198.

[231] E. Olson, "AprilTag: A robust and flexible visual fiducial system," *2011 IEEE International Conference on Robotics and Automation*, pp. 3400–3407, 2011.

[232] Q. Li, J. Wu, Y. Chen, J. Wang, S. Gao, and Z. Wu, "High Precision Position Measurement Method for Laguerre-Gaussian Beams Using a Quadrant Detector," *Sensors*, vol. 18, no. 11, p. 4007, Nov. 2018.

[233] G. F. Barranco, M. Tröbs, V. Müller, O. Gerberding, F. Seifert, and G. Heinzel, "Spatially resolved photodiode response for simulating precise interferometers," *Applied Optics*, vol. 55, no. 24, p. 6688, Aug. 20, 2016.

[234] Hamamatsu, "Multi-element photodiodes for surface mounting," Datasheet, Oct. 2017.

[235] Cree, "LED Luminaire Design Guide," Application Note, 2016.

[236] A. Arafa, X. Jin, M. H. Bergen, R. Klukas, and J. F. Holzman, "Characterization of Image Receivers for Optical Wireless Location Technology," *IEEE Photonics Technology Letters*, vol. 27, no. 18, pp. 1923–1926, Sep. 2015.

[237] A. G. Dempster, "Dilution of precision in angle-of-arrival positioning systems," *Electronics Letters*, vol. 42, no. 5, pp. 291–292, Mar. 2006.

[238] S. Cincotta, A. Neild, and J. Armstrong, "Visible Light Positioning Receiver Arrangement and Two Stage Positioning Method," pat. WO2020000021 (A1).

[239] B. Huang, Z. Yao, X. Cui, and M. Lu, "Dilution of Precision Analysis for GNSS Collaborative Positioning," *IEEE Transactions on Vehicular Technology*, vol. 65, no. 5, pp. 3401–3415, May 2016.

[240] Y. Lu, D. Zhongliang, Z. Di, and H. Enwen, "Quality assessment method of GNSS signals base on multivariate dilution of precision," in *2016 European Navigation Conference (ENC)*, May 2016, pp. 1–6.

[241] W. Huihui, Z. Xingqun, and Z. Yanhua, "Geometric dilution of precision for GPS single-point positioning based on four satellites," *Journal of Systems Engineering and Electronics*, vol. 19, no. 5, pp. 1058–1063, Oct. 2008.

[242] T. Sun, F. Xing, and Z. You, "Optical System Error Analysis and Calibration Method of High-Accuracy Star Trackers," *Sensors (Basel, Switzerland)*, vol. 13, no. 4, pp. 4598–4623, Apr. 8, 2013.

[243] "AS/NZS 1680.2.4:2017 Interior and workplace lighting Industrial tasks and processes."

[244] T. Kim, L. Yong, and Q. Xu, "Robust design study on the wide angle lens with free distortion for mobile lens," in *AOPC 2017: Optical Storage and Display Technology*, vol. 10459, International Society for Optics and Photonics, Oct. 24, 2017, 104590Y.

[245] B. Ma, K. Sharma, K. P. Thompson, and J. P. Rolland, "Mobile device camera design with Q-type polynomials to achieve higher production yield," *Optics Express*, vol. 21, no. 15, p. 17 454, Jul. 29, 2013.

[246] Y. Zhuang, J. Yang, Y. Li, L. Qi, and N. El-Sheimy, "Smartphone-Based Indoor Localization with Bluetooth Low Energy Beacons," *Sensors*, vol. 16, no. 5, p. 596, Apr. 26, 2016.